LBL-7811



**Energy and Environment Division**

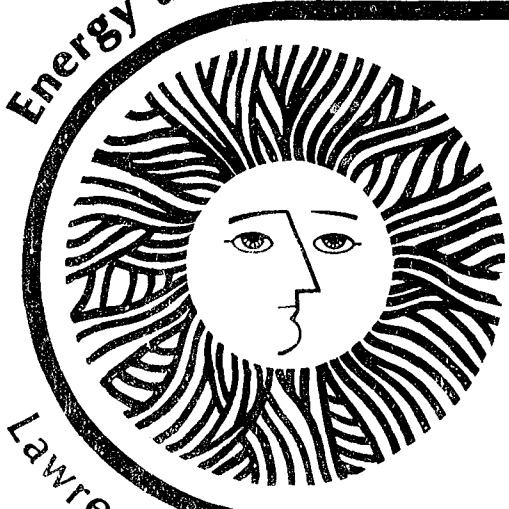

# Some Analytic Models Of Passive Solar Building Performance: A Theoretical Approach To The Design of Energy-Conserving Buildings

*David Baird Goldstein*
*(Ph.D. thesis)*

November 1978

Lawrence Berkeley Laboratory University of California/Berkeley

Prepared for the U.S. Department of Energy under Contract No. W-7405-ENG-48

LBL-7811

# SOME ANALYTIC MODELS OF PASSIVE SOLAR BUILDING PERFORMANCE: A THEORETICAL APPROACH TO THE DESIGN OF ENERGY-CONSERVING BUILDINGS

David Baird Goldstein

Lawrence Berkeley Laboratory
University of California
Berkeley, California

TABLE OF CONTENTS

Foreword . . . . . iii

List of Symbols . . . . . vi

1. INTRODUCTION: ENERGY CONSERVATION IN BUILDINGS AND ANALYTIC MODELING . . . . . 1

Footnotes to Section 1 . . . . . 12

Figures for Section 1 . . . . . 14

2. PASSIVE SOLAR . . . . . 18

2.1 Introduction . . . . . 18

2.2 The Passive Solar Building Model: The Basic Equations and Their Interpretation . . . . . 24

2.2.1 Heat Balance Equations . . . . . 25

2.2.2 Distributed Parameter Description . . . . . 28

2.2.3 Lumped Parameter Description . . . . . 29

2.2.4 Solution of the Equations . . . . . 31

2.2.5 Interpretation of the Equations . . . . . 33

2.3 Solution of the Lumped Parameter Model . . . . . 43

2.4 Solution of the Distributed Parameter Model . . . . . 49

2.4.1 Weather Response . . . . . 54

2.5 Evaluation of the Lumped Parameters . . . . . 59

2.6 Summary and Conclusions . . . . . 67

Footnotes to Section 2 . . . . . 69

Tables to Section 2 . . . . . 75

Figures for Section 2 . . . . . 93

3. EXPERIMENTAL VALIDATION OF THE MODELS . . . . . 104

3.1 Introduction and Overview of Results . . . . . 104

3.2 Determination of the Heat Capacity of LASL Concrete . . . 108

# FOREWORD

This paper describes an application of the fundamental methods of physics to solve a problem of environmental and economic interest: the description of the thermal performance of passive solar buildings. Such a description is of great practical interest to building designers; however, this paper is not intended to be of use to architects and engineers in its present form. Its intention is to provide a theoretical basis for understanding passive solar buildings; further effort is needed to develop rules of solar engineering.

The reader of this paper is assumed to have a background in physics and its application to buildings. Since building physicists have not yet developed analytic models of general applicability, this paper must derive its equations from first principles. This has resulted in a lengthy exposition. Because of the length, I have attempted to summarize the results of Section 2 early in the section. This summary is meant only as a guide to the reader, and so it presents many of its statements without proof or full explanation. More complete derivations are found later in the paper.

The passive solar problem has been of interest to physicists for several years. It was discussed in detail in the American Physical Society's summer study on efficient uses of energy (Ref. 1). Both of my advisors on this project (Prof. Sam Berman and Prof. Art Rosenfeld) were involved in the summer study and are highly interested in passive solar. Working with them provided many opportunities to look at passive solar buildings in more analytical detail.

comings in that regard remain the responsibility of the author.

I would like to thank Bob McFarland and Doug Balcomb of Los Alamos for the data they provided on their test buildings. There is a dearth of good hourly data on free-floating passive solar buildings; the LASL group has the only reliable and complete set of data I was able to find. I am also grateful to the Technical Information people at LBL for their help in the production of this paper from the original handwritten text and scrawled figures. Paula Bjork took responsibility for the typing with some assistance from Deberah Craig. Drawings were done by Antoinette Czerwinski.

Members of my thesis committee, Profs. Owen Chamberlain and John P. Holdren, supplied thoughtful comments on the content and exposition of this paper, which have been incorporated into its present form.

Finally, some mention is needed of the larger community of Berkeley. This community has been supportive of creativity and intellectual freedom throughout the nine years I have spent here; the feelings of acceptance and freedom that I have experienced were a crucial ingredient in the accomplishment of this project and others.

| | |
|---|---|
| $d_n$ : | Fourier expansion coefficients of the diurnal solar gain function |
| d (subscript) : | day |
| e (subscript) : | envelope walls |
| f (subscript) : | floor |
| h : | film heat transfer coefficient |
| $\hat{h}$ : | film heat transfer coefficient times area |
| i : | imaginary number ($\sqrt{-1}$) |
| i (subscript) : | inside of material (room side) |
| j (subscript) : | indexing subscript |
| k : | extinction coefficient |
| $\ell$ (subscript) : | lumped model |
| n (subscript) : | night, also an index for summation |
| o (subscript) : | outside of material |
| $p_n$ : | $n^{th}$ pole of a function |
| p (subscript) : | partition wall |
| q (subscript) : | quick |
| r (subscript) : | thermal resistance |
| s (subscript) : | surface |
| t : | time |
| $t_d$ : | the time at which the building ceases to collect solar energy for the day |
| t (subscript) : | thermostat |
| w (subscript) : | wall; also weather-frequency |
| x,y,z : | distance into a material |
| $z_n$ : | $n^{th}$ zero of a function |
| $\alpha$ : | fraction of solar gain absorbed on a given surface |

# 1. INTRODUCTION

Energy is used in a wide variety of ways in the developed world, but in almost all its uses, the desired result is the accomplishment of some non-energy-related task. The physicist's approach to analyzing patterns of energy consumption has been to compare the energy requirements of present technologies or devices for accomplishing a task with the theoretical limits to energy use. This method reveals where present processes are inefficient and can suggest where new ideas might be sought.

Analysis of energy uses in the United States economy shows that almost all tasks that use significant amounts of energy are done very inefficiently, both thermodynamically and economically. The American Physical Society study on efficient energy use (Ref. 1) found that most processes have second-law efficiencies of 10% or less. Our research at Lawrence Berkeley Laboratory has shown more detailed examples of energy waste; we have never found any process for which the life cycle costs of energy use have been minimized. That is, in all tasks we have studied, the economic return on an additional investment in energy conservation (beyond existing practice) would have been justified at existing energy prices and interest rates.

To illustrate the conservation potential implied by present inefficiencies, we display in reference 22 a list of several dozen conservation measures all of which have acceptably large returns on investment which would, taken as a whole, save 25% of California's gas and electricity use in ten years. Collectively, they have an

Different strategies are applicable for different uses and for different time scales. In the short run, the properties of energy using equipment are fixed and one can save energy only by better management (e.g. turning off lights in unoccupied offices or rooms) or by changes in habit or comfort (such as turning down thermostats at night). These changes generally result in relatively small savings unless the operation was grossly mismanaged in the first place.

In the longer run, retrofits of existing equipment can be attempted, such as insulating the ceiling or walls of originally uninsulated structures. This process is more costly than it would be for new construction, but the savings can be large: 30% of original energy use for ceiling insulation and another 30% for walls, based on computer simulation of northern California climates.[2]

On a similar time-scale, replacement of appliances with the more efficient models currently on the market can save 40% or more of existing energy needs.[3] New buildings can be constructed in more energy-efficient ways. Mandatory efficiency standards in California will lead to a savings of 15% or more for commercial buildings[4] and as much as 60% for residential buildings.[5]

Over a longer time period, more fundamental design changes can be made. One recent study of refrigerator redesigns estimated potential savings of 2/3 through a few relatively simple and high-payback improvements.[6] The effects of adding some more advanced insulation measures for houses are shown in Fig. 2, which graphs space heating needs as a function of conservation expenditures for

treat quite precisely the heat transfers driven by temperature differences, their treatment of solar gains is much more approximate.

In a real building, some fraction of sunlight incident on a window is transmitted into the interior. The direct beam component first strikes the floor or a piece of furniture, or perhaps an interior partition wall. Depending on the properties of the receiving surface, some portion of the energy is absorbed, and the rest is reflected. The reflected light, plus the diffuse sunshine from the window, strikes other surfaces in the room, is re-reflected, etc. Eventually all the sunshine is absorbed on some surface.

If the building models treated solar gain in detail, they would use their calculations of solar position in the sky to find the directly illuminated area within the building, and calculate solar absorption for each area of interior surface for each hour. They would then use these solar heat gains in calculating surface temperature for different sections of each material.

In fact, the treatment of solar gains is highly simplified compared to this description. The U.S. National Bureau of Standards computer program NBSLD (Ref. 11) assumes that solar gain from a window is absorbed uniformly over all interior surfaces (floor, ceiling, etc.) for all hours of the day. The Lawrence Berkeley Laboratory program DOE-1 (Cal/ERDA) (Ref. 18) is designed to simulate NBSLD runs in which the average solar gain for each surface is adjusted to be consistent with the exact modeling described above for only one specific hour and one specific building geometry and one set of surface reflectances. Only the thermal mass of the room is varied. Weighting factors are used to calibrate DOE-1 to these runs for light, medium, or heavy-weight

store more solar heat before it reaches an unacceptably hot temperature the next day. This results in a tradeoff between comfort and amount of solar energy stored. Such tradeoffs are difficult to treat in general because one cannot measure comfort in units which are comparable to heat or cost. They can be treated in an individual way by a resident about to construct or buy a house, but only if he can understand the thermal performance of the building in advance.

The rest of this paper is devoted to the derivation of an analytic model of building performance which can be used to develop an understanding of building response. Extensions and amplifications of this model can probably be developed as a design tool for new or retrofit buildings. The model is developed with the idea of describing buildings like the one discussed in Fig. 3 with large solar gain and tight insulation, but the theory should be generally applicable.

Section 2 describes the central equations and assumptions used in the model, and gives the solutions to a lumped-parameter and a distributed-parameter model. The derivations are performed in detail in a set of appendices whose numbers (2.3, 2.4, etc.) correspond to their analogous parts of Sec. 2.

Section 3 describes some experimental tests of the relationships derived in Sec. 2. Using data from the test buildings at Los Alamos Scientific Laboratory (LASL), we compute model response and compare it to measurements. Agreement between the data and the predictions is good.

there is no way to determine *a priori* which factors are responsible for the major features of a building's performance and which ones are unimportant. In addition, any errors in the model or approximations which are not accurate for a particular situation cannot readily be seen unless the model starts giving absurd results. One loses physical intuition in such an approach; the only way to find out what is really going on in the model is to make a large number of parametric runs, varying parameters which the modeller guesses will be important.

An analytic model, in contrast, will often show by its structure or the form of its equations which effects are dominant. For example, the distributed parameter model of Sec. 2.4 gives the response of room temperature in terms of relatively simple functions; the form of the key equation provides some insight into the expected results.

Also, a simple model of a building allows the determination of some of the parameters experimentally using a comparatively simple setup. Some of the linearities that show up in Sec. 2 can be exploited in reducing experimental complexity. In Sec. 3, we average over some large areas to obtain interesting theory vs. experiment comparisons with only a few measurements.

However, the models derived in this paper have more limitations than the computer models. The description of the building must be more elementary, and the response to complicated management schemes and even normal thermostatic control of a furnace cannot be handled. But, one can learn a lot about the heating and cooling needs

There is a large need for such improved modelling; very few new buildings are taking advantage of passive techniques, in part because of the lack of proven design rules.

Passive solar modelling is worthwhile as a tool for implementing one important conservative strategy — the use of building design to take advantage of "free" energy from the environment. As only one element of good energy-conserving design, it cannot be credited with a fixed or definable energy savings potential. However, the whole range of building energy strategies can reduce space-heating use to near zero, eliminating one of the major causes of energy demand.

Section 1 Footnotes (cont.)

in buildings which use 15% less energy than the average new building, based on simulations using DOE-1 (Cal-ERDA) (see Ref. 18). However, some buildings will use less energy than the legal maximum (some already do), so actual savings will be much larger than 15%.

5. The 60% savings are for northern California climates where, in 1979, double glazed windows will be required. A double-glazed, insulated house uses 60% less heat than a pre-standards house with only attic insulation, according to Ref. 8.
6. The refrigerator study is listed as Ref. 26; its significance for overall patterns of energy demand is discussed in Ref. 24.
7. Personal communication, G. P. Mitalas, 4 July 1978.

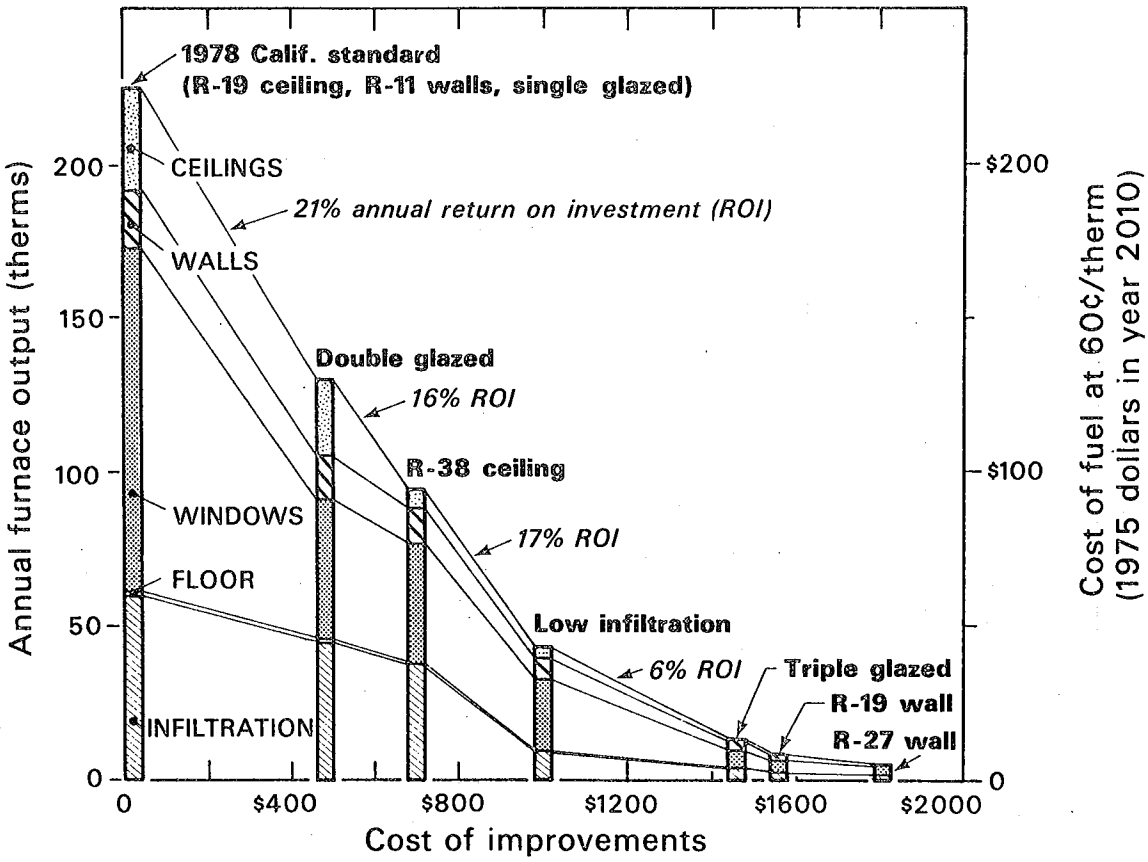


Figure 2 (A)
Heating loads calculated for Sacramento

Fig. 2. Heating energy use for a new house as a function of expenditure on insulation. Heating loads are calculated for Sacramento (Fig. 2A) and Chicago (Fig. 2B). The bar at the left illustrates a house insulated with R-19 ceiling insulation, R-11 wall insulation, R-19 floor insulation, and with single-pane windows. The bar is divided into segments labelled "ceiling, walls", etc. to indicate which part of the house is responsible for what fraction of heating energy. The next bars progressively add insulation measures such as double-glazing, better sealing for lower air infiltration, etc. The right-hand scale gives the annual cost of heating; it is equal to heat load (left scale) divided by the furnace efficiency of 60% and multiplied by the cost of fuel. For Sacramento we use future fuel prices of 60¢ per therm (see Ref. 24); for Chicago we assume present fuel prices of 25¢ per therm.

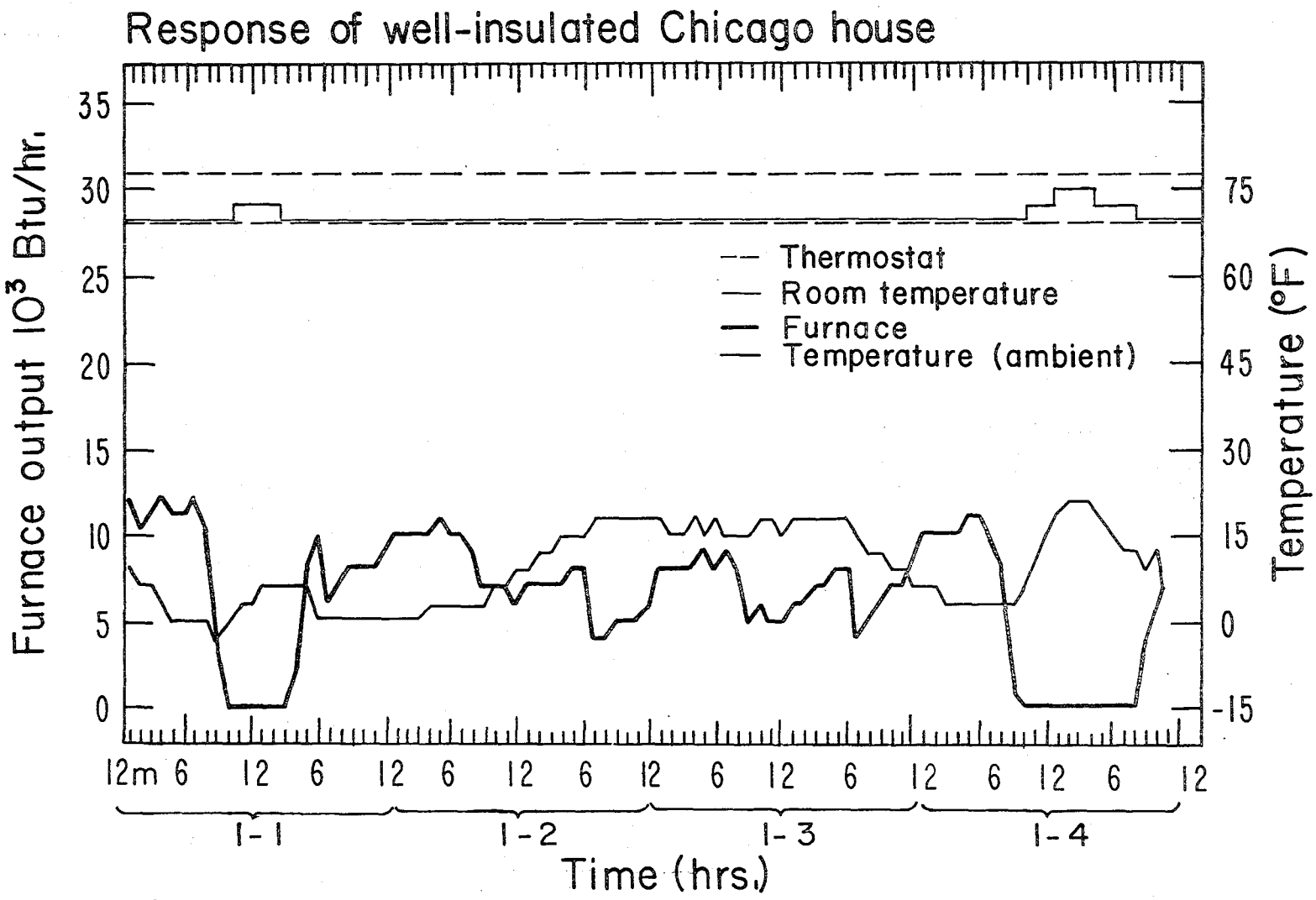


XBL 789-11389

Fig. 3. Predicted furnace load as a function of time (hours) for the Chicago house at the right of Fig. 2b, for the first four days in January. We also display outside temperature, thermostat settings of 70°F for heating and 78°F to open the windows, and inside room temperature. This figure was generated by TWOZONE (Ref. 8).

underwent several retrofits after the first winter to mitigate problems observed by its occupants.[21] Several other passive structures have required similar modification. This iterative approach is more costly than installing all the needed features during construction. Conversely, many passive houses have performed much better than expected. This, too, may be a problem if it results in oversizing the heating and cooling equipment. Additionally, the possibility that the building may not work "as planned" is a deterrent to the widespread application of passive solar designs.

To design a predictably well-performing passive building requires the use of an accurate model predicting building response, as well as an intuitive understanding of the heat transfers which are responsible for this performance. To this end, we present in this section a simple analytic model for calculating passive solar building response. The emphasis is on scientific clarity and simplicity. While it is our intent that the model be developed into a design tool for architects and building designers, in its present form it is not suitable for general use.

This model is most easily used to calculate "floating" or non-thermostated room temperature as a function of the driving forces of solar energy gain, ambient (outside air) temperature, and heater output (or internal heat generation from lights, appliances, etc.) It can also be used to calculate heater output needed to maintain a fixed room temperature, but this solution is generally of less interest. The mixed mode, in which room temperature floats between fixed thermostat positions, is much messier to handle and is not discussed here.

all interior surfaces in the room.[16] In contrast, our model allows the user to specify varying proportions of solar absorption on each surface (e.g. more sunlight absorbed on one wall than on another) or in the room air. This option makes a substantial difference in thermal response, as shown in Fig. 2.

Figure 2 graphs the room temperature of a passive solar building with wood frame walls and concrete floor under four sets of assumptions about solar energy absorption. The solid line labelled 'A' gives room temperature as a function of time for the case in which 6/7 of the sunlight is absorbed on the floor and 1/7 is absorbed on the walls and ceiling. Line 'B' describes the same house with 2/7 of the sunlight absorbed on the walls and 5/7 on the floor; while in case 'C' 4/7 of the sunlight is absorbed on the walls and 3/7 on the floor. The dotted line labelled 'D' graphs the case in which all the sunlight is absorbed on light furniture or carpets.

As show in the figure, there is a noticeable difference between the four curves; this difference illustrates the importance of being able to specify where solar energy is absorbed. Any model which does not allow this specification (or calculate it) implicitly assumes that one of these curves is always correct.

The importance of correctly modelling where solar energy is absorbed comes about because the response of a passive solar building involves considerable amounts of heat storage. The quantity of heat stored by a building depends strongly on the heat capacity ("thermal mass") of the materials exposed to direct sunlight, (along with other properties). The fact that solar absorption on surfaces of materials

can be studied using the simple model to determine which effects are significant enough to include in a revised computer model. For example, if it turns out that changing the solar radiation balance each hour as the sun moves across the sky does not strongly affect thermal response, then this feature need not appear in the computer models.

A simple model can also be used to decide what criteria to use in optimizing the thermal response of a building. As we will show, a building designed to minimize fluctuations in room temperature without heat input will be quite different from one designed to minimize annual energy use under fixed-thermostat conditions. When the various indices of thermal "quality" in a building disagree, a greater degree of understanding is needed to choose among alternate designs; a simple model can provide more insight into the physical process being modeled.

We now proceed to the derivation of the model. We will first present in Sec. 2.2 the basic equations of motion for the heat transfers within the building. These equations are developed along parallel paths for a "lumped-parameter" model and a "distributed-parameter" model. Next we will discuss the motivation for using each form of equation, and what the consequences and implications of the equations are. Finally, we solve the equations for the lumped parameter model in Sec. 2.3, and then for the distributed parameter or continuum model in Sec. 2.4. Comparisons between the lumped parameter and distributed parameter models are discussed in Sec. 2.5. The solution is sketched out in the text and redone with more technical detail in the appendices.

lumped parameter approach is an approximation which is useful in describing the response of managed buildings, and in modelling irregular weather patterns. The distributed-parameter solution is more exact, and gives a more elegant solution, but is incapable of modelling managed buildings. Heat transfers through light elements, such as windows, insulation-filled wall cavities, and air leakage ("infiltration") are handled by steady-state methods which only consider inside and outside air temperatures.

We consider the large solar gains through south-facing windows. (Windows facing other directions can also be treated in the model). Sunlight enters the house through the window, and is absorbed, either directly or after one or more reflections, on the surfaces of heavy elements in the room (such as floors, partition walls, and envelope walls). This process is sketched in Fig. 3. This absorbed solar heat warms the room air in the manner described below.

### 2.2.1 Heat Balance Equations

The most central equations in this model are surface heat balances. After sunlight enters a window, it is absorbed on some inside surface (labelled 'j') which heats up to satisfy the following heat balance equation:

$$\hat{h}_j (T_{s_j} - T_R) - \alpha_j S + Q_{in} = 0 \qquad (1)$$

where $\hat{h}_j$ is the combined radiation/convection surface film coefficient times the area of the surface (for the $j^{th}$ surface) (Btu/hr-°F or W/°C);

$T_{s_j}$ is the surface temperature (°F or °C) of the $j^{th}$ surface;

$T_R$ is the room temperature (room <u>air</u> temperature) (°F or °C);

materials with nontrivial heat capacity, and involve heat transfers from the room to the material surface, and then from the surface through the material. These materials attenuate variations in outside air temperature and delay their influence on the room air. Delayed heat transfers will be discussed shortly; at present they are considered indirectly in the terms $\hat{h}_j\ (T_{s_j} - T_R)$ describing heat transfers from the room air to the material surfaces, since the magnitude of $T_{s_j}$ is determined by the internal heat flows.

The room heat balance is given by:

$$\sum_{j=1}^{N} \hat{h}_j\ (T_R - T_{s_j}) + \hat{U}_q (T_R - T_A) = H + \alpha_R\ S \qquad (2)$$

where $U_q$ = heat transfer coefficient (Btu/(hr-°F) or W/°C) for quick heat transfers; the sum of the products of U-values times areas.

$T_A$ = ambient temperature

$H$ = heater output (Btu/hr or W)

$\alpha_R$ = fraction of sunlight absorbed directly into the room air

This equation states that the heat losses from the room always equal the heat gains. The first term is the sum of heat losses from the room air to each of the heavy material surfaces which surround it. Note that the surface temperature $T_{s_j}$ will be influenced by both outside air ("ambient") temperature and sunlight. The second term combines into

where $A_j$ is the area of the $j^{th}$ surface ($ft^2$ or $m^2$). The fundamental solution to the diffusion equation (3) with frequency $\omega$ can be written as (the real part of)

$$T_j(x,t) = \left(T_j^{(+)}\ e^{+k_j x} + T_j^{(-)}\ e^{-k_j x}\right) e^{i\omega t}$$

or

$$\left(T_j^{(c)}\ \cosh k_j x + T_j^{(s)}\ \sinh k_j x\right) e^{i\omega t} \tag{5}$$

where $$k_j = \sqrt{\frac{i\omega(\rho C_p)_j}{K_j}} = \sqrt{\frac{\omega(\rho C_p)_j}{2K_j}}\,(1+i)$$

The boundary conditions which determine the amplitudes $T_j^{(+)}$ and $T_j^{(-)}$ are the surface heat balance (1) and a condition on the temperature of the outside surface; usually the condition is that the outside surface temperature equals the ambient temperature.

The result can be visualized by looking at its limiting form for a very thick material. Only the negative sign in the exponential appears, and the solution is in the form of an exponentially damped sinusoidal traveling wave.

The solution (5) assumes a single-layer wall or floor. Extension to two or more layers is straightforward. If the second layer is a pure resistance, then the extension is especially easy; this two-layer wall will be used in some of the solutions of the model.

### 2.2.3 Lumped Parameter Description

For the lumped parameter case, we approximate the wall or floor as a sandwich of a lumped heat capacity $C_j$ (Btu/°F or Joules/°C) surrounded

2.2.4 Solution of the Equations

The solutions for room temperature as a function of time are generally the most interesting. We briefly describe their form below. Solutions can be computed using Tables 1 and 2. These solutions are derived for typical daily weather conditions where the solar gain, S(t), is given by (the real part of)

$$S(t) = \begin{cases} S_1 e^{i\omega_1 t} & \text{day } (0 \leq t < t_d) \\ 0 & \text{night } (t_d \leq t < 24 \text{ hrs}) \end{cases}$$

S(t) is sketched in Fig. 5.[17] The ambient temperature $T_A(t)$ is equal to (the real part of) $\Delta T_A e^{i\omega_o t} + \overline{T}_A$, where $\omega_o = 2\pi/1$ day. The heater output is taken as $H_o$, a constant. (However, this constant can change values from day to night.) All temperatures are measured with respect to average ambient temperature, so we set $\overline{T}_A = 0$.

We use the lumped model primarily for buildings whose parameters change from day to night (e.g. because the collector windows are insulated at night). The model generates two solutions, one for the day period and one for the night period.

Solving the lumped parameter equations for N heavy materials (j = 1,N) requires solving several sets of N simultaneous equations in N unknowns, so the solution becomes very difficult to compute by hand for $N \geq 3$. For N = 2, the result for room temperature can be written as

$$T_R(t) = \begin{cases} A_{1d} e^{-\Lambda_{1d} t} + A_{2d} e^{-\Lambda_{2d} t} + \chi_{A_d} \Delta T_A e^{i\omega_o t} + \chi_s S_1 e^{i\omega_1 t} + T_{H_d} & \text{[day]} \\ A_{1n} e^{-\Lambda_{1n} t} + A_{2n} e^{-\Lambda_{2n} t} + \chi_{A_n} \Delta T_A e^{i\omega_o t} + T_{H_n} & \text{[night]} \end{cases} \quad (8)$$

where the subscripts d and n indicate day or night values. The X's

the top of the table.

Descriptions of the solutions are provided in Sections 2.3 and 2.4. Modifications needed to describe Trombe wall or water-wall collectors are discussed in Appendices 2.3 and 2.4

### 2.2.5 Interpretation of the Equations

This set of equations (1-7) idealizes a building as a room with zero heat capacity, surrounded by a small number of materials of finite heat capacity, and a pathway for instantaneous conductive heat losses. Sunlight enters the room through windows, and is absorbed or reflected from the various surfaces in the room. The reflectances, absorptances, and room geometry produce a radiation balance; this balance is described by the $\alpha$ parameters.

a surface heats up due to absorption of sunlight) must be excluded from the measurement. In practice, one can measure all radiation at wavelengths shorter than 3μ, since longer-wave sunlight will be filtered out by the window glass.

As mentioned in the introduction, varying the fraction of the sunlight absorbed on each surface makes a large difference in the response of the building. Returning to Fig. 2 we see the difference in the response of a passive solar building with wood frame walls and concrete slab floor[5] for four different sets of α's. All four lines on the graph describe the same house. The solid line labeled A describes the case where $\alpha_{floor} = 6/7$ ; $\alpha_{walls} = 1/7$ and $\alpha_R = 0$. The lines labeled B and C successively double $\alpha_w$ at the expense of $\alpha_f$, with $\alpha_R$ remaining zero. The dotted line labeled D sets $\alpha_f = \alpha_w = 0$ and $\alpha_R = 1$, corresponding to solar absorption in the room air.

As shown in the figure, the response of the building is noticeably different as we vary the α's. Going from case A to case B, the house is 1°F hotter during the afternoon but 1/2°F cooler at night. Moving to case C where 57% of the sunlight is absorbed on the light, wood-frame walls, the house overheats 2-1/2°F during the afternoon and is another 1/2° colder at night.

Case D with solar absorption in the room, differs most dramatically from any of the other cases; it overheats by almost 8°F compared to case A while cooling off 2-1/2°F more at night. Thus correctly accounting for solar absorption within the building makes a significant difference in the predictions of performance. Getting the exact radiation balance solved for a given house (i.e. evaluating the α's correctly) is

in Sec. 2.4. This equation shows that as long as heat transfers are linear in temperature difference, the distribution of sunlight received over a surface doesn't affect the solution; the only important parameter is the total amount of sunlight absorbed on the whole surface.

In fact, we assume that in general temperatures do not vary from one point on a surface to another; in other words, that the floor surface temperature $T_{fs}$ represents an average over the whole floor surface. This assumption of 1-dimensional heat flows is common to all calculational methods; it is valid here as long as heat transfers are linear.

Linearity of the heat transfer equations is an assumption which is common to all building models; heat flows are taken as proportional to temperature differences. In fact, film coefficients are the sums of terms which involve the differences of fourth powers of temperature for radiation terms and roughly the 5/4 power of temperature difference for convective terms. These heat transfers can be approximated as linear because temperature differences are typically much smaller than absolute temperatures, so a Taylor expansion which drops all terms of higher order than 1 in $\Delta T$ will not introduce serious error. For example for a room temperature of 300°K and a temperature difference of 10°K, the error in a linear approximation for radiative heat transfer is 5%.

thick, plus stucco siding, can be approximated as a 4" thick slice of wood for most purposes, since wood has[8]

$$\rho C_p \cong 9 \text{ Btu/°F-ft}^3 , \quad \text{and} \quad K \cong 0.068 \text{ Btu/hr-°F-ft} ,$$

while gypsum board has

$$\rho C_p \cong 13 \text{ Btu/ft}^3\text{-°F} , \quad \text{and} \quad K \cong 0.075 \text{ Btu/hr-°F-ft} ,$$

not significantly different. This one-layer approximation yields a substantial reduction in algebraic manipulation needed to solve the equations. The response functions of Sections 2.4 and 2.5 can provide a check on the validity of this approximation. However, a two-layer model is used when there is substantial difference in material properties (e.g. concrete block with polyurethane foam exterior).

Similarly, materials of similar parameters are combined to form a single "surface" j; this also reduces the amount of computation needed. For example, wood-frame walls can be treated together with the ceiling as a single surface. Combined or average parameters are used for this approximation.

Room heat capacity is taken as zero in Eq. (2), which says that heat losses from the room equal heat gains, with no heat storage term. This is a good approximation; even a light house has a heat capacity of about 2.25 Btu/°F per square foot of floor area, while with 8-foot ceilings, the heat capacity of the air is only 0.14 Btu/°F per ft.$^2$ A more realistic passive solar house[7] has 12 Btu/°F of heat capacity per ft$^2$ of floor. To confirm that this assumption is unimportant, we calculated the 3 time constants for the lumped parameter model with

In addition to these assumptions are the usual ones assumed in all building models -- no intra-zone temperature variations, one-dimensional heat flows, known materials properties, construction which follows designs (e.g. no forgotten insulation or air leaks), known behavior of thermostat, etc. In fact, the "standard" assumptions probably lead to about 10-20% uncertainty in any model, no matter how exact the mathematical modelling.[19] This "acceptability range" of ± 10%-20% justifies a number of the simplifications described above; if the description of the house is only correct within 10-20%, then 5% calculational errors are not crucial.

In addition to the simplifying assumptions about the building, an analytic model requires a different type of weather input than a numerical model. Weather data is available as a function of time only with 1-hour or 3-hour sampling periods. Numerical models use special forms of response functions to account for this.[9] An analytic model must be driven by continuous functions of time. Connecting data points with a smooth curve could lead to very long Fourier series for the weather and correspondingly messy solutions to the differential equations. In this model we approximate outside weather by simple, continuous functions of time, typically sinusoids. Weather conditions are usually treated by Fourier-analyzing the actual weather and only taking a few dominant frequencies in the series, typically $\omega_o = 2\pi/\text{day}$, $2\omega_o$, $3\omega_o$, and 0.

This procedure is in line with the intended uses of the model as a design optimization tool and as a method for gaining an understanding of how the building works. For either of these two

## 2.3 Solution of the Lumped Model

This section discusses the solution of the lumped parameter model, using Eqs. (1), (2), (6), (7), and a simplified description of weather which is described below. In order to carry out this solution numerically one must first evaluate the lumped parameters. Evaluation is not trivial; $C_w$ is not just the heat capacity of the bulk material which makes up the wall, neither is $\hat{U}_{wi}$ or $\hat{U}_{wo}$ equal to the U value times area. This problem is discussed in Sec. 2.5. The discussion in this section describes the solution of the lumped parameter model in general terms. The detailed algebraic manipulations are contained in Appendix 2.3. We first solve the equations for the free-floating (unheated) house.

We consider two surfaces with heavy materials behind them; call them "floor" and "walls". The floor and wall temperatures ($T_f$ and $T_w$) are the important variables in the calculation; they express the temperatures of massive elements. Thus we will derive differential equations which involve only $T_w$ and $T_f$. The solution to these differential equations will then be used to derive room temperature $T_R$. The room temperature is usually the desired result of the calculation. It is given by Eq. (11) below.

We next describe the derivation, which is carried out in Appendix 2.3.

We use Eqs. (1) and (2) to derive a relationship between the room temperature and the dynamic temperatures $T_w$ and $T_f$. This relationship shows that room temperature is a linear function of the dynamic temperatures and the driving forces S, H, and $T_A$; it is given by

The inhomogeneous solution depends on the form of the driving functions. We approximate the driving forces by simple functions and then derive the inhomogeneous solution for each one.

The heater output is taken as a constant $H_o$, which may be different during the day and night ('$H_{o_d}$' and '$H_{o_n}$'). Then the inhomogeneous solution to the differential Eqs. (10a) is

$$T_w = T_{H_w}$$

$$T_f = T_{H_f}$$

constant temperatures given by Table 1.

The solar gain function S(t) is given by a sine wave during the day or zero at night.[17] We take t = 0 to be when the sunlight first enters the windows and $t = t_d$ to be when it last enters. Then

$$S(t) = \begin{cases} S_1 e^{i\omega_1 t} & 0 \leq t < t_d \\ 0 & t_d \leq t < 24 \text{ hrs.} \end{cases}$$

We assume that S(t) is the same each day. Then the inhomogeneous solutions to (10a) is

$$T_w = \chi_{s_w} S_1 e^{i\omega_1 t} \qquad 0 \leq t < t_d$$

$$T_f = \chi_{s_f} S_1 e^{i\omega_1 t} \qquad 0 \leq t < t_d$$

and $T_f = T_w = 0$ for $t_d \leq t < 24$ hours (at night).

These four boundary conditions fix the four constants $B_{1d}$, $B_{2d}$, $B_{1n}$ and $B_{2n}$. Knowing the B's, we now have the complete solution to (10a) for both day and night periods. We can finally use this solution with (10) to find room temperature.

The complete solution can be expressed as

$$T_w(t) = \begin{cases} B_{1d}\, e^{-\Lambda_{1d}t} + B_{2d}\, e^{-\Lambda_{2d}t} + \chi_{A_{wd}} \Delta T_A\, e^{i\omega_o t} + \chi_{s_w} S_1\, e^{i\omega_1 t} + T_{H_{wd}} & \text{(day)} \\ B_{1n}\, e^{-\Lambda_{1n}(t-t_d)} + B_{2n}\, e^{-\Lambda_{2n}(t-t_d)} + \chi_{A_{wn}} \Delta T_A\, e^{i\omega_o t} + T_{H_{wn}} & \text{(night)} \end{cases}$$

(11)

$$T_f(t) = \begin{cases} B_{1d}K_{1d}\, e^{-\Lambda_{1d}t} + B_{2d}K_{2d}\, e^{-\Lambda_{2d}t} + \chi_{Af_d} \Delta T_A\, e^{i\omega_o t} + \chi_{s_f} S_1\, e^{i\omega_1 t} + T_{H_{fd}} & \text{(day)} \\ B_{1n}K_{1n}\, e^{-\Lambda_{1n}(t-t_d)} + B_{2n}K_{2n}\, e^{-\Lambda_{2n}(t-t_d)} + \chi_{A_{fn}} \Delta T_A\, e^{i\omega_o t} + T_{H_{fn}} & \text{(night)} \end{cases}$$

$$T_R(t) = \frac{N_w}{N_R} T_w(t) + \frac{N_f}{N_R} T_f(t) + \frac{1}{N_R} \Delta T_A\, e^{i\omega_o t} + \frac{N_s}{N_R} S_1\, e^{i\omega_1 t} + \frac{1}{\hat{U}_q N_R} H$$

Table 1 below gives a program for calculating the functions described by (11) from building and weather parameters. In most cases, the interesting result of the calculation is the room temperature curve. Given design day weather conditions, the room temperature function describes whether the building will overheat during the day or cool off too much during the evening.

## 2.4 Solution of the Distributed Parameter Model

This section discusses the solution of the continuum model at a similar level of overview to the previous section. Algebraic details are in Appendix 2.4A. The continuum model solves the heat transfer equations in Fourier-transform space. It can only be used when house parameters are time independent; time-dependent parameters generate extra terms which, although they can be calculated analytically (see Appendix 2.5B) are tedious to compute.

The continuum model is most useful in cases where the response of the building to several-day weather cycles is important. As we will show, the response to weather cycles can be derived relatively easily from the solution to daily cycles.

This model also handles more than two material surfaces without undue complication of the algebra. We will therefore display the equations of heat transfer for a slightly more complicated system than used in the lumped parameter model. We will use three material surfaces in this derivation, with subscript "e" for envelope walls, "p" for partition walls, and "f" for floor. Extension to a larger number of surfaces is straightforward.

The continuum model is solved in Fourier transform space; instead of looking at, say, the room temperature $T_R(t)$, we look at its Fourier transform $\tilde{T}_R(\omega) = 1/(2\pi)\int_{-\infty}^{\infty} dt\ T_R(t)\ e^{-i\omega t}$. $\tilde{T}_R(\omega)$ is a function of the driving forces of solar gain $\tilde{S}(\omega)$, ambient temperature $\tilde{T}_A(\omega)$ and heater output $\tilde{H}(\omega)$. If these driving forces can be expressed as sums over only a few frequencies, then we can write $T_R(t)$ as a Fourier sum over a small number of frequencies. These relationships are summarized in Table 2. We derive them below:

partition walls, and semi-infinite floor slab) in Table 2 and Eq. (A2.4-21). Some typical $R_1$ functions are plotted in Figs. 8, 9, A2.5-2 and A2.5-3. With slight redefinitions, these response functions are the Fourier form of the response factors used in computer models.

The expression for surface temperature can be used in the room heat balance to produce the equation:

$$T_R(\omega)\left\{\hat{U}_q + \hat{h}_e(1-h_eR_{1e}) + \hat{h}_p(1-h_pR_{1p}) + \hat{h}_f(1-h_fR_{1f})\right\}$$
$$= S(\omega)\ (\alpha_R + h_e\alpha_eR_{1e} + h_p\alpha_pR_{1p} + h_f\alpha_fR_{1f})$$
$$+ T_A(\omega)\ (\hat{U}_q + \hat{h}_eR_{2e}) + H(\omega) \qquad (14)$$

This equation relates the Fourier transform of the room temperature to those of the driving forces S, $T_A$ and H. It can be written simply in the form

$$T_R(A(\omega)) = S(B(\omega)) + T_A(C(\omega)) + H \qquad (14a)$$

where A, B, and C, are frequency dependent functions given by (14). All of these functions are linear combinations of heat transfer coefficients times materials response functions. All the frequency dependence is contained in the response functions; materials properties such as conductivity do not appear except in these functions.

The response functions will be important in choosing values for the lumped parameters; they are plotted and tabulated for several representative materials in Sec. 2.5 and Appendix 2.5A.

The response of the building is driven by the Fourier transforms of ambient temperature $T_A(t)$ and solar gain S(t). Fourier transformation produces very short series, since $T_A$ can be modelled acceptably by 1-3 terms. If we take the same function for S as in the lumped-

such that $\frac{B(0)}{A(0)}$ is large but $\frac{B(\omega_o)}{A(\omega_o)}$ is small.

We can also see what design criteria apply to a constant-thermostat house which is continuously heated. In that case, we can write (14a) as

$$H(\omega) = T_R(\omega)\ A(\omega) - S(\omega)\ B(\omega) - T_A(\omega)\ C(\omega)$$

We note that $H(\omega)$ integrates to zero unless $\omega = 0$, so that to minimize heating requirements, we want $B(0)$ large and $C(0)$ small. (Of course, if $H(t)$ goes negative in this solution, it means that air conditioning is required and our model is then unrealistic). We show in Appendix 2.4 that $C(0)$ is just the steady-state heat transfer coefficient of the house; so the strategy of minimizing $C(0)$ is satisfied by simply insulating the building.

Thus we see that the design strategy for optimizing thermal performance of a house depends on whether the house is free-floating or thermostated. Design strategies for the thermostated house will not differ radically from those implied by the degree-day method, while those for the free-floating house will be more complex.

We can also use Eqs. (14) and (14a) to see some of the physical significance of the response functions. To get $A(\omega)$, we add the quick heat transfer coefficient $\hat{U}_q$ to terms of the form $\hat{h}_j(1-h_jR_{1j})$. These terms act as heat transfer coefficients (or U-values times areas) for their heavy materials. For $\omega \to 0$, they reduce to the conventional steady-state heat transfer coefficients, as shown in Appendix 2.4. For

To add slowly varying insolation, we assume that solar gain is still sinusoidal every day, but that the amplitude of the solar gain varies sinusoidally over a weather cycle. That is, we express S(t) as

$$S(t) = \begin{cases} (\bar{S} + \Delta S_w \cos \omega_w t) \sin \omega_1 (t - (24 \text{ hr})\, m); & \text{daytime} \\ 0 \quad \ldots\ldots\ldots\ldots\ldots\ldots & \text{nighttime} \end{cases}$$

m = largest integer that allows a positive argument for sin.

We assume that $\omega_o/\omega_w$ is an integer for simplicity. Thus solar intensity is approximately $\bar{S} + \Delta S_w$ at noon on the sunniest day and $\bar{S} - \Delta S_w$ at noon on the cloudiest day.

S(t) can be Fourier analyzed into relatively few frequencies (in principle, all integer multiples of $\omega_w$ are possible). We show in Appendix 2.4 that the only frequencies which appear are $\omega_w$, $\omega_o$, $\omega_o \pm \omega_w$, $2\omega_o \pm \omega_w$ .... The amplitudes are found as follows:

| The amplitude at frequency | | is | |
|---|---|---|---|
| | 0 | | $d_o \times \bar{S}$ |
| | $\omega_w$ | | $d_o \times \Delta S_w$ |
| | $\omega_o$ | | $d_1 \times \bar{S}$ |
| | $\omega_o \pm \omega_w$ | | $d_1 \times \frac{\Delta S_w}{2}$ |
| | $n\omega_o$ | | $d_n \times \bar{S}$ |
| | $n\omega_o \pm \omega_w$ | | $d_n \times \frac{\Delta S_w}{2}$ |

This can be understood as follows: a term $Sd_n e^{i\omega_n t}$ from the Fourier expansion of the daily solar gain function is replaced by the terms

We have derived in this section a simple expression for room temperature response to ambient temperature and solar gain, which uses truncated Fourier series. A model which considers approximately weekly weather variations will express $T_R$ as a sum of 8 terms, which can be computed by hand.

As mentioned earlier, this model will only work for unmanaged passive buildings; that is, buildings which do not open windows or add insulation in response to weather conditions or time of day. However, for these unmanaged buildings, the solution derived is an exact solution of the heat transfer equations (to arbitrary accuracy depending on how many terms of the Fourier expansion are retained). In other words, all the simplifications in the model occur in the writing of Eqs. ((1), (2), (3), and (4)), not in their solution.

Also, it is often possible to produce an approximate solution to a managed building by changing the value of H(t), the heater output function. For example, suppose we assume that a window is insulated at night. We estimate the expected change in heat loss due to this change in insulation, and assume that much energy is released to the room air by the heater. An exact solution would require equivalent heater output to equal $\Delta UA(T_R-T_A)$ where $\Delta U$ is the change in conductance of the windows. The approximate solution (or iterative approach to the exact solution) assumes that we already know $(T_R-T_A)$ and adjusts H(t) to equal the guessed value of $\Delta UA(T_R-T_A)$. This approximation moves the time-dependence from the building parameters (which we can't handle) to the input functions.

The form of the equations in this section assume single-layer heavy materials; however, the use of multi-layer materials will only produce

## 2.5 Evaluation of the Lumped Parameters

The section on the lumped parameter model (Sec. 2.3) shows how to calculate the response of a building as a function of a few lumped parameters. However, it did not describe how to calculate values for these parameters if they were to be used to model a continuous wall. In this section, we derive methods for choosing values of lumped parameters which optimally simulate the response of continuum materials. The purpose of this exercise is to provide a way of simulating a managed building whose parameters change from day to night or as a function of weather.

Lumped parameters are a mathematical construct used to simplify solution of the equations. A continuum wall's temperature is described by a function of position $T_w(x,t)$; to describe it by a single temperature $T_w$ is not physically meaningful. That is, the lumped temperature $T_w$ cannot be measured. However, $T_w$, along with the lumped parameters $\hat{U}_{wi}$, $\hat{U}_{wo}$ and $C_w$, will determine a wall surface temperature which can be measured. If $\hat{U}_{wi}$, $\hat{U}_{wo}$, and $C_w$ can be chosen such that this wall surface temperature agrees with that derived from the exact solution, then the lumped model will be useful.

We derive optimal values for the lumped parameters by calculating surface temperatures for an isolated material (floor or wall) in both the lumped and continuum models.

The calculation proceeds along the same lines as that used to derive the response functions of Sec. 2.4. The result is an expression for response functions for the lumped model, along with the previously-derived response functions.

interest in the passive solar heating problem. The driving functions $T_A$ and S have spectra which are large for $\omega = 0$ or $\omega = 2\pi/yr$ and for frequencies around $\omega_o = 2\pi/day$. However, their components at high frequency ($\omega > 3\ \omega_o$) are generally not very large, so if we can choose the lumped parameters such that $R_{1_\ell}$ and $R_{1_c}$ agree $0 \leq \omega \lesssim 3\ \omega_o$ we should expect good agreement for the lumped and continuum models.

We present two methods for simulating the lumped parameters, one for thin walls and one for thick walls. The definitions of thin and thick will become clear from the analysis; in practice walls thinner than 5" of wood or 10" of concrete are "thin".

For the thin wall model, we use an adaptation of a method suggested by Sonderegger.[13] We look at the poles and zeroes of the response functions. Noting that the $R_2$ functions have no zeroes, and that their poles are the same as those of the $R_1$ functions, we can look at $R_1$ only. Functions of a complex variable can be expanded as a ratio infinite products $F \cdot \dfrac{\prod_{i=1}^{\infty}\left(1-\frac{z}{z_i}\right)}{\prod_{i=1}^{\infty}\left(1-\frac{z}{p_i}\right)}$ where the z's and p's are zeroes and poles and F is the value of the function for $z = 0$. If $z \ll z_i$ the term $\left(1 - \frac{z}{z_i}\right)$ will be close to 1. Thus if we look at the function for $z \ll z_i$ and $p_i$ we can approximate the function by truncating the product with i terms, since all terms of higher order than i will equal 1.

The function $R_{1_\ell}$ has only one pole and one zero, while $R_{1_c}$ has an infinite string of alternating poles and zeroes. All poles and zeroes of all four functions occur along the positive imaginary

resistance R to get the new value of $\frac{1}{\hat{U}_i}$ or $\frac{1}{\hat{U}_o}$ ; instead the whole process of matching poles and zeroes of response functions must be repeated. The results for inside insulation, outside insulation, and partition walls are shown in Table 3. The derivation is shown in Appendix 2.5A.

As mentioned earlier, the thin wall approximation only works for $\omega << p_1$ or $z_1$. Sonderegger shows that this will be true for all $\omega \leqslant \omega_{max}$ when $d \lesssim \sqrt{\frac{3K}{\rho C_p \omega_o}}$ ($\omega_{max} \cong 3\ \omega_o$), (see Appendix 2.5A).

As an example, we present the comparison between the exact (continuum) response functions and the lumped response functions for 2" concrete in Table 4. This table shows good agreement for both response functions for $\omega \leqslant 8\ \omega_o$ . Table 5 for 4" wood also shows good agreement for $\omega \lesssim 3\ \omega_o$ , except for some loss of phase lag in the lumped functions. The magnitude of $R_1$ is graphed for this case in Fig. 8; the solid line represents $|R_{1_c}|$ while the light dashed line represents $|R_{1_\ell}|$.

But the agreement worsens for thick materials. Table 6 lists the continuum and lumped response functions for 1½ - foot concrete; and Fig. 9 graphs $|R_{1_c}|$ and $|R_{1_\ell}|$. As shown, the agreement becomes poor for $\omega \gtrsim \omega_o$.

For thick walls, a number of poles and zeroes of $R_{1C}$ occur whose magnitude is less than $3\omega_o$. Since $R_1$ has only 1 pole and zero, the locations of these points must be chosen to approximately simulate

$|R_{1_\ell}|$ for 6" wood; while Fig. 9 is for 1½' concrete. In both figures, the continuum response functions are plotted with solid lines, while the thick-wall lumped parameter functions are plotted with heavily dashed lines. For comparison, the thin-wall functions are plotted with lightly dashed lines. Figure 9 also shows the comparison in the limit of a semi-infinite concrete slab. The comparisons between both $R_1$ and $R_2$ are also listed in Tables 7, 8, and 9, respectively.

Another feature of the thick-wall method is that its values for the lumped parameters join smoothly with those given by the thin wall model. That is, when $C_{thin} = C_{thick}$, $\hat{U}_{i\ thin} \cong \hat{U}_{i\ thick}$ for both wood and concrete. Figure 10 graphs the values of lumped parameters as a function of wall thickness for concrete, and illustrates this smooth transition. The numerical values for the lumped parameters are tabulated in Table 10 for concrete and Table 11 for wood. Because of this transition, we can provide a rule for distinguishing thin walls from thick: whenever $C_{thin\ model} > C_{thick\ model}$, we use the thick model. Physically, this is because the effective heat capacity of a finite-thickness wall can never exceed that of a semi-infinite wall.[15]

The thick-wall parameters of (21) are chosen to represent a single-layer thick wall. Extension to two-layer walls is done in Appendix 2.5A; the results are summarized in Table 3. Because of the use of the penetration depth in the equations for the lumped parameters, the thick wall approximation should be valid only for $d > \frac{\sqrt{2}}{|k|}$. But the thin wall model is valid for $d < \sqrt{\frac{3}{2}}\ \frac{\sqrt{2}}{|k|}$. Thus, the two models overlap and either one or the other should be valid for all thicknesses

## 2.6 Summary and Conclusions

This section is intended to present a method for calculating the response of a simple passive solar building to idealized weather. Such a calculation can be used in finding optimum window areas, insulation levels, amounts of heat capacity, etc., for a given climate.

We have described two approaches: a distributed parameter model, which is useful in developing an intuitive understanding of the building, and which works only for unmanaged buildings; and a lumped parameter model, which provides a more approximate solution, but is capable of handling time-dependent building parameters (e.g. night insulation). The results of these approaches are summarized in Tables 1 and 2.

We have developed arguments to show that the approximations made in deriving our results appear to be justified and have shown that for one test case, the results of the lumped parameter approach agree with the exact solution. We will show the agreement with experiment in Sec. 3.

However, much work remains to be done before these models can be used for practical design applications.

First, sample optimization calculations should be done for a few typical climate areas to see which parameters change dramatically with climate and which are relatively unaffected. Optimum free-floating houses should be compared with optimum thermostated units; the habits of the occupants will apparently change the optimal window areas.

Second, further approximations should be made to simplify the arithmetic. The end-product should be a model which can be used by

Footnotes to Section 2

1. Ref. 1 describes the heat balance (solar radiation in minus conduction/convection out) on a south-facing window for several typical U.S. climates.
2. Ref. 2 discusses heat balances for different types of glazing.
3. These houses are described in Refs. 5, 10 and 20, and are catalogued in Ref. 6. Ref. 7 contains several-page write-ups of the architecture and thermal performance of 5 passive buildings.

3a. See Ref. 3a and the discussion in the beginning of Ref. 4.

4. Ref. 4.

4a. Balcomb defines passive solar buildings as those in which energy flows by natural means (Ref. 3c). Our definition of passive is a little more restrictive: we exclude systems which use collectors which are distinct from the building itself.

4b. A Trombe wall is a south-facing heavy wall with one or more layers of glazing covering the south or outside surface. The sunlight is absorbed after passing through the glazing (see Fig. 7). The air in the channel between the wall surface and the glazing may be coupled convectively to the room air through slots in the bottom of the wall. The inventor of the Trombe wall discusses some of its attributes in Ref. 20.

5. See next page.

6. The method for deriving lumped parameters is specific to the surface-absorption model, so it is not clear what values of heat capacity to use for $C_{room}$. But the form of the two curves is

sufficiently different that even if we were to choose a different value for $C_{room}$, the agreement would still be poor. (Note that the value of U that is used is not ambiguous. The model must always give the same steady-state heat loss as the exact solution).

7. See Appendix 2.3 for description of house parameters.
8. Values are from Ashrae Handbook of Fundamentals, Ref. 15, for gypsum board $\rho$ = 50 lbs/ft$^3$; K = 0.075 Btu/°F-ft-hr. Heat capacity $C_p$ is not listed, so we use the value of 0.259 Btu/°F for gypsum.
9. The discrete form of the Laplace transform is called the z-transform; it is described in some detail for building models in Ref. 29.
10. This is apparent looking at the output of the TWOZONE program (for a description of the program see Ref. 8). TWOZONE provides as output a graph of room temperature, ambient temperature, furnace output, and thermostat setting as a function of time. (see Fig. 1.3) The graph covers the first four days of each month.

    One can get an idea of the passive performance of the TWOZONE house by setting the thermostat very low (e.g. 55 or even 40 F) and looking at the fluctuations in room temperature. But to do so, requires first trying to find typical circumstances of outside weather - which hopefully occur during the first four days of the month - and then looking at the response of the building to custom-selected typical weather. It would be much easier to simply program in the desired "typical" weather.
11. Concrete and soil both have thermal properties which depend on the detailed description of the individual specimen. Moisture

15. cont. is $\frac{1}{|k|}$, since for $\Pi > |\frac{kd}{\sqrt{2}}| > \frac{\Pi}{2}$, T(x) is negative and the increasing thickness slightly diminishes the heat stored in the wall. However, this optimum thickness varies with frequency, so for a range of frequencies, a thicker wall should always store slightly more heat than a thinner wall.

16. The NBSLD program (see Ref. 11 for program description) assumes that the solar gain is spread uniformly over all interior surfaces. The Cal/ERDA or DOE-1 program (see Ref. 18) and NECAP (see Ref. 12) both use the weighting factors given by ASHRAE (Ref. 15). The derivation of these weighting factors has never been described in a paper, but is based on some computer runs by G. P. Mitalas, assuming typical office building conditions, such as light-colored floors, relatively small windows (less than half of wall area). These conditions would not be appropriate for simulating passive solar buildings (personal communication, G. P. Mitalas, telephone 4 July 1978). The TWOZONE program (see Ref. 8) uses weighting factors for solar absorption based on the above results, also. In addition, the results used in the programs simply distinguish between light, medium, or heavy-weight rooms; they do not consider the precise materials properties (conductively, heat capacity, etc.) of the walls.

17. This sinusoidal solar gain function is shown to be a good approximation to the data for at least one particular climate in Ref. 21.

18. See Ref. 9, Chapter IV.

Table 1

A PROGRAM FOR EVALUATING THE LUMPED PARAMETER EQUATIONS

$$N_w = \frac{1}{\hat{U}_q} \frac{\hat{h}_w \hat{U}_{wi}}{\hat{h}_w + \hat{U}_{wi}}$$

$$N_f = \frac{1}{\hat{U}_q} \frac{\hat{h}_f \hat{U}_{fi}}{\hat{h}_f + \hat{U}_{fi}}$$

$$N_R = 1 + N_w + N_f$$

$$N_s = \frac{N_w \alpha_w}{\hat{U}_{wi}} + \frac{N_f \alpha_f}{\hat{U}_{fi}} + \frac{\alpha_R}{\hat{U}_q}$$

$$\lambda_w = \frac{\hat{U}_q}{C_w} N_w$$

$$\lambda_f = \frac{\hat{U}_q}{C_f} N_f$$

$$\Lambda_p = \lambda_w \left(1 - \frac{N_w}{N_R}\right) + \frac{\hat{U}_{wo}}{C_w}$$

$$\Lambda_G = \lambda_f \left(1 - \frac{N_f}{N_R}\right) + \frac{\hat{U}_{fo}}{C_f}$$

$$\Lambda_F = \frac{\lambda_w N_f}{N_R} = \frac{\hat{U}_q N_f N_w}{C_w N_R}$$

Table 1 (cont.) p.3

$$\chi_{A_w} = \frac{a_3(\Lambda_G+i\omega_o) + a_6\ \Lambda_F}{(\Lambda_P+i\omega_o)(\Lambda_G+i\omega_o) - \Lambda_F\Lambda_Q}$$

$$\chi_{A_f} = \frac{a_6(\Lambda_P+i\omega_o) + a_3\ \Lambda_Q}{(\Lambda_P+i\omega_o)(\Lambda_G+i\omega_o) - \Lambda_F\Lambda_Q}$$

$$\chi_{S_w} = \frac{a_2(\Lambda_G+i\omega_1) + a_5\ \Lambda_F}{(\Lambda_P+i\omega_1)(\Lambda_G+i\omega_1) - \Lambda_F\ \Lambda_Q}$$

$$\chi_{S_f} = \frac{a_5(\Lambda_P+i\omega_1) + a_2\ \Lambda_Q}{(\Lambda_P+i\omega_1)(\Lambda_G+i\omega_1) - \Lambda_F\ \Lambda_Q}$$

$$T_{H_w} = \frac{a_1\Lambda_G + a_4\ \Lambda_F}{\Lambda_X} H_o$$

$$T_{H_f} = \frac{a_4\Lambda_P + a_1\ \Lambda_Q}{\Lambda_X} H_o$$

$$\Lambda_{1_2} = \frac{1}{2}(\Lambda_P+\Lambda_G) \mp \frac{1}{2}\sqrt{(\Lambda_P+\Lambda_G)^2 - 4\Lambda_x}$$

$$K_{1_2} = \frac{-\Lambda_{1_2}+\Lambda_P}{\Lambda_F}$$

$$t_n = 24 \text{ hours} - t_d$$

Table 1 (cont.)$_{p.5}$

$$Q_5 = K_{2d} - Y_2 K_{1n} e^{-\Lambda_{1n} t_n} - Y_5 K_{2n} e^{-\Lambda_{2n} t_n}$$

$$Q_6 = K_{1d} - Y_1 K_{1n} e^{-\Lambda_{1n} t_n} - Y_4 K_{2n} e^{-\Lambda_{2n} t_n}$$

$$B_{1d} = \frac{Q_3 Q_4 + Q_1 Q_5}{Q_2 Q_5 - Q_3 Q_6}$$

$$B_{2d} = \frac{Q_1 - Q_2 B_{1d}}{Q_3}$$

$$B_{1n} = Y_1 B_{1d} + Y_2 B_{2d} + Y_3$$

$$B_{2n} = Y_4 B_{1d} + Y_5 B_{2d} + Y_6$$

$$T_w = \begin{cases} B_{1d} e^{-\Lambda_{1n} t} + B_{2d} e^{-\Lambda_{2d} t} + \chi_{A_{wd}} \Delta T_A e^{i\omega_o t} + \chi_{Sw} S_1 e^{i\omega_1 t} + T_{H_{wd}} & 0 \leqslant t < t_d \\ B_{1n} e^{-\Lambda_{1n}(t-t_d)} + B_{2n} e^{-\Lambda_{2n}(t-t_d)} + \chi_{A_{wn}} \Delta T_A e^{i\omega_o t} + T_{H_{wn}} & t \leqslant t_d < +24 \text{ hours} \end{cases}$$

Table 1a

Definitions: Trombe Wall Case

$$N_w = \frac{\hat{h}_{wc}\,\hat{U}_{CR}\,\hat{U}_{wi}}{\hat{U}_q\,\hat{\Sigma}\,(\hat{U}_{wi}+U_a)} + \frac{\hat{U}_{wo}}{\hat{U}_q}$$

$$N_f = \frac{1}{\hat{U}_q}\,\frac{\hat{h}_f\,\hat{U}_{fi}}{\hat{h}_f + \hat{U}_{fi}}$$

$$N_R = 1 + N_f + \frac{\hat{U}_{wo}}{\hat{U}_q} + \frac{\hat{U}_{CR}}{\hat{\Sigma}\,\hat{U}_q}\left(\hat{h}_{wc} + \hat{U}_{CA} - \frac{\hat{h}_{wc}^2\,\hat{U}_{CR}}{\hat{\Sigma}(\hat{U}_{wi}+\hat{U}_a)}\right)$$

$$N_S = \frac{\alpha_w\,\hat{h}_{wc}\,\hat{U}_{CR}}{\hat{U}_q(\hat{U}_{wi}+\hat{U}_a)\,\hat{\Sigma}} + \frac{\alpha_f\,N_f}{\hat{U}_{fi}} + \frac{\alpha_R}{\hat{U}_q}$$

$$N_A = 1 + \frac{\hat{U}_{CA}\,\hat{U}_{CR}}{\hat{U}_q\,\hat{\Sigma}} + \frac{\hat{h}_{wc}^{\,2}\,\hat{U}_{CA}\,\hat{U}_{CR}}{\hat{\Sigma}^2(\hat{U}_{wi}+\hat{U}_a)}$$

$$\lambda_f = \frac{1}{C_w}\left(\frac{\hat{U}_{fi}\,\hat{h}_f}{\hat{U}_{fi}+\hat{h}_f}\right)$$

$$\lambda_R = \frac{1}{C_w}\left(\hat{U}_{wo} + \frac{\hat{h}_{wo}\,\hat{U}_{CR}\,\hat{U}_{wi}}{\hat{\Sigma}(\hat{U}_{wi}+\hat{U}_a)}\right)$$

$$\Lambda_p = \frac{1}{C_w}\left[\frac{\hat{U}_{wi}\,\hat{U}_a}{\hat{U}_{wi}+\hat{U}_a} + \hat{U}_{wo}\right] - \lambda_R\,\frac{N_w}{N_R}$$

Table 1a (cont.) p.2

$$\Lambda_G = \lambda_f\left(1 - \frac{N_f}{N_R}\right) + \frac{\hat{U}_{fo}}{C_f}$$

$$\Lambda_F = \lambda_R \frac{N_f}{N_R}$$

$$\Lambda_Q = \lambda_f \frac{N_w}{N_R}$$

$$a_1 = \frac{\lambda_R}{N_R \hat{U}_q}$$

$$a_2 = \frac{\alpha_w}{C_w} \frac{\hat{U}_{wi}}{\hat{U}_{wi} + \hat{U}_a} + \lambda_R \frac{N_S}{N_R}$$

$$a_3 = \lambda_R \frac{N_A}{N_R} + \frac{\hat{U}_{wi}\ \hat{h}_{wc}\ \hat{U}_{CA}}{C_w\ \hat{\Sigma}\ (\hat{U}_{wi} + \hat{U}_a)}$$

$$a_4 = \frac{\lambda_f}{N_R \hat{U}_q}$$

$$a_5 = \lambda_f\left(\frac{\alpha_f}{\hat{h}_f} + \frac{N_s}{N_R}\right)$$

$$a_6 = \lambda_f \frac{N_A}{N_R} + \frac{\hat{U}_{fo}}{C_f}$$

Table 2 (cont.) p.2

$$B(\omega) = \alpha_R + h_e \alpha_e R_{1e} + h_p \alpha_p R_{1p} + h_f \alpha_f R_{1f}$$

$$C(\omega) = \hat{U}_q + \hat{h}_e R_{2e} + \hat{h}_f R_{2f}$$

where the subscripts e, p, and f stand for envelope walls, partition walls, and floor

The response functions $R_{1j}$ and $R_{2j}$ are functions of frequency which depend on materials properties. They are:

$$R_{1,e \text{ or } f} = \frac{\cosh kd + \frac{1}{RKk} \sinh kd}{(h + \frac{1}{R}) \cosh kd + (Kk + \frac{h}{RKk}) \sinh kd}$$

$$R_{2,e \text{ or } f} = \frac{\frac{1}{R}}{(h + \frac{1}{R}) \cosh kd + (Kk + \frac{h}{RKk}) \sinh kd}$$

where $k = \sqrt{\frac{i\omega\rho c_p}{K}} = \sqrt{\frac{\omega\rho c_p}{2K}} (1+i)$

$R$ is the thermal resistance of the insulation on the outside of the wall,

$R_{1_p}$ has the same form for $R \to \infty$ ,

$R_{2_p} = 0$ ,

and $\cosh x(1+i) = \cosh x \cos x + i \sinh x \sin x$

$\sinh x(1+i) = \sinh x \cos x + i \cosh x \sin x$

for $x$ real

Table 4

Response Functions for 2" Thick Concrete*

| | continuum model | | lumped model | |
|---|---|---|---|---|
| $\omega$ | $R_1$ | $R_2$ | $R_1$ | $R_2$ |
| 0 | .211 | .684 | .211 | .684 |
| $2\pi$/month | $.211\ e^{-.002i}$ | $.684\ e^{-.004i}$ | $.211\ e^{-.002i}$ | $.684\ e^{-.003i}$ |
| $2\pi$/week | $.211\ e^{-.010i}$ | $.683\ e^{-.017i}$ | $.211\ e^{-.009i}$ | $.683\ e^{-.013i}$ |
| $2\pi$/day | $.210\ e^{-.064i}$ | $.681\ e^{-.119i}$ | $.210\ e^{-.060i}$ | $.681\ e^{-.091i}$ |
| $2\pi$/12 hrs. | $.208\ e^{-.136i}$ | $.672\ e^{-.236i}$ | $.208\ e^{-.119i}$ | $.672\ e^{-.181i}$ |
| $2\pi$/ 8 hrs. | $.204\ e^{-.200i}$ | $.659\ e^{-.351i}$ | $.204\ e^{-.176i}$ | $.659\ e^{-.267i}$ |
| $2\pi$/ 3 hrs. | $.175\ e^{-.456i}$ | $.548\ e^{-.855i}$ | $.175\ e^{-.391i}$ | $.552\ e^{-.631i}$ |

* Assumes ASHRAE properties: $\rho = 144\ \text{lbs/ft}^3$ $C_p = .156\ \frac{\text{Btu}}{\text{lb.-°F}}$

$h = 1.5\ \frac{\text{Btu}}{\text{ft}^2\text{-hr-deg F}}$ $K = .54\ \frac{\text{Btu}}{\text{°F-hr-ft}}$

Table 6

Response Functions for $1^{1/2}$" Thick Concrete

Thin Wall Model*

| | continuum model | | lumped model(thin wall) | |
|---|---|---|---|---|
| $\omega$ | $R_1$ | $R_2$ | $R_1$ | $R_2$ |
| 0 | .538 | .194 | .538 | .194 |
| $2\pi$/month | $.535\ e^{-.052i}$ | $.192\ e^{-.188i}$ | $.536\ e^{-.039i}$ | $.192\ e^{-.122i}$ |
| $2\pi$/week | $.503\ e^{-.198i}$ | $.170\ e^{-.768i}$ | $.505\ e^{-.142i}$ | $.171\ e^{-.483i}$ |
| $2\pi$/day | $.329\ e^{-.428i}$ | $.035\ e^{+3.137i}$ | $.379\ e^{-.116i}$ | $.051\ e^{-1.305i}$ |
| $2\pi$/8 hrs. | $.233\ e^{-.535i}$ | $.003\ e^{+.467i}$ | $.366\ e^{-.043i}$ | $.017\ e^{-1.480i}$ |

*Assumes ASHRAE properties $\rho = 144\ \frac{lbs}{ft^3}$ $C_p = .156\ \frac{Btu}{lb.-°F}$

$K = .54\ \frac{Btu}{°F\text{-}hr\text{-}ft}$ $h = 1.5\ \frac{Btu}{°F\text{-}ft^2\text{-}hr}$

Table 8

RESPONSE FUNCTIONS FOR 1½-FOOT THICK CONCRETE*

| | continental model | | lumped model | (thick wall) |
|---|---|---|---|---|
| $\omega$ | $R_1$ | $R_2$ | $R_1$ | $R_2$ |
| 0 | .538 | .194 | .538 | .194 |
| $2\pi$/month | $.535\ e^{-.052i}$ | $.192\ e^{-.188i}$ | $.537\ e^{-.933i}$ | $.193\ e^{-.062i}$ |
| $2\pi$/week | $.503\ e^{-.198i}$ | $.170\ e^{-.768i}$ | $.524\ e^{-.137i}$ | $.187\ e^{-.259i}$ |
| $2\pi$/2-days | $.392\ e^{-.364i}$ | $.083\ e^{-2.045i}$ | $.429\ e^{-.343i}$ | $.142\ e^{-.748i}$ |
| $2\pi$/day | $.329\ e^{-.428i}$ | $.035\ e^{+3.137i}$ | $.336\ e^{-.367i}$ | $.092\ e^{-1.076i}$ |
| $2\pi$/8 hours | $.233\ e^{-.535i}$ | $.003\ e^{+.467i}$ | $.262\ e^{-.193i}$ | $.034\ e^{-1.343i}$ |

*Assumes ASHRAE materials properties of $\rho = 144\ \frac{\text{lbs}}{\text{ft}^3}$, $C_p = .156\ \frac{\text{Btu}}{\text{lb.-}^\circ\text{F}}$

$$K = .54\ \frac{\text{Btu}}{\text{ft-deg F-hr}} \qquad h = 1.5\ \frac{\text{Btu}}{\text{ft}^2\text{-deg F-hr}}$$

Table 10

VALUES OF THE LUMPED PARAMETERS, CONCRETE*

| d | $U_i$ (Btu/°F-hr-ft$^2$) | | $U_o$ (Btu/°F-hr-ft$^2$) | | C (Btu/°F-ft$^2$) | |
|---|---|---|---|---|---|---|
| | thin wall model | thick wall model | thin | thick | thin | thick |
| $\frac{1}{2}$ inch | 51.8 | | 17.3 | | .51 | |
| 1 inch | 25.6 | | 8.68 | | 1.00 | |
| 2 inch | 12.62 | | 4.36 | | 1.99 | |
| 3 inch | 8.30 | | 2.92 | | 2.96 | |
| 8 inch | 2.97 | 2.52 | 1.114 | 1.194 | 7.65 | 9.64 |
| $10^{\frac{1}{4}}$ inch | 2.28 | 2.52 | .875 | .844 | 9.70 | 9.64 |
| 1 foot | 1.93 | 2.52 | .750 | .687 | 11.28 | 9.64 |
| 1½ foot | 1.245 | 2.52 | .506 | .420 | 16.61 | 9.64 |
| 3 foot | | 2.52 | | .194 | | 9.64 |
| ∞ | | 2.52 | | 0 | | 9.64 |

*Assumes ASHRAE materials properties $\rho = 144 \frac{\text{lbs}}{\text{ft}^3}$, $C_p = .156 \frac{\text{Btu}}{\text{°F-lb.}}$

$K = .54 \frac{\text{Btu}}{\text{°F-ft-hr}}$ $h = 1.5 \frac{\text{Btu}}{\text{°F-ft}^2\text{-hr}}$

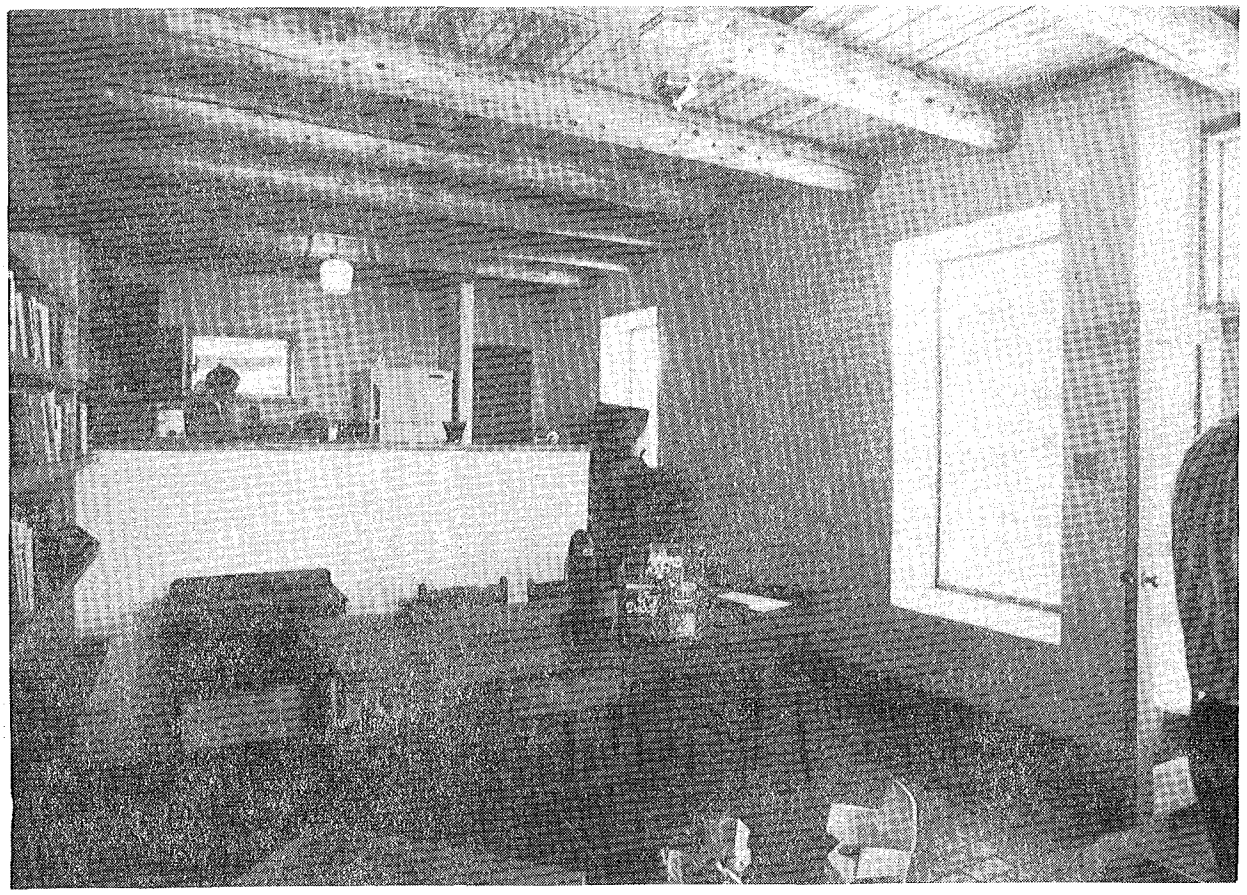

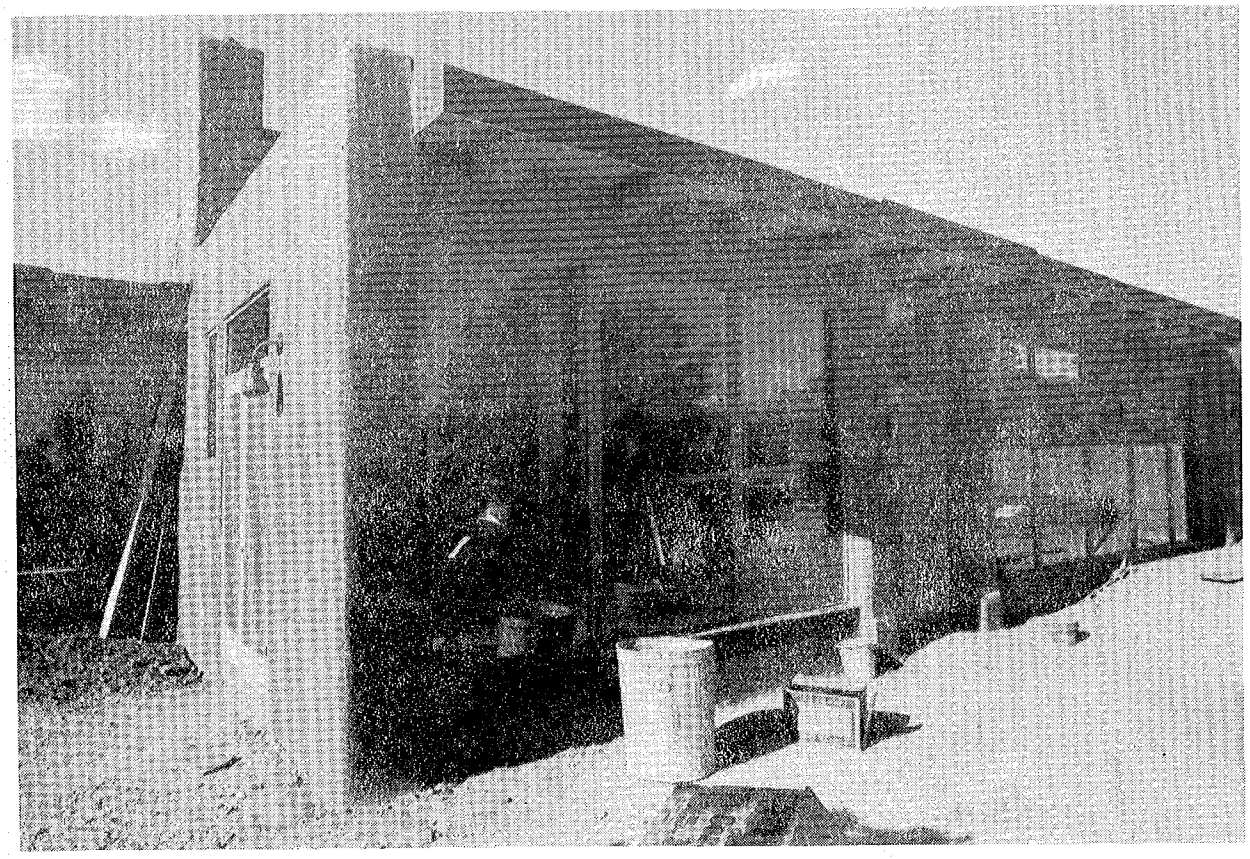

Fig. 1. Interior and exterior photographs of a passive solar house at First Village in Santa Fe, New Mexico. Some of the windows seen in the exterior view provide direct solar gain to the inside, where the sunlight falls on the brick floor. Other windows illuminate Trombe walls of 1½ foot concrete. (Photos by the author.)

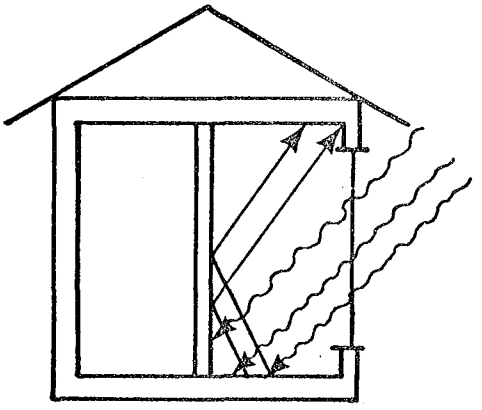

XBL 787-1267

Fig. 3. Sketch of the path of solar energy as it is absorbed and reflected from surfaces in a direct gain building. Actual reflections are likely to be diffuse rather than specular.

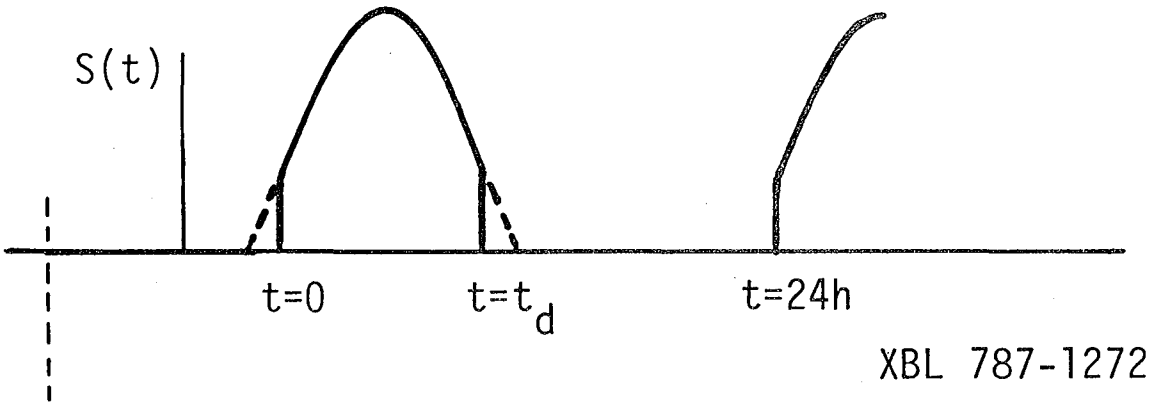


Fig. 5. Assumed form of the solar gain through a south window as a function of time. The same function repeats every day. In this sketch the function jumps discontinuously from zero to a finite value at $t = 0$ and jumps back at $t = t_d$. In most cases the curve begins and ends smoothly at zero at these times.

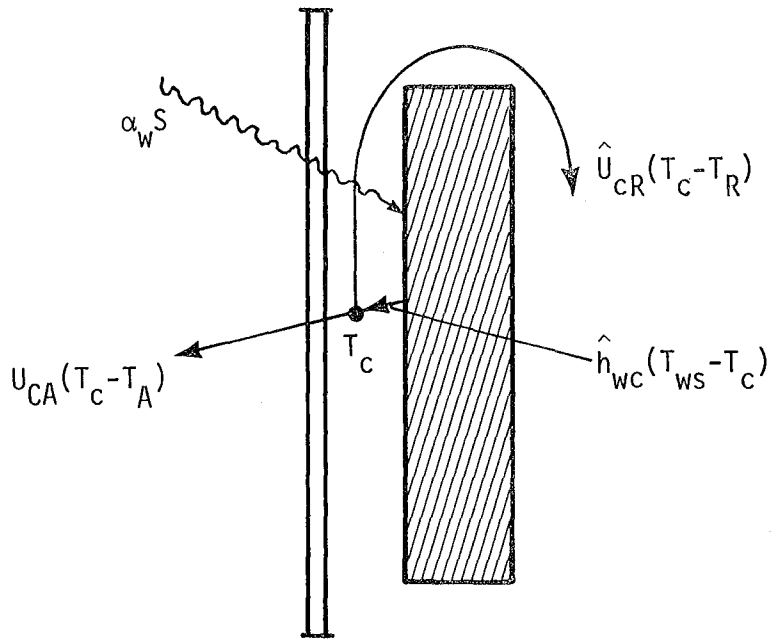


Fig. 7. Heat transfers for the Trombe wall model. Sunlight enters through the window at left and is absorbed on the left-hand surface of the Trombe wall. This wall surface is in thermal contact with the channel air which is at a temperature of $T_c$. The channel can lose heat to the outside air at left or to the room at at right.

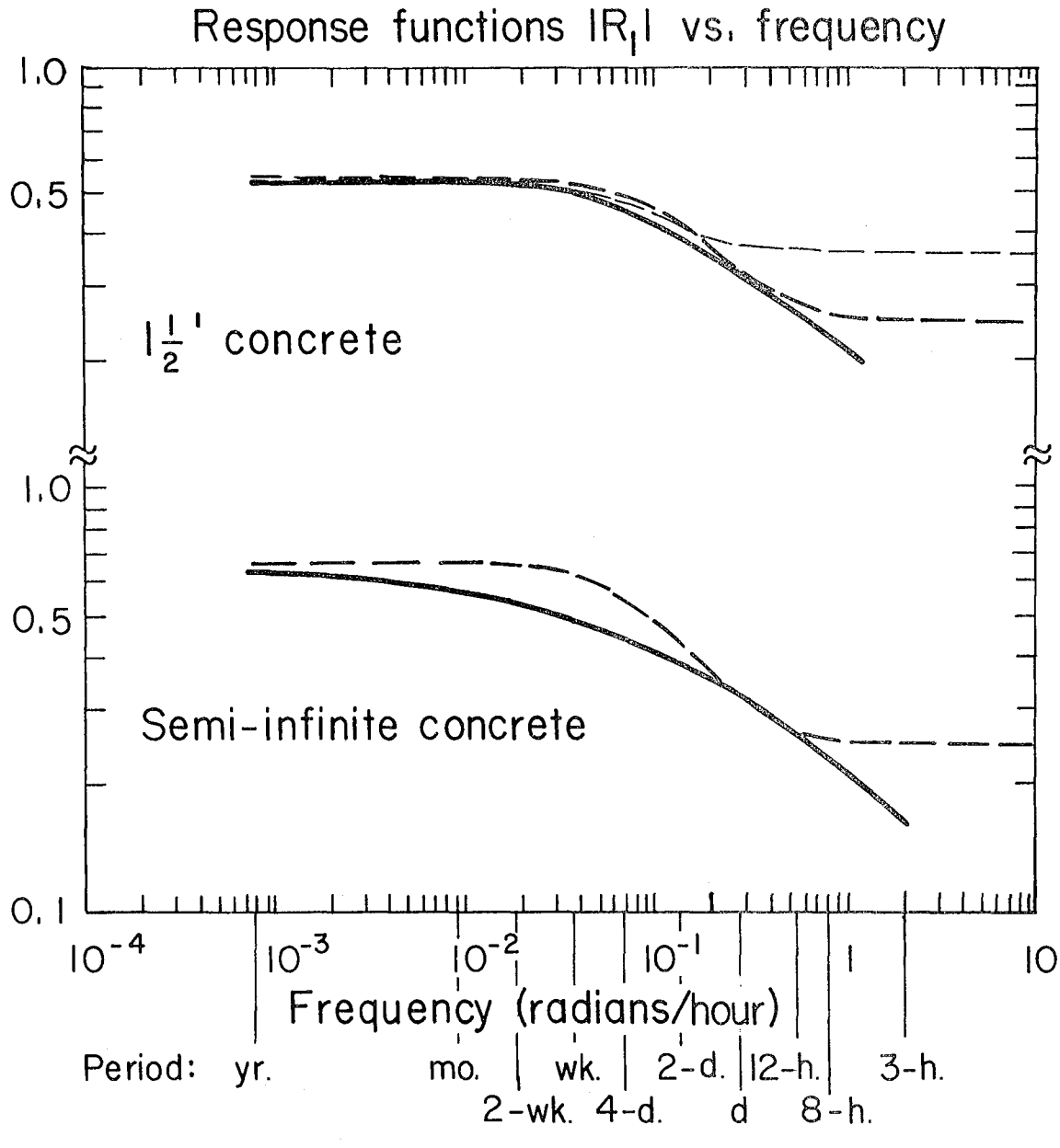


XBL 786-1103A

Fig. 9. Response functions as a function of frequency. This figure plots $\log|R_1|$ vs. $\log \omega$ for 1½ foot thick and semi-infinite concrete. The solid lines represent the continuum response functions; the heavy dashed lines describe the thick-wall lumped model response functions; and the light dashed lines represent thin-wall functions.

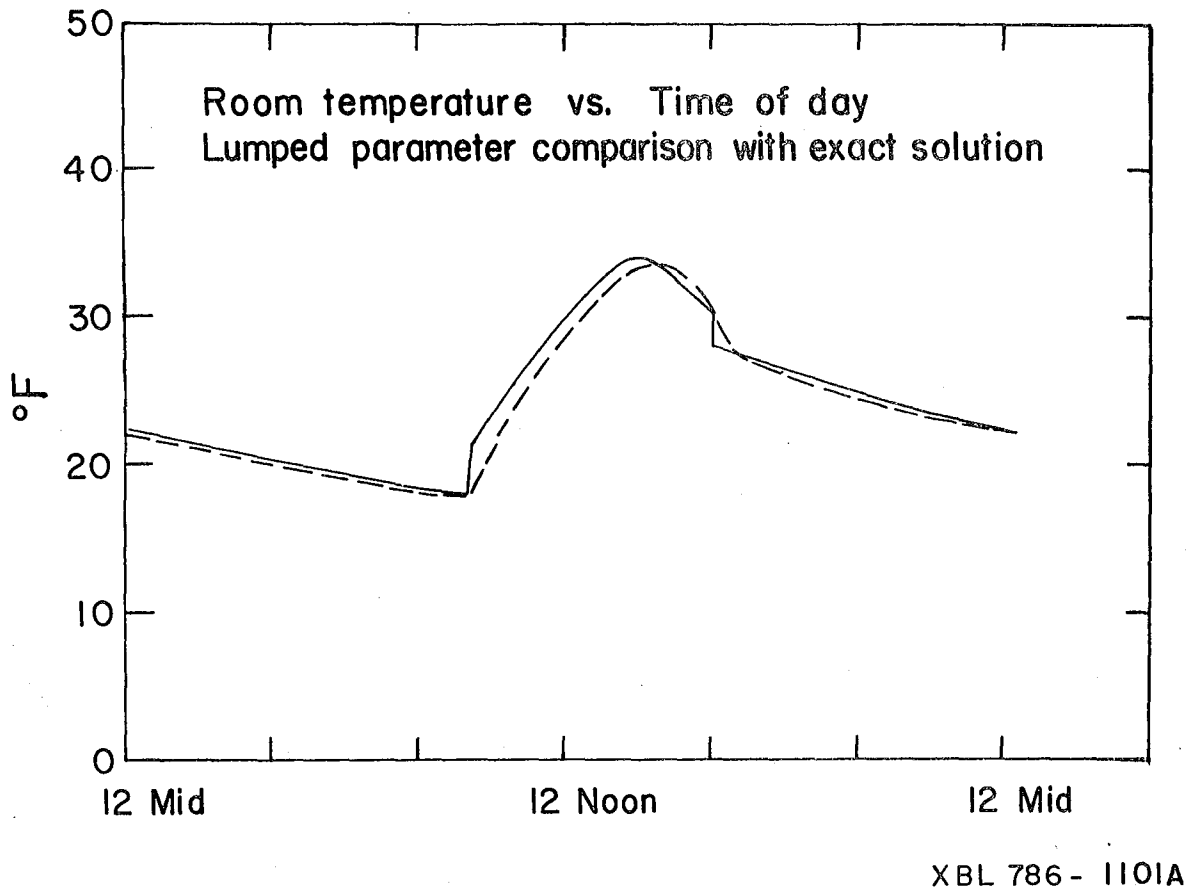


Fig. 11. Room temperature elevation vs. time for comparing the lumped parameter approximation to an exact solution. The exact solution for room temperature of the building described in Appendix 2.5B is graphed as a dotted line; the lumped parameter approximation is plotted as a solid line.

non-circulating Trombe wall — a thick concrete wall which is located directly behind the window. The air channel between the wall and the window is sealed to prevent air exchange between the channel and the room; thus the path for solar heat gain into the house requires absorption on the front surface of the Trombe wall and diffusion through the wall into the room.

Accurate modelling of the test buildings requires knowledge of the materials properties of the concrete. This is not a trivial look-up exercise, since the conductivity and heat capacity of concrete can vary over a factor of two range even at fixed density.[1] Los Alamos staff measured the conductivity; their estimate appears to be consistent with the data to high accuracy. However, the heat capacity was not measured, and handbook values appear to give inaccurate results.

We therefore begin our discussion of data analysis with a derivation of the heat capacity of Los Alamos concrete from data obtained using thermocouples buried inside the concrete. We conclude that the heat capacity per unit volume is 18 Btu/°F-ft$^3$ to within about 7%. This determination is described in Sec. 3.2.

We next discuss modelling the direct gain test cell in Sec. 3.3. We first describe the cell, and then evaluate model parameters. Using these parameters, and a design day chosen for time-independent weather patterns, we compare room temperature measurements with predictions of

(~ 150 $m^2$ in floor area) can be adequately described by single-zone models. However, the application of our model to the small buildings described here should provide some insight into what temperatures should be measured to make that comparison efficiently.

If we know the temperature $T(\omega)$ for the front and back surfaces of the material, we can determine A and B from (2) evaluated at $\xi = 0$ and $\xi = 1$, respectively. If we then know $T(\omega)$ for some intermediate value of $\xi$, we can determine k such that the prediction from (2) most closely agrees with the measurement. Knowing k gives us the heat capacity $\rho c_p$ provided that K, the conductivity, is known.

In fact, K was measured at Los Alamos, it is equal to .80 Btu/°F-hr-ft, which is consistent with our model. Thus we will use the interior temperature data from the LASL concrete walls to find $\rho c_p$ as described.

We perform the experiments using the component of temperature at frequency $\omega_o = 2\pi / 24$ hours since there is a large signal at that frequency. The Fourier-transformed temperature for a cycle of length P is given by

$$T(\omega) = \frac{2}{P} \int_{t=o}^{t=P} T(t)\ e^{-i\omega t}\ dt \qquad (3)$$

Our data is available only at hourly intervals, so we use the approximation

$$T(\omega_o) \cong \frac{2}{P} \sum_{n=0}^{P-1\,hr} T(t)\ e^{-i\omega_o t} \qquad (4)$$

We describe four experiments, one using the Trombe cell data for 24 February 1978, which was chosen for having time-independent weather patterns; the second uses the direct gain cell for the same date; the third uses the Trombe cell data for 8 March 1978; and the

These are apparently pretty close; we shall measure closeness of fit by calculating the squared fractional error for each temperature and adding. We find that $\Delta_{43}^2 = 0.0191$; $\Delta_{44}^2 = 0.0027$, so $\Delta^2 = 0.0217$

For $\rho c_p = 18$ Btu/ft$^3$-°F, we calculate

$$T_{43} = 9.325e^{-5.2491i}$$
$$T_{44} = 6.24e^{-5.8512i}$$

The errors are: $\Delta_{43}^2 = 0.00319$; $\Delta_{44}^2 = 0.00145$, so $\Delta^2 = 0.00464$, considerably smaller than for $\rho c_p = 20$.

For $\rho c_p = 17$ Btu/ft$^3$-°F,

$$T_{43} = 9.60e^{-5.2072i}$$
$$T_{44} = 6.28e^{-5.8276i}$$

The errors are: $\Delta_{43}^2 = 0.00187$; $\Delta_{44}^2 = 0.00288$ so $\Delta^2 = 0.00475$. We see that reducing $\rho c_p$ from 18 to 17 improves the fit for $T_{43}$ but worsens it for $T_{44}$; the total squared error is slightly larger for $\rho c_p = 17$.

As a check on this experiment, if we really have a day with no long-term weather trends, the average temperatures (that is, the Fourier coefficient for $\omega = 0$) should be along a straight line. We calculate the steady state terms $\overline{T}$ ; they are

$$\overline{T}_{41} = 108.33$$
$$\overline{T}_{43} = 96.48$$
$$\overline{T}_{44} = 89.17$$
$$\overline{T}_{45} = 86.94$$

Using the average temperature data, we find that the depth of the Channel 53 thermocouple is 2.20 inches into the $5^{5/8}$-inch-thick concrete, so $\xi = 0.3913$ for this measurement.

We next use $T_{54}$ and $T_{52}$ and our guesses for $\rho c_p$ to determine A and B from (2) and use (2) to predict $T_{53}$.

We first check $\rho c_p = 28$ Btu/°F-ft$^3$. We find that the prediction for $T_{53}$ is $T_{53} = 21.165e^{+i1.6445}$. This is off in both magnitude and phase; the fractional error squared is $7.55 \times 10^{-3}$.

Our next guess for $\rho c_p$ is 18 Btu/°F-ft$^3$. Then our prediction is $T_{53} = 21.480e^{+i1.727}$. The fractional squared error is $3.49 \times 10^{-5}$; considerably smaller than the previous estimate.

We next try $\rho c_p = 17.5$ Btu/°F-ft$^3$ based on the results of the previous experiment. We find that

$$T_{53} = 21.494e^{+i1.7312}$$

The error-squared $\Delta^2 = 2.14 \times 10^{-5}$, slightly smaller than the previous case.

For $\rho c_p = 17$ Btu/°F-ft$^3$, $T_{53} = 21.506e^{+i1.7354}$ and $\Delta^2 = 4.39 \times 10^{-5}$

(We also note that if we had assumed $\xi = 1/2$ or the interior thermocouple located in the exact center of the concrete, the fits would not be very good until $\rho c_p \sim 12$ Btu/ft$^3$-°F, which is implausibly small.)

From this test, we conclude that $\rho c_p$ is between 17.5 and 18 Btu/°F-ft$^3$; and much closer to 17.5. This agrees with the previous result.

For $\rho c_p = 18$

$$T_{43} = 9.414e^{i0.9820}$$

$$T_{44} = 6.601e^{i0.5882}$$

Here $\Delta_{43}^2 = 0.062$ and $\Delta_{44}^2 = 0.021$ so $\Delta^2 = 0.083$

For $\rho c_p = 16$

Then $$T_{43} = 9.970\ e^{i1.0689}$$

$$T_{44} = 6.733e^{i0.6387}$$

$\Delta_{43}^2 = 0.0271$ and $\Delta_{44}^2 = 0.0128$ so $\Delta^2 = 0.0399$. Since $\Delta^2$ is still decreasing, we check $\rho c_p = 15$.

Then $$T_{43} = 10.257e^{i1.1150}$$

$$T_{44} = 6.792e^{i0.6658}$$

$\Delta_{43}^2 = 0.0157$; $\Delta_{44}^2 = 0.0105$ so $\Delta^2 = 0.0257$.

We next try $\rho c_p = 14$ :

$$T_{43} = 10.547e^{i1.1628}$$

$$T_{44} = 6.845e^{i0.6943}$$

$\Delta_{43}^2 = 0.00946$; $\Delta_{44}^2 = 0.00969$; $\Delta^2 = 0.01915$

For $\rho c_p = 13$

$$T_{43} = 10.841e^{i1.2126}$$

$$T_{44} = 6.891e^{i0.7241}$$

$\Delta_{43}^2 = 0.00941$; $\Delta_{44}^2 = 0.01055$ so $\Delta^2 = 0.01996$

both times, but for March 8, they are 8 or 9° F higher at the end of the day than at the beginning.

Trombe Cell Data, 9-day period

We attempt to correct for the errors in the previous experiment caused by long-term weather variations in two ways. First, we use a longer test period P, and second, we end the period such that the final period temperatures are lower than the initial temperatures, in contrast to the previous cases.

This will produce a higher estimate for $\rho c_p$. This high estimate allows the estimation of upper and lower bounds for $\rho c_p$: the estimate for 24 February when temperatures were slowly rising provides a lower bound and the one for this period will provide an upper bound.

We find that

$$T_{41} = 19.767e^{i2.31954}$$
$$T_{43} = 6.0351e^{i0.98950}$$
$$T_{44} = 4.3015e^{i0.25921}$$
$$T_{41} = 3.9946e^{i0.26404}$$

We check $\rho c_p = 28$ to confirm that it gives unrealistic results in this case; we then try $\rho c_p = 18,19$, and 20.

For $\rho c_p = 18$ Btu/°F-ft$^3$

$$T_{43} = 6.227e^{i1.0643}$$
$$T_{44} = 4.224e^{i0.2828}$$

$\Delta_{41}^2 = 0.0067$; $\Delta_{44}^2 = 0.00087$; $\Delta^2 = 0.00766$.

changes in weather would affect the response of these two walls in different ways. The fact that both produce nearly identical estimates of $\rho c_p$ (to 1%) suggests that their value is close to the truth.

Thus we conclude that heat capacity per unit volume of the Los Alamos concrete is 18 ± 1 Btu/°F-ft$^2$ with the error most likely occurring on the high side, and use this value in subsequent calculations. We note that 5-10% errors in $\rho c_p$ will introduce imperceptibly small errors into the predictions that follow; however, larger errors (~ 50%) will produce noticeable disagreements.

sunlight on a winter day near the solstice . Thus all the direct sunlight hits the concrete at all times.

There are only four channels for heat loss from the room air: infiltration, loss through the glass (collector), heat transfer to the styrofoam envelope wall surfaces, and heat transfer to the concrete. The first three channels are all relatively fast heat transfers, so we lump their effects into $\hat{U}_q$. We treat the concrete as being the only heavy material, since the properties of the blocks lining the walls are identical to those of the concrete on the floor. (The film coefficients may be slightly different, but the results are not very sensitive to the exact value of h chosen, as shown later in this section.)

Evaluation of Building Parameter

We next use the materials properties of the elements used in construction of the cell along with the measurements in Fig. 2 to derive building parameters for the lumped parameter and for the distributed parameter models.

We first evaluate the parameters for the concrete. We consider as concrete surface area only those areas which face the inside of the cell; that is, we ignore the small areas of concrete which are parallel to the glazing and only two inches behind it. Thus the surface areas of concrete are:

| | | |
|---|---|---|
| side walls: | $2 \text{ walls} \times \{8.92' \times 3.92' + 1.30' \times 4.49'\}$ | $= 80.60 \text{ ft}^2$ |
| back walls: | $4.50' \times 5.25'$ | $= 22.57 \text{ ft}^2$ |
| floor : | $4.30' \times 6.88'$ | $= 29.58 \text{ ft}^2$ |
| Total concrete surface area | | $133.75 \text{ ft}^2$ |

floor to the top of the glass less the $2^{7/8}$" of horizontal wood framing in the window: 8.885 ft. Thus the effective collector area is 38.2 $ft^2$.

We calculate the rest of $\hat{U}_q$ by adding infiltration losses to conduction losses through the styrofoam. Infiltration losses are calculated by assuming 1/4 air change per hour, and multiplying by the volume times the heat capacity of air at Los Alamos elevation: 0.014 Btu/°F-$ft^3$. We use 1/4 air change as a guess based on the LASL scientists' feeling that the house was "very tight" and a comparison with a very tight Princeton retrofit townhouse (see Ref. 25 ) which had 1/4 air change per hour in ~ 5 mph winds. The approximate volume is equal to the volume of a parallelopiped whose sides correspond to the surfaces of concrete, plus a set of irregular volumes one concrete block in thickness where no concrete is present:
Volume $\cong$ 9.67' × 4.30' × 7.04' + 2 × [(9.67' × 7.04' - 40.80 $ft^2$) × .469 ft] + [(5.25' × 9.67' - 22.57 $ft^2$) × 4.69 ft] $\cong$ 331.5 $ft^3$; thus the heat transfer coefficient is 1.16 Btu/degF-hr.

Finally, the heat losses for the styrofoam are equal to the area of styrofoam times the U-value of 1/16. (The resistance is 15 for the styrofoam-plus-wood-frame and 1 for the film coefficient). The area of styrofoam includes only one side wall (since the other is a party wall with the adjoining cell). It is:

| | | | |
|---|---|---|---|
| ceiling | 5.25' × 7.56' | = | 39.69 $ft^2$ |
| side wall | (9.67' × 7.04' - 40.80 $ft^2$) | | |
| | + (9.67' - 4.50') × 0.469 $ft^2$ | = | 29.70 $ft^2$ |
| back wall | 5.25' × 9.67' - 22.57 $ft^2$ | = | 28.20 $ft^2$ |
| Total styrofoam area is | | | 97.59 $ft^2$ |

re-reflected out the window. This 5% loss is consistent with the fluxes calculated in determining the $\alpha$'s. So the net transmissivity of the collector is 70%. Since the transmission was not measured, this estimate could be in error by 5-10%.

3.3.2 Weather Parameterization

As input to the models, we need weather which has sinusoidal form. We will fit ambient temperature to the form $T_A(t) = \bar{T}_A + \Delta T_A e^{i\omega_o t}$ or else to the form $T_A(t) = \bar{T}_A + \Delta T_A e^{i\omega_o t} + \Delta T_{A_w} e^{i\omega_w t}$. The first form can be calculated using Eq. (4) for each day; the results for $\bar{T}_A$ and $\Delta T_A$ are given for each day in Table 1. The term $\Delta T_{A_w}$ can be found by guessing at $\omega_w$ and then using (4) on the daily estimates of $\bar{T}_A$ to find $\Delta T_{A_w}$. This process of fitting a sinusoidal model to the observed data is illustrated in Fig. 3.

Solar gain is also assumed to be sinusoidal: $S(t) = \begin{cases} S_1 e^{i\omega_1 t} & \text{day} \\ 0 & \text{night} \end{cases}$

We have as input data LASL measurements of solar flux incident on a south-facing vertical plane; the measurements were taken each hour. We first add all the solar gain values for the whole day; this gives an estimate of daily solar gain. These values are listed in Table 1 and graphed in Fig. 3.

We use this data to pick test days. We first look for a day with little change in weather patterns from previous days. From Table 1, the best choice is apparently February 24. We see this more clearly from Fig. 4, which graphs solar gain as a function of time for several days around the 24th of February. As seen in the figure, there have

The daily solar gain totals are shown in Table 1. If we normalize the solar gains to their value for 78/02/24 and Fourier-analyze the data for 78/02/21-78/03/06 using Eq. (4) with $\omega_w = 2\pi/14$ days, we find that $S(t) = (.6403 + .3566\, e^{i\omega_1(t-2.82 \text{ days})})\, |S_1|$ where t is measured in days, with t = 0 at noon on the 21st of February and where all solar gain values are assumed to take place at noon on their respective days. Extending this expression to the 7th and 8th of March, we get excellent agreement as shown in Fig. 3, especially for the last few days. For the test of March 8, the (non-normalized) expression for solar gain leads to an estimate of 1702 Btu/day, compared with the observed value of 1753, or a 3% error.

To find $\Delta T_{A_w}$, we find best agreement for $\omega_w' = 2\pi/10$ days; applying Eq. (4) to the data for $\bar{T}_A$ for 78/02/27 to 78/03/08 we derive $T_A(t) = 37.5\ ^\circ\text{F} + 4e^{i\omega_w'(t-5.5 \text{ days})}$ where t = 0 at noon on February 21, 1978. The predicted temperature for March 8 is thus 41.3 °F compared to the 41.2°F observed. The overall agreement, shown in Fig. 3, is not as good as for S(t), but is reasonably close. The predictions for $T_R$ will not depend very sensitively on the precise modelling of long-term fluctuation in $T_A$. (Note that there is no reason to want the same value of $\omega_w$ for the ambient temperature term as for the solar gain term).

We take $\omega_1$ to be time-independent because seasonal changes in sunrise and sunset are not very large over the 3-week span of data. Thus we always take sunrise to be 7 a.m., sunset to be 6.52 p.m. and $\omega_1$ to be 0.273 radians/hr.

This completes our parameterization of weather; these results will be used below and also in the Trombe wall modelling discussion.

$$\Lambda_p = .0312 \text{ hr}^{-1}$$

$$a_2 = 8.513 \times 10^{-4} \text{ °F/(Btu/hr)}$$

$$a_3 = \Lambda_p$$

$$N_c = 3.316$$

$$N_R = 4.316$$

$$N_s = .01103 \quad \text{°F-hr/Btu}$$

We calculate $T_w$ using the solutions to (7) and the boundary conditions $T_w(0^+) = T_w(24 \text{ hrs}^-); T_w(t_d^+) = T_w(t_d^-)$; the result is (measured with respect to the average temperature of 37 °F)

$$T_w = \begin{cases} 66.82\, e^{-.0312t} + 1.89\, e^{i\omega_o(t-13.55)} + 21.13\, e^{i\omega_1(t-11.10)} & \text{day} \\ 67.63\, e^{-.0312(t-t_d)} + 1.89\, e^{i\omega_o(t-13.55)} & \text{night} \end{cases}$$

Then by (6), we can derive $T_R$:

$$T_R = \begin{cases} 51.34\, e^{-.0312t} + 4.14\, e^{i\omega_o(t-9.36)} + 25.13\, e^{i\omega_1(t-8.316)} & \text{day} \\ 51.96\, e^{-.0312(t-t_d)} + 4.14\, e^{i\omega_o(t-9.36)} & \text{night} \end{cases}$$

This gives temperature elevation $(T_R - T_A)$ for 78/02/24; the result is plotted in Fig. 5 for comparison with the data. Room temperature is the label for the y-axis, although the zero of temperature is taken as $\overline{T}_A$ to allow the reader to see relative error.

The LASL measurement of room temperature was performed by enclosing a thermocouple inside a plastic sphere, so their room temperature is really some average of room temperature and mean radiant

$$T_{s_{styro}} = T_R + \frac{\bar{\alpha}_R S}{h} \quad \text{or since } h = 1 \text{ Btu/ft}^2\text{-degF-hr},$$

$$T_{s_{styro}} = T_R + \bar{\alpha}_R S$$

Finally, the glass temperature is determined by looking at the glazing as consisting of two resistances in series - the outside resistance from the surface and the inside resistance. The inside resistance, accounting for radiant heat transfers to the other walls as well as convection to the air, should look like $R_{in} \cong 1/h \cong 1/(1.5$ Btu/hr- F-ft$^2$). The inside and outside resistances add to the inverse of the U-value, or 1/0.55. Then the glass surface temperature is given by

$$T_{gs} = \frac{R_{total}-R_{in}}{R_{total}} (T_R - T_A) + T_A \cong 0.633 (T_R - T_A) + T_A$$

$$= 0.633\, T_R + 0.367\, T_A$$

We can now evaluate mean radiant temperature as follows.

$$MRT = \frac{1}{A_{styro} + A_c + A_{gl}} (A_{styro}\, T_{s_{styro}} + A_c\, T_{cs} + A_{gl}\, T_{gs})$$

where the A's represent areas.

Using the previous numerical results, we find that

$$MRT = 0.509\, T_R + 0.436\, T_{cs} + 0.055\, \Delta T_A + 4.447\, e^{i\omega_1 (t-5.763)},$$

or

$$MRT = \begin{cases} 53.94\, e^{-.0312t} + 3.60\, e^{i\omega_o (t-9.65)} + 26.40\, e^{i\omega_1 (t-8.31)} & \text{day} \\ 54.59\, e^{-.0312(t-t_d)} + 3.60\, e^{i\omega_o (t-9.65)} & \text{night} \end{cases}$$

because the response to ambient temperature fluctuations is relatively small.

To see the sensitivity to correct evaluation of the $\alpha$'s, we try another set of assumptions. One reasonable assumption is that even more of the light is absorbed on the concrete, since shaded concrete subtends most of the solid angle seen by the illuminated concrete. Suppose we set $\alpha_c = 0.9$ and $\alpha_R = 0.1$. Then we can calculate $T_R$ as we did before; the result is

$$\begin{cases} 52.39\, e^{-.0312t} + 4.14\, e^{i\omega_o(t-9.36)} + 22.54\, e^{i\omega_1(t-8.76)} & \text{day} \\ 53.02\, e^{-.0312(t-t_d)} + 4.14\, e^{i\omega_o(t-9.36)} & \text{night} \end{cases}$$

Neither this result nor the calculation for mean radiant temperature differs by more than a degree or two from the previous calculation; so we conclude that the result is insensitive to small errors in determining the $\alpha$'s.

We will later check the sensitivity to errors in $h_c$. We assume for this test that $h_c = 1.5$ Btu/ft$^2$-deg F-hr instead of 1; the former being the usual combined film coefficient. This test also shows small sensitivity to the change. The calculation is performed later in conjunction with the distributed parameter model.

### 3.3.4 Distributed Parameter Model

For the distributed parameter (continuum) model, the calculations are relatively straightforward applications of the results of section 2.4. Since the concrete walls are within the domain of the thin-wall

$$T_R(t) = 48.98 + 15.60\, e^{i\omega_o(t-8.9\ \text{hrs})} + 4.188\, e^{2i\omega_o(t-6.793\ \text{hrs})} +$$

$$0.266\, e^{3i\omega_o(t+1.68\ \text{hrs})} + 0.694\, e^{4i\omega_o(t-3.137\ \text{hrs})}$$

The first term is referred to ambient average temperature (37° F) for 78/02/24; so the Fahrenheit temperature would be 37° higher. This result is graphed in Fig. 5; it is seen to be almost identical to the lumped parameter result, but with slightly better agreement with the data during the early morning hours.

We next repeat the calculation for $h_c$ = 1.5 Btu/ft$^2$-deg F-hr to check the sensitivity to $h_c$. We find that

$$T_R = 49.55 + 14.88\, e^{i\omega_o(t-9.23\ \text{hrs})} + 3.96\, e^{2i\omega_o(t-6.96\ \text{hrs})} + \ldots.$$

We truncate after two terms because it is evident that there will be very little change in the results. The insensitivity to $h_c$ probably is due to two competing effects cancelling. As h is increased, more of the heat absorbed on the concrete surface is conducted directly into the room, tending to increase diurnal fluctuations in temperature. But in addition, the (unheated) room is then more tightly coupled to the concrete walls, which damps fluctuations. Over this particular range of $h_c$ , these effects cancel.

### 3.3.5 Varying Weather Experiment, 8 March 1978, Direct Gain Cell

We apply the results of our model to predict the response of the test cell on March 8, a day for which the previous two weeks of weather can be accurately modelled as a sinusoidal fluctuation added to a constant term, as shown in Fig. 3. This situation can most

$$T_R(t) = \bar{S}\,\frac{B(0)}{A(0)}\,d_o + \Delta S_w\,\frac{B(\omega_w)}{A(\omega_w)}\,d_o\,e^{i\omega_w t} + \left(\bar{S} + \Delta S_w\,e^{i\omega_w t}\right)\left(\sum_{n=1}^{4}\frac{B(n\omega_o)}{A(n\omega_o)}\,d_n\,e^{in\omega_o t}\right) \tag{8}$$

$$+\ \bar{T}_A + \Delta T_{A_w}\,\frac{C(\omega_w')}{A(\omega_w')}\,e^{i\omega_w t} + \Delta T_A\,e^{i\omega_o t}$$

The first term is just .6403 times the old steady-state term of 48.98°F. For the second term, $\Delta S_w\,d_o$ is just .3566 times the old steady-state solar heat gain. The sum in the third term is the same sum as in the daily solution, but multiplied by a time-varying factor. This factor, evaluated at noon on March 8, when t = 15 days, is equal to .8844. The rest of the terms are relatively straightforward to understand.

Numerically (8) is equivalent to:

$$T_R(t) = 30.88 + 14.90\,e^{i\omega_w(t-3.92\text{ days})} + \Big(10.35\,e^{i\omega_o(t-8.72\text{ hrs})} + 3.70\,e^{2i\omega_o(t-6.793\text{ hrs})} + .24\,e^{3i\omega_o(t+1.68\text{ hrs})} + .61\,e^{4i\omega_o(t-3.14\text{ hrs})}\Big) + 37.5 + 3.08\,e^{i\omega_w'(t-6.33\text{ days})} + 3.336\,e^{i\omega_o(t-9.65\text{ hrs})} \tag{9}$$

Equation (9) follows the form of (8) term-for-term. A more compact version of (9) would combine the two terms at frequency $\omega_o$ into one term. It would also evaluate the terms at frequencies $\omega_w$ and $\omega_w'$ numerically. Note that such an evaluation is not constant over the

long-term weather fluctuations. This response is fairly large: the test cell has a long time-constant and stores significant heat over two-week cycles. The model is apparently tracking the dynamic response to both daily and multi-week cycles. Response to long-term weather variations is an important feature of good passive solar performance; if a building can store heat from a week or more before a severely cloudy spell, it has a better chance of going through a design cold day without requiring artifical heat input.

### 3.3.6 2-1/2-week Historic Weather Experiment

In this experiment we attempt to solve for the lumped parameter model's response to historic weather. By historic weather, we mean the observed random day-to-day fluctuations in weather conditions as opposed to "typical" weather conditions. Historic weather is not periodic and so the Fourier transformation of the continuum model won't work; so we are limited to the lumped parameter model.

We treat this modelling exercise as an initial conditions problem. That is, we begin with the solution for 24 February 1978. We then solve the equations for the pre-dawn period of 25 February, using the weather conditions for that date (shown in Table 1) and using the initial condition that $T_c$, the concrete mass temperature, does not change discontinuously. We then proceed with solutions for each period of each successive day (pre-dawn, daylight, past-sunset), matching the initial value of $T_c$ to the previous period's final value of $T_c$.

To simplify the algebra, we assume that ambient temperature can be modelled as an average temperature $\overline{T}_A$ plus a sinusoidal term

see in Fig. 7 that the model recovers from errors (perhaps caused by missing data) and tracks the measurements as well on the 18th day as on the eighth day. This stability is reassuring, particularly in light of the large amount of long-term heat storage demonstrated in Fig. 6.

This exercise demonstrates the flexibility of the lumped parameter model in describing conditions which would be impossible to model using the distributed parameter model. The two models are complementary in many ways; one may be more useful than another in solving any particular problem (or they may both work or both fail).

The response of the Trombe cell is governed by Eq. (A2.4-39). Ordinarily, we would model the cell as consisting of one heavy element - the Trombe wall - and would lump the effects of the envelope walls into $\hat{U}_q$, the quick heat transfer coefficient. But for the LASL Trombe cell, the envelope walls are the only significant channel for heat loss from the cell, so we must model them as massive envelope walls and calculate response functions for them. The form of (A2.4-39) which we use in this section can therefore be written as:

$$T_R \left\{ \hat{U}_q + \hat{h}_e \ (1 - h_e R_{1e}) + \hat{U}_{cR} \left( 1 - \frac{1}{\Sigma} \left( U_{cR} + h_{Tc} \left[ R_{2T} + \frac{U_{cR} h_{Tc}}{\Sigma} \ R_{1T} \right] \right) \right) \right.$$

$$\left. + \ \hat{U}_{TR} \left( 1 - U_{TR} \left( R'_{1T} + \frac{1}{U_{TR}^2} \ \frac{U_{cR} h_{Tc}}{\Sigma} \ R_{2T} \right) \right) \right\}$$

$$= S \left( \alpha_T \left( \frac{U_{cR} h_{Tc}}{\Sigma} \ R_{1T} + R_{2T} \right) \right) \qquad (10)$$

$$+ \ T_A \left( \hat{U}_q + \hat{h}_e \ R_{2e} + \frac{\hat{U}_{cR} \ \hat{U}_{cA}}{\hat{\Sigma}} + \frac{\hat{h}_{Tc} \hat{U}_{cA}}{\hat{\Sigma}} \left( R_{2T} + \frac{U_{cR} h_{Tc}}{\Sigma} \ R_{1T} \right) \right)$$

where the subscript 'T' refers to Trombe wall, and where the parameters for the Trombe wall are defined in Fig. 2.7 and in Appendix 2.3.

We evaluate the parameters needed for Eq. (10) next. To begin with, $\hat{U}_q$ consists only of infiltration losses. The volume of the cell consists of the volume of the main room (5.25' × 5.75' × 10.08' according to the author's measurements as displayed in Fig. 8) plus the volume of the small area over the Trombe wall (5.25' × 0.58' × 1.63')

| | | | |
|---|---|---|---|
| floor: | 5.75' × 5.25' | = | 30.19 $ft^2$ |
| side wall: | 5.75' × 10.08' | = | 57.96 $ft^2$ |
| ceiling: | 7.39' × 5.25' | = | 38.77 $ft^2$ |
| back wall: | 5.25' × 10.08' | = | 52.92 $ft^2$ |
| walls above air channel: | (1.63' + 5.25') × 0.58' | = | 3.99 $ft^2$ |
| | TOTAL | | 183.8 $ft^2$ |

So $A_e$ = 183.8 $ft^2$. We assume $h_e \cong 1$ Btu/deg F-$ft^2$-hr because the envelope walls see mostly other walls.

We next calculate solar transmission. The transparent area of the glazing is 8.58' × 4.58'. The transmissivity of the glass is assumed to be 75%; the amount of light reflected back out of the glass is apparently somewhat less than for the direct gain cell; we assume 72% for net transmissivity. Thus the solar gain is for 24 February when the peak solar gain is 255 Btu/hr-$ft^2$ is 7215 Btu/hr. We take $\alpha_T = 1.00$.

Finally, we list some materials properties necessary in calculating response functions. For the Trombe wall, K = .80 Btu/hr-deg-ft, $\rho c_p$ = 18 Btu/°F-$ft^3$, and d = 1.3021 ft. For the envelope walls, we have two 2-layer walls in parallel. Both have styrofoam as an inside layer. Using ASHRAE handbook values, we find that for styrofoam, $\rho$ = 2.2 lbs/$ft^3$, $c_p$ = 0.29 Btu/lb, K = 0.01667 Btu/°F-hr-ft, and d = 1/12 ft.

The second (outside) layer is fiberglas in one case ($\rho c_p$ = 0.143 Btu/°F-$ft^3$, K = 0.0238 Btu/°F-ft-hr, d = 3.5/12 ft) and wood ($\rho c_p$ = 9 Btu/°F-$ft^3$, K = .068 Btu/°F-ft-hr, d = 4.5/12 ft) in the

For example, we omit $C(2\omega_o)$ because there is no input of temperature variation at frequency $2\omega_o$.

The room temperature response is given by (2.15), which is repeated below. Recall that $|S_1| = 7215$ Btu/hr and the d's are given in Sec. 3.3.3.

$$T_R = |S_1|\left\{ d_o \frac{B(o)}{A(o)} + \sum_{n=1}^{2} \frac{B(n\omega_o)}{A(n\omega_o)} d_n e^{in\omega_o t} \right\} + \overline{T}_A + \frac{C(\omega_o)}{A(\omega_o)} \Delta T_A \; e^{i\omega_o t} \qquad (11)$$

We evaluate (11) term-by-term below, and point out some interesting effects:

$$T_R = 41.08^o \text{ F} + 4.973 \; e^{-4.313i} e^{i\omega_o t} + .695 \; e^{-.552i} \; e^{2i\omega_o t}$$

$$+ 37^o\text{F} + 2.458 \; e^{-2.842i} e^{i\omega_o t} \qquad (12)$$

We first note that the response to sunlight is very heavily damped by passage through the Trombe wall; the daily fluctuations in temperature due to solar input are only $\pm 5^\circ$F. In addition, they are phase delayed by about $0.9\,\pi$, or almost half a day. Thus even though the solar gain peaks at 12:30 p.m. and the ambient temperature peaks at 3 p.m., the effects of sunlight are felt six hours later than the effects of temperature.

This last effect illustrates why we had to model the envelope walls as massive objects. Comparing the last term $\left(\frac{C(\omega_o)}{A(\omega_o)} \Delta T_A\right)$ to the second term $\left(\frac{B(\omega_o)}{A(\omega_o)} d_1 \; S_1\right)$, we see that they are separated in phase by 1/4 cycle. This means that if the phase difference were to increase, these two terms would begin to interfere with each other. In other

Note the very fast convergence of the series $\sum d_n \frac{B(n\omega_o)}{A(n\omega_o)}$ in Eqs. (12) and (13). This convergence is due to the fact that $B(n\omega_o) \approx R_{2T}$, which decreases very rapidly with $\omega$, coupled with the slower $1/\omega^2$ dependence of the $d_n$. For this reason, we can completely ignore harmonics with $n \geq 3$; even the 2nd harmonic is buried in the noise of the calculation.

Finally, we can check the conductivity measurement of LASL concrete in a very approximate way using the results derived above. We find that they are consistent with the LASL measurement of .80 Btu/°F-hr-ft. Our check consists of calculating the steady-state heat transfer from the Trombe wall into the room and comparing this with the steady-state heat losses from the room. The former is estimated by calculating $U_T A_T(\overline{T}_{41} - \overline{T}_{45})$ where $\overline{T}_{41}$ and $\overline{T}_{45}$ are the front and back Trombe wall surface temperature at mid-height, averaged over the day (see Sec. 3.2 for values), $U_T$ is the Trombe wall U-value of $K_T/d_T$ = 0.6144 Btu/ft$^2$-deg F-hr. This should overestimate heat transfers, since the temperature of the wall is not uniform and the bottom is much colder than the middle or the top. (That is, the average back-surface temperatures for February 24 are: top: 88.79° F; middle: 86.94°F; bottom: 78.50°F. The middle temperature is thus somewhat hotter than the average temperature). The result is a heat transfer to the room of 615 Btu/hr.

The losses from the room are given by $\left\{\hat{U}_q + \hat{h}_e\ (1 - h_e R_{1e})\Big|_{\omega=o}\right\} \times (\overline{T}_R - \overline{T}_A)$. This is numerically equal to 12.33 Btu/°F-hr × 41.08°F or

We use Table 7 to evaluate this term-by-term, as follows:

$$T_R(t) = 26.30^\circ F + 12.19\, e^{i\omega_w(t-4.365 \text{ days})} + 4.398\, e^{-i4.313}\, e^{i\omega_o t}$$

$$+ \quad 0.615\, e^{2i\omega_o(t-1.05 \text{ hrs})} + 37.5^\circ F + 2.96\, e^{i\omega_w'(t-6.52 \text{ days})}$$

$$+ \quad 2.072\, e^{-i2.897}\, e^{i\omega_o t} \qquad (14)$$

As in the daily solution, the solar response term at frequency $\omega_o$ is out of phase by 1/4 cycle with the ambient temperature response at that frequency.

We note that in (14), the time t is measured in <u>days</u> in the second and sixth terms; that at noon on March 8 t = 15.0 days (i.e. t = 0 at noon on February 21).

What is the effect of long-term weather storage on the system? We note several effects. First, on the peak day of the cycle, the temperature elevation due to solar gain is 26.30 + 12.19°F, or 38.49°F. This is 2-1/2 degrees cooler than the steady-state result for 24 February, indicating that the storage of "coolth" is considerable. This is also evident in the reduced amplitude of the response to ambient temperature; $\Delta T_{A_w}$ is 4°F, but the room temperature response to it is only 3°F.

Also, note the phase lag in the second term of (14). The response to weather-varying solar amplitude is delayed 1-1/2 days. This results in the second term contributing almost nothing to room temperature on March 8, but if there were no phase lag the contribution from a 12°F amplitude would have been 8.3°F (that is, the room would have been about 8° warmer).

$$T_R(t) = \begin{cases} 62.7 \\ 66.2^\circ F \\ 69.6^\circ F \end{cases} + 5.14\, e^{i\omega_o(t-14.92\ \text{hrs})} + .61\, e^{2i\omega_o(t-1.05\ \text{hrs})} \qquad (15)$$

where the first term includes the effects of weather varying terms evaluated at $\begin{cases} \text{previous midnight} \\ \text{noon March 8} \\ \text{following midnight} \end{cases}$. Values for intermediate times can be approximated by linear interpolation. In comparing with (8), we are making the assumption that the second and fifth terms of (8) must be evaluated for each hour of each day (e.g. t = 15 days + 2 hours) while the expression $\Delta S_w\, e^{i\omega_w t}$ in the third term can be evaluated for t = noon on March 8 and held constant throughout the day. The good agreement in Figs. 10 and 6 seems to validate this approximation.

effort at Sonoma was spotty. Hourly values of $T_R$ are generally available, but $T_A$ was obtained from the campus weather station, which was frequently out of order. The calculations also require knowledge of when the collector window cover was opened and closed; this data was collected about half the time, and is sometimes incorrect (e.g. the data show that the cover was not opened on a given day, yet $T_R$ increases as quickly as on sunny days when the collector was used).

The net result is that the only day for which all the data were available was December 13, 1975. Fortunately, the condition of time-independent weather was satisfied to good approximation on this date. Figure 12 graphs the results $T_R - (\overline{T}_A)$ vs time; the solid line gives the data, the flatter dotted line gives the model predictions. The more curved dotted line gives the results of an extension of the model which accounts in an approximate way for the solar gain through the small west-facing windows. West window solar gain was assumed to be sinusoidal in time and centered at 2:30 p.m. To the extent that the real function was skewed towards later time, the house response should also be delayed further. The model also calculates the collector ("floor") temperature $T_f$, which was measured in a few spot checks. Measurements put the afternoon collector temperature $T_f$ in the range of 125-140°F, which is consistent with the calculation.

The predictions agree reasonably well with the data, considering the amount of judgment required in evaluating the parameters of a house which was demolished before it could be seen by the authors, and considering the uncertainties in the weather data.

We next describe the details of the modelling.

$\hat{U}_{fo}$ is the loss rate from the collector; it is the U value of the collector glazing. This ranges from about 1.1 for still air inside to about 2 for quickly circulating inside air, so $\hat{U}_{fod} \cong 220\ ft^2 \times (1.1\text{-}2) = 230 - 440$. Discussions with people at Cal State suggest the higher part of the range is more believable, since a jet of fast-moving air blew past the receiver and into the room when the sun was shining. So we take $\hat{U}_{fod} = 400\ \frac{Btu}{°F\text{-}hr}$.

We estimate the collector heat capacity $C_f$ as the sum of the contributions of the water and of the wood frame. The water has a heat capacity of $407\ gal \times \frac{8.33\ lbs}{gal} \times \frac{1\ Btu/deg}{lb} = 3390\ Btu/deg$.

The frame consists of 2 × 6 studs 12" apart in a 240 gross square foot assembly. We use the entire heat capacity, since the lumped parameters for 1" half-thickness of interior wood are very nearly the steady-state parameters. Heat capacity of the frame is

$240\ ft^2 \times \frac{6"}{12"} \times \frac{1\frac{5}{8}"\ of\ stud}{12"\ of\ space} \times 9\ \frac{Btu}{ft^3\text{-}deg} = 146\ Btu/deg\ F.$ Thus

$C_f = 3390 + 146 \cong 3535\ Btu/deg\ F.$

To evaluate wall parameters, we use a thickness of 6" corresponding to an average wood thickness for ceiling and floor joints and wall studs. Thus for $\rho c_p = 9\ Btu/ft^3\text{-}deg$ and $K_w = 0.068\ Btu/ft\text{-}deg\ F\text{-}hr$, we have $U_{wi} = 0.564\ Btu/ft^2\text{-}deg\ F\text{-}hr$, $C_w = 2.164\ Btu/ft^2\text{-}deg$.

$U_{wo}$ is normally chosen such that $U_{wi}^{-1} + U_{wo}^{-1} = U_w$ where $U_w = \frac{K_w}{d}$ in order to assure the correct steady-state heat loss. However, in this problem, we use "wall" subscripts to describe both walls and some building contents, so that to get the correct steady state heat loss

The lumped parameters for interior walls 2" thick (that is, assuming that the "wall" extends 2" below the surface and no heat flow occurs out the other side) are $U_i = .910 \frac{Btu}{ft^2\text{-deg-hr}}$; $U_o = 0$, $C = 1.356$ Btu/ft$^2$-deg. Thus, adding the contributions for 156 ft$^2$ of lumber to the wall stud contribution, we get

$$h_w = 198 + \left(156 \text{ ft}^2 \times 1 \frac{Btu}{\text{hr-deg F-ft}^2}\right) = 354 \text{ Btu/deg F-hr}$$

$$U_{wi} = 112 + \left(156 \text{ ft}^2 \times .91 \frac{Btu}{\text{hr-deg F-ft}^2}\right) = 254 \text{ Btu/deg F-hr}$$

$$C_w = 428 + \left(156 \text{ ft}^2 \times 1.356 \frac{Btu}{\text{deg F-ft}^2}\right) = 637 \text{ Btu/deg F}$$

We take $\hat{U}_{wo}$ such that $\hat{U}_{wi}$ and $\hat{U}_{wo}$ add in series to the steady-state U-value of 198 ft$^2$ x $U_w$; where $U_w = \frac{K_w}{d} = .136$ Btu/ft$^2$-deg F-hr. Thus $\hat{U}_{wo} = 30.1$ Btu/deg F-hr.

$\hat{U}_q$ is estimated using the steady-state U-values for the insulated spaces (cavities) in the envelope, the non-collector window, and air exchange.

The U-value for R-11 walls with no interior sheathing is .08 Btu/ft$^2$-deg F-hr, for ceiling about .05, for floor about .06 including the crawl space. Infiltration was not measured; we estimate it at 1 air exchange per hour (which is rather high for a 1-room, 1-story building) corresponding to the description of the house as "leaky".

We calculate $\hat{U}_q$ as follows:

Not all of this reflected light will reach the receiver window; since the receiver is not infinitely wide, some of the early-morning or late-evening light will miss the window to the west or east. However, all specularly reflected light at noon will reach the receiver. The intensity of the reflected light should be about $S_o$ x (reflectivity) x sin 20° for a solar gain of $S_o$; this equals about .2 $S_o$ for a reflectivity of 60%.

Solar gain is thus approximately 1.2 x 278 $\frac{\text{Btu}}{\text{ft}^2}$ x 200 (net $\text{ft}^2$ of glazed area) = 66,700 Btu/hr.

This is rounded to 65,000 Btu/hr.

We have used solar gain data for a south facing vertical window, although the actual collector is tilted 30° upward. This should not make too much difference, since for the latitude of this house, maximum solar elevation angle is 27½°. Thus at noon, solar heat gain through a vertical window is reduced to approximately cos 27½° or .89 of its maximum value for the tilted window. For other hours, this ratio is larger, until in the early morning and late afternoon it exceeds 1. Weighting the cosine of the angle between solar flux and collector normal by ASHRAE solar heat gain factor for December 21 at 40° latitude, we find that a vertical collector receives 7% less solar gain than the tilted collector, this 7% is better than the accuracy of the calculation and is ignored.

Sunrise was at t = -1.7 hrs, where t = 0 is 9:30 a.m. when the collector cover was opened; sunset was at t = 7.5 hrs = $t_d$ + 1.0. Thus $\omega_1 = \frac{\pi}{7.5-(-1.7)} = .3415\ \text{hr}^{-1}$. The phase of solar gain is such that it is centered between sunrise and sunset, thus $S = 65{,}000\ e^{i[\omega_1(t) - .9903]}$.

Solving the lumped parameter model gives the temperature curves of Table 8 which are plotted for collector temperature and room temperature in Fig. 12.

NOTE: Modifications to the lumped parameter model for two sources of solar gain.

This exercise is motivated by the desire to see the effect of explicitly modelling the solar gain through the west facing windows in the Sonoma house. This solar gain function has a different shape than the primary solar gain function, thus it generates new inhomogeneous solutions.

Assume that the secondary solar function has the form

$$S_2(t) = \begin{cases} S_2 e^{i\omega_2 t} & t_1 < t < t_2, \\ 0 & \text{otherwise.} \end{cases}$$

This is also a sinusoidal form, but $\omega_2 \neq \omega_1$ and $t_1$ and $t_2$ have no relationship to the other times in the problem. In the Sonoma case, $\omega_2$ would be faster than $\omega_1$, since the west windows collect sunlight for only about half the day. The time at which solar gain begins is $t_1$; this would be about noon for a west window; $t_2$ would correspond to sunset, at about 5:30 p.m. Note that for the example given $t_2$ would occur at "night," while $t_1$ would be during the "day."

The inhomogeneous solution produced by this new excitation is:

$$T_w = \chi_{S_{w2}} e^{i\omega_2 t}$$

$$T_f = \chi_{S_{f2}} e^{i\omega_2 t}$$

$$T_f = \begin{cases} A_1 K_{1d} e^{-\Lambda_{1d} t} + A_2 K_{2d} e^{-\Lambda_{2d} t} + \chi_{A_{fd}} \Delta T_A e^{i\omega_o t} + \chi_{S_f} S_1 e^{i\omega_1 t} & 0 \leq t < t_1 \\ A_3 K_{1d} e^{-\Lambda_{1d} t} + A_4 K_{2d} e^{-\Lambda_{2d} t} + \chi_{A_{fd}} \Delta T_A e^{i\omega_o t} + \chi_{S_f} S_1 e^{i\omega_1 t} \chi_{f2d} S_2 e^{i\omega_2 t} & t_1 \leq t < t_d \\ A_5 K_{1n} e^{-\Lambda_{1n}(t-t_d)} + A_6 K_{2n} e^{-\Lambda_{2n}(t-t_d)} + \chi_{A_{fn}} \Delta T_A e^{i\omega_o t} + \chi_{S_{f2n}} S_2 e^{i\omega_2 t} & t_d \leq t < t_2 \\ A_7 K_{1n} e^{-\Lambda_{1n}(t-t_d)} + A_8 K_{2n} e^{-\Lambda_{2n}(t-t_d)} + \chi_{A_{fn}} \Delta T_A e^{i\omega_o t} & t_2 \leq t < 24 \text{ hrs} \end{cases}$$

(16b)

These solutions for $T_w$ and $T_f$ must be matched at each transition time: that is, $T_w(t_1^-) = T_w(t_1^+)$ $T_f(t_1^-) = T_f(t_1^+)$, etc. This procedure generates eight equations in the eight unknowns A. These are relatively easy to solve and can be expressed analogously to the ordinary lumped parameter case in terms of some nested definitions. The results are written in the form of a program below; see the final equations for the overall form.

$$F_1 = \frac{(K_{1n} - K_{1d})\, e^{-\Lambda_{1n} t_n}}{K_{2d} - K_{1d}}$$

$$F_2 = \frac{(K_{2n} - K_{1d})\, e^{-\Lambda_{2n} t_n}}{K_{2d} - K_{1d}}$$

$$F_3 = (K_{2d} - K_{1d})^{-1} \left\{ \left( \chi_{A_{f_n}} - \chi_{A_{f_d}} \right) \Delta T_A - \chi_{Sf}\ S_1 - K_{1d} \left( \left( \chi_{A_w n} - \chi_{A_w d} \right) \Delta T_A - \chi_{Sw}\ S_1 \right) \right\}$$

$$F_4 = e^{-\Lambda_{1n} t_n} - F_1$$

$$F_5 = e^{-\Lambda_{2n} t_n} - F_2$$

(17)

$$F_{12} = e^{-\Lambda_{1d} t_d} - F_9$$

$$F_{13} = e^{-\Lambda_{2d} t_d} - F_{10}$$

$$F_{14} = \left(\chi_{Awd} - \chi_{Awn}\right) \Delta T_A \, e^{i\omega_o t_d} + \chi_{Sw} \, S_1 \, e^{i\omega_1 t_d} + \left(\chi_{Sw_2 d} - \chi_{Sw2n}\right) S_2 \, e^{i\omega_2 t_d} - F_{11}$$

$$F_{15} = \left\{\left(K_{2n} - K_{1n}\right) e^{-\Lambda_{2n}(t_2 - t_d)}\right\}^{-1} \left(\chi_{Sf2n} - K_{1n} \chi_{Sw2n}\right) S_2 \, e^{i\omega_2 t_2}$$

$$F_{16} = \chi_{Sw2n} \, S_2 \, e^{i\omega_2 t_2} \, e^{+\Lambda_{1n}(t_2 - t_d)} - F_{15} \, e^{(\Lambda_{1n} - \Lambda_{2n})(t_2 - t_d)}$$

$$Q_1 = F_9 \, F_4 + F_{10} \, F_1$$

$$Q_2 = F_9 \, F_5 + F_{10} \, F_2$$

$$Q_3 = F_{11} + F_9(F_6 + F_8) + F_{10}(F_3 + F_7)$$

$$Q_4 = F_{12} \, F_4 + F_{13} \, F_1$$

$$Q_5 = F_{12} \, F_5 + F_{13} \, F_2$$

$$Q_6 = F_{14} + F_{12}(F_6 + F_8) + F_{13}(F_3 + F_7)$$

and floor area which is located between the studs, and $\alpha_w = 1-\alpha_R$. Thus $\alpha_R = 0.723$ $\alpha_w = 0.277$. (Note that $0.277 = \frac{198\ ft^2 + 156\ ft^2}{450\ ft^2 + 828\ ft^2}$).

Solar gain is derived from the ASHRAE solar heat gain values for west windows. We total the solar gain for the 6 hours 12 noon to 5 p.m. and find a sine wave whose integral gives this same value. We assume that the sine wave starts at 11:30 a.m. and ends at 5:30 p.m. Since $\int_0^{\omega x=\pi} \sin \omega x dx = \frac{2}{\omega}$, we have that $S_2$ = (sum of solar gains) $x \frac{\omega_2}{2} \times 0.9$ (for double-pane glass transmission factor) $\times 0.9$ (for net area of window) $\times 30\ ft^2 = 2475$ Btu/hr for $\omega_2 = \frac{\pi}{6}$ hrs $= 0.5236\ hr^{-1}$. Solar gain peaks at 2:30 p.m. in this model; since t = 0 occurs at 9:30 a.m. second solar gain is given by $S_2(t) = 2475\ e^{i\omega_2(t-5\ hrs)}$. The times are then: $t_1 = 2$ hrs, $t_d = 6.5$ hrs, $t_2 = 8$ hrs.

The algebra is then straightforward; we display the results below. The room temperature curve is plotted in Fig. 12.

As seen in the figure, the solution differs from the 1-solar-gain-function solution only during the late afternoon, when it provides a closer fit to the data. Considering that the actual shape of the west-window solar gain function is skewed toward sunset from a sine wave, a solution using more Fourier terms for the west-window solar gain would be even closer to the data.

It is also evident from the A's that the 2-solar-gain solution could be obtained much more simply in this example as a perturbation onto the 1-solar-gain case.

Section 3 Footnotes

1. The thermal properties of concrete are known to be dependent on the exact composition of the specimen, as well as on its moisture content and density. There are no canonical values for any of these parameters, and the building literature contains several inconsistencies with regard to concrete's heat capacity.

   The Ashrae 1977 Handbook of Fundamentals (Ref. 15) lists concrete heat capacity as 0.21-0.22 Btu/°F-lb; depending on composition, in Chapter 22, Table 3A. However, the sources for data in this table are not listed, and the footnotes to the table warn the reader that the values it tabulates "are intended as design (not specification) values for materials in normal use. For properties of a particular product, use the value specified by the manufacturer or by unbiased tests."

   As if to add emphasis to this cautionary statement, the same handbook gives a different estimate for concrete heat capacity in Table 3 of Chapter 37; in that table the heat capacity is listed as 0.156 Btu/°F-lb., and attributed to Perry's (Ref. 30).

   Unfortunately, Perry's is also self-inconsistent on the heat capacity of concrete. Table 3-201 does indeed say that $C_p$ = 0.156 Btu/°F-lb. for concrete between 70°F and 312°F, but on the same line it also says that $C_p$ = 0.219 Btu/°F-lb. for concrete between 72°F and 1472 °F. No explanation is provided, nor is there a reference.

   In addition, Perry's also discusses heat capacity of concrete on page 3-235, where it says that concrete components ("sand, crushed rock, cement mortars, etc.") all have heat capacity within

Table 1 Los Alamos Weather Patterns

| Date | $\overline{T}_A$ (°F) | $\Delta T_A$ (°F) | Solar Gain (Btu/day) |
|---|---|---|---|
| 2/21 | 32.5 | | 1923 |
| /22 | 35.0 | | 1915 |
| /23 | 36.7 | $16\, e^{i\omega_o (t-15:00)}$ | 1909 |
| /24 | 37.0 | | 1924 |
| /25 | 40.2 | $14.3\, e^{i\omega_o (t-14.71:00)}$ | 1851 |
| /26 | 43.6 | $11.19\, e^{i\omega_o (t-14.62:00)}$ | 1086 |
| /27 | 42.4 | $3.96\, e^{i\omega_o (t-12.46:00)}$ | 785* |
| /28 | 39.4 | $7.96\, e^{i\omega_o (t-14.69:00)}$ | 775*** |
| 3/1 | 39.6 | $2.82\, e^{i\omega_o (t-11.95:00)}$ | 144 |
| /2 | 39.9 | $8.07\, e^{i\omega_o (t-13.43:00)}$ | 950** |
| /3 | 25.0 | $4.11\, e^{i\omega_o (t-18.61:00)}$ | 785** |
| /4 | 36.0 | $10.92\, e^{i\omega_o (t-14.65:00)}$ | 1392* |
| /5 | 40.3 | $7.44\, e^{i\omega_o (t-12.62:00)}$ | 710* |
| /6 | 36.3 | $9.36\, e^{i\omega_o (t-14.57:00)}$ | 1107 |
| /7 | 39.7 | $8.36\, e^{i\omega_o (t-14.71:00)}$ | 1322 |
| /8 | 41.2 | $13.49\, e^{i\omega_o (t-15.21:00)}$ | 1753 |

Table 2 Response Functions for Los Alamos Direct Gain Wall

| $\omega$ | $R_1$ | $R_2$ |
|---|---|---|
| 0 | .940 | .0603 |
| $2\pi$/month | $.937\ e^{-.0665i}$ | $.0601\ e^{-.0875i}$ |
| $2\pi$/14 days | $.9265\ e^{-.1411i}$ | $.0594\ e^{-.1861i}$ |
| $2\pi$/10 days | $.9143\ e^{-.1953i}$ | $.05858\ e^{-.2584i}$ |
| $2\pi$/2 days | $.615\ e^{-.672i}$ | $.038\ e^{-.982i}$ |
| $2\pi$/day | $.3991\ e^{-.787i}$ | $.0228\ e^{-1.380i}$ |
| $2\pi$/12 hours | $.2645\ e^{-.726i}$ | $.0118\ e^{-1.764i}$ |
| $2\pi$/8 hours | $.2225\ e^{-.665i}$ | $.0077\ e^{-2.021i}$ |
| $2\pi$/6 hours | $.2017\ e^{-.639i}$ | $.0055\ e^{-2.238i}$ |

Table 4a Response of the Concrete Mass Temperature* to Historic Weather, Direct Gain Cell

| Date | Period | $T_c - \overline{T}_A$ |
|---|---|---|
| 1978 | | |
| 02/24 | day | $66.82e^{-.0312(t-7:00)} + 1.89e^{i\omega_o(t-20.55:00)} + 21.13e^{i\omega_1(t-18.10:00)}$ |
| | night | $67.63e^{-.0312(t-18.52:00)} + 1.89e^{i\omega_o(t-20.55:00)}$ |
| /25 | morning | $54.03e^{-.0312(t-0:00)} + 1.69e^{i\omega_o(t-20.26:00)}$ |
| | day | $63.63e^{-.0312(t-7:00)} + 1.69e^{i\omega_o(t-20.26:00)} + 20.33e^{i\omega_1(t-18.1:00)}$ |
| | evening | $64.62e^{-.0312(t-18.52:00)} + 1.69e^{i\omega_o(t-20.26:00)}$ |
| /26 | morning | $51.29e^{-.0312(t-0:00)} + 1.32e^{i\omega_o(t-20.17:00)}$ |
| | day | $53.08e^{-.0312(t-7:00)} + 1.32e^{i\omega_o(t-20.17:00)} + 11.93e^{i\omega_1(t-18.1:00)}$ |
| | evening | $48.90e^{-.0312(t-18.52:00)} + 1.32e^{i\omega_o(t-20.17:00)}$ |
| /27 | morning | $43.13e^{-.0312(t-0:00)} + 0.47e^{i\omega_o(t-18.01:00)}$ |
| | day | $43.23e^{-.0312(t-7:00)} + 0.47e^{i\omega_o(t-18.01:00)} + 8.62e^{i\omega_1(t-18.1:00)}$ |
| | evening | $38.74e^{-.0312(t-18.52:00)} + 0.47e^{i\omega_o(t-18.01:00)}$ |
| /28 | morning | $35.13e^{-.0312(t-0:00)} + 0.94e^{i\omega_o(t-20.24:0)}$ |
| | day | $36.70e^{-.0312(t-7:00)} + 0.94e^{i\omega_o(t-20.24:00)} + 8.51e^{i\omega_1(t-18.1:00)}$ |
| | evening | $34.07e^{-.0312(t-18.52:00)} + 0.94e^{i\omega_o(t-20.24:00)}$ |
| 03/1 | morning | $29.08e^{-.0312(t-0:00)} + 0.33e^{i\omega_o(t-17.50:00)}$ |
| | day | $24.95e^{-.0312(t-7:00)} + 0.33e^{i\omega_o(t-17.50:00)} + 1.58e^{i\omega_1(t-18.1:00)}$ |
| | evening | $18.98e^{-.0312(t-18.52:00)} + 0.33e^{i\omega_o(t-17.50:00)}$ |

*Concrete temperature for each day is measured with respect to $\overline{T}_A$ <u>for that day</u>. Since $\overline{T}_A$ changes discontinuously at midnight, the definition and value of $T_c - \overline{T}_A$ will also change, but the actual temperature will be constant. $\overline{T}_A$ is given in Table 1.

Table 4a (cont.)

| Date 1978 | Period | $T_c - \overline{T}_A$ |
|---|---|---|
| /08 | morning | $31.33e^{-.0312(t-0:00)} + 1.59e^{i\omega_o(t-20.76:00)}$ |
| | day | $44.32e^{-.0312(t-7:00)} + 1.59e^{i\omega_o(t-20:76:00)} + 19.25e^{i\omega_1(t-18.1:00)}$ |
| | evening | $50.06e^{-.0312(t-18.52:00)} + 1.59e^{i\omega_o(t-20.76:00)}$ |
| 03/09 | morning | $40.00e^{-.0312(t-0:00)} + 1.62e^{i\omega_o(t-20.40:00)}$ |
| | day | $48.53e^{-.0312(t-7:00)} + 1.62e^{i\omega_o(t-20.40:00)} + 16.48e^{i\omega_1(t-18.1:00)}$ |
| | evening | $50.25e^{-.0312(t-18.52:00)} + 1.62e^{i\omega_o(t-20.40:00)}$ |
| 03/10 | morning | $49.60e^{-.0312(t-0:00)} + 0.14e^{i\omega_o(t-18.33:00)}$ |
| | day | $44.28e^{-.0312(t-7:00)} + 0.14e^{i\omega_o(t-18.33:00)} + 4.44e^{i\omega_1(t-18.10:00)}$ |
| | evening | $35.32e^{-.0312(t-18.52:00)} + 0.14e^{i\omega_o(t-18.33:00)}$ |
| /11 | morning | $27.22e^{-.0312(t-0:00)} + 1.03e^{i\omega_o(t-19.38:00)}$ |
| | day | $33.11e^{-.0312(t-7:00)} + 1.03e^{i\omega_o(t-19.38:00)} + 11.30e^{i\omega_1(t-18.10:00)}$ |
| | evening | $34.34e^{-.0312(t-18.52:00)} + 1.03e^{i\omega_o(t-19.38:00)}$ |
| /12 | morning | $32.29e^{-.0312(t-0:00)} + 0.77e^{i\omega_o(t-17.62:00)}$ |
| | day | $32.47e^{-.0312(t-7:00)} + 0.77e^{i\omega_o(t-17.62:00)} + 6.56e^{i\omega_1(t-18.10:00)}$ |
| | evening | $29.18e^{-.0312(t-18.52:00)} + 0.77e^{i\omega_o(t-17.62:00)}$ |
| /13 | morning | $25.38e^{-.0312(t-0:00)} + 1.28e^{i\omega_o(t-19.65:00)}$ |
| | day | $36.97e^{-.0312(t-7:00)} + 1.28e^{i\omega_o(t-19.65:00)} + 16.67e^{i\omega_1(t-18.10:00)}$ |
| | evening | $42.37e^{-.0312(t-18.52:00)} + 1.28e^{i\omega_o(t-19.65:00)}$ |

Table 4b(cont.)

| Date 1978 | Period | $T_R - \overline{T}_A$ |
|---|---|---|
| 03/02 | morning | $11.8e^{-.0312(t-0.00)} + 2.1e^{i\omega_o -14.79:00)}$ |
| | day | $17.5e^{-.0312(t-7:00)} + 2.1e^{i\omega_o(t-14.79:00)} + 12.41e^{i\omega_1(t-15.32:00)}$ |
| | evening | $20.2e^{-.0312(t-18.52:00)} + 2.1e^{i\omega_o(t-14.79:00)}$ |
| /03 | morning | $28.3e^{-.0312(t-0:00)} + 1.1e^{i\omega_o(t-19.90:00)}$ |
| | day | $29.3e^{-.0312(t-7:00)} + 1.1e^{i\omega_o(t-19.90:00)} + 10.25e^{i\omega_1(t-15.32:00)}$ |
| | evening | $27.0e^{-.0312(t-18.52:00)} + 1.1e^{i\omega_o(t-19.90:00)}$ |
| /04 | morning | $14.2e^{-.0312(t-0:00)} + 2.8e^{i\omega_o(t-16.01:00)}$ |
| | day | $23.1e^{-.0312(t-7:00)} + 2.8e^{i\omega_o(t-16.01:00)} + 18.18e^{i\omega_1(t-15.32:00)}$ |
| | evening | $27.8e^{-.0312(t-18.52:00)} + 2.8e^{i\omega_o(t-16.01:00)}$ |
| /05 | morning | $20.6e^{-.0312(t-0:00)} + 1.9e^{i\omega_o(t-13.98:00)}$ |
| | day | $22.5e^{-.0312(t-7:00)} + 1.9e^{i\omega_o(t-13.98:00)} + 9.28e^{i\omega_1(t-15.32:00)}$ |
| | evening | $21.7e^{-.0312(t-18.52:00)} + 1.9e^{i\omega_o(t-13.98:00)}$ |
| /06 | morning | $20.9e^{-.0312(t-0:00)} + 2.4e^{i\omega_o(t-1\ 5.92:00)}$ |
| | day | $26.1e^{-.0312(t-7:00)} + 2.4e^{i\omega_o(t-15.92:00)} + 14.46e^{i\omega_1(t-1\ 5.32:00)}$ |
| | evening | $27.5e^{-.0312(t-18.52:00)} + 2.4e^{i\omega_o(t-15.92:00)}$ |
| /07 | morning | $20.6e^{-.0312(t-0:00)} + 2.2e^{i\omega_o(t-16.07:00)}$ |
| | day | $27.6e^{-.0312(t-7:00)} + 2.2e^{i\omega_o(t-16.07:00)} + 17.27e^{i\omega_1(t-15.32:00)}$ |
| | evening | $30.4e^{-.0312(t-18.52:00)} + 2.2e^{i\omega_o(t-16.07:00)}$ |

Table 5. Response Functions for Trombe Cell Envelope Wall

| $\omega$ | $R_{1e}$ | $R_{2e}$ |
|---|---|---|
| 0 | .9388 | .06119 |
| $2\pi/14$ days $\equiv \omega_w$ | $.9387e^{-.002i}$ | $.06104e^{-.0379i}$ |
| $2\pi/10$ days $\equiv \omega_w'$ | $.93864e^{-.0025i}$ | $.06090e^{-.0528i}$ |
| $2\pi$/day | $.9319e^{-.0165i}$ | $.04803e^{-.2892i}$ |
| $2\pi/12$ hrs | $.9279e^{-.0255i}$ | $.04175e^{-.2593i}$ |

Table 7. Building Response Functions for the LASL Trombe Wall Cell

| $\omega$ | A | B | C |
|---|---|---|---|
| 0 | 23.79 | .4437 | 23.79 |
| $2\pi$/14 days | $27.35e^{.3116i}$ | $.4243e^{-.3816i}$ | * |
| $2\pi$/10 days | $29.92e^{.3739i}$ | * | $22.17e^{-.2664i}$ |
| $2\pi$/day | $56.90\ e^{+.3007i}$ | $.08224e^{-2.504i}$ | $8.741e^{-.447i}$ |
| $2\pi$/12 hours | $63.95\ e^{+.2765i}$ | $.02726e^{+2.741i}$ | * |

*not required for solution of the model

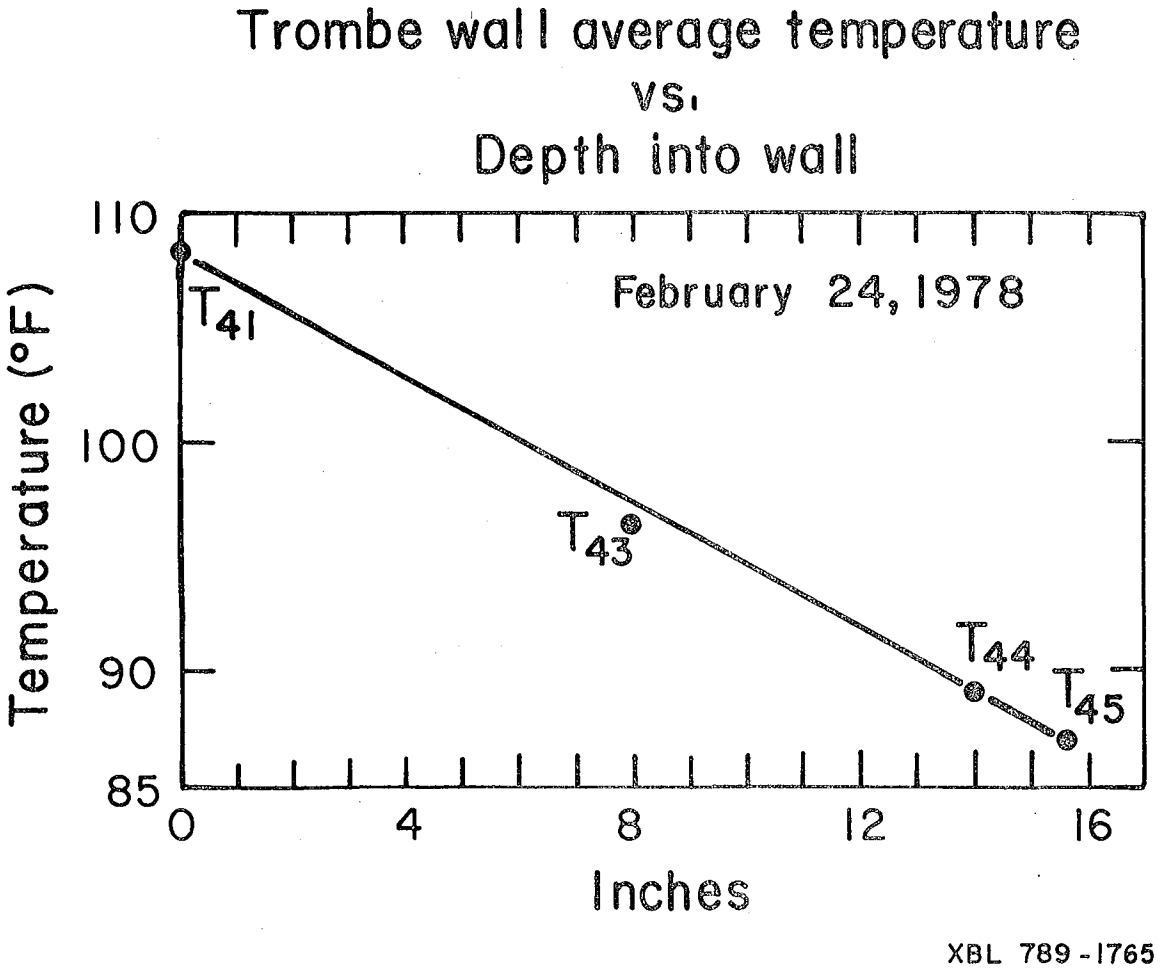


Fig. 1. Trombe wall steady-state temperature as a function of thickness into the wall. The temperatures are averages for the day of 24 February 1978.

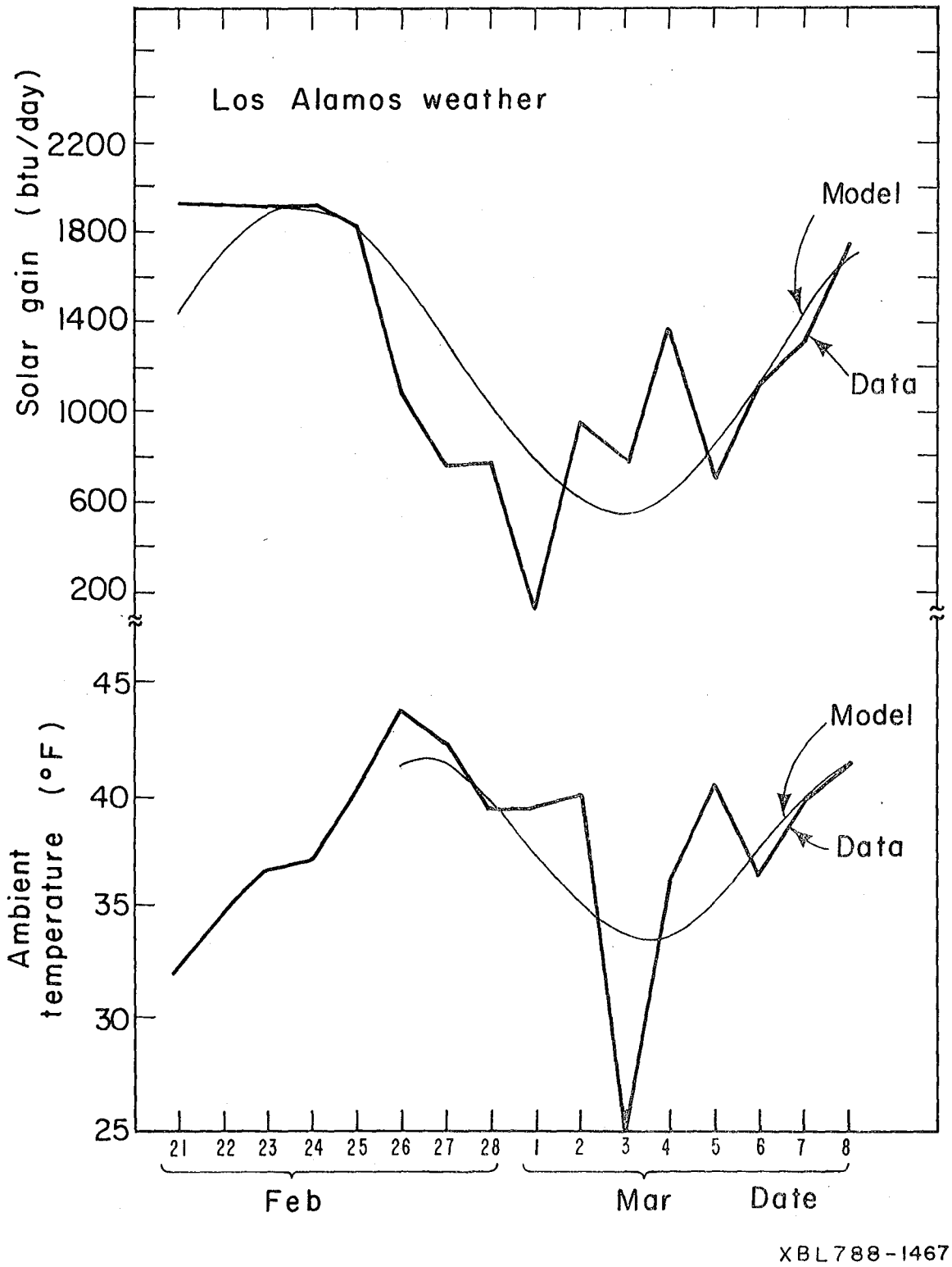


Fig. 3. Los Alamos weather as a function of date. This figure shows total solar gain (the sum of hourly solar flux for the whole day), and average ambient temperature. We model the variations in weather using a constant term plus one sinusoidally-varying term; the result is labelled "model." This idealized weather is used to predict building response for March 8.

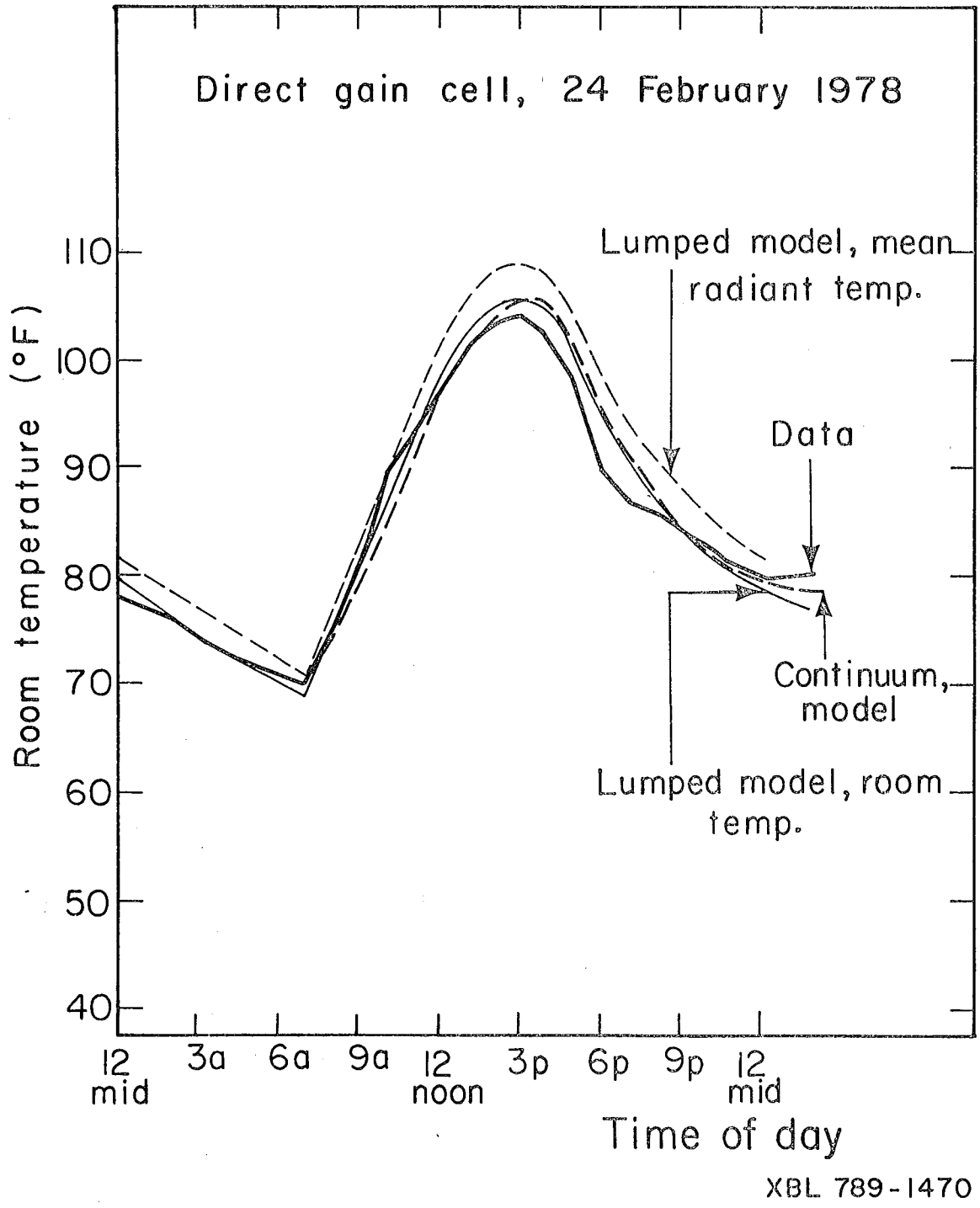


Fig. 5. Predicted room temperature and observed data as a function of time of day for the direct gain cell for 24 February 1978.

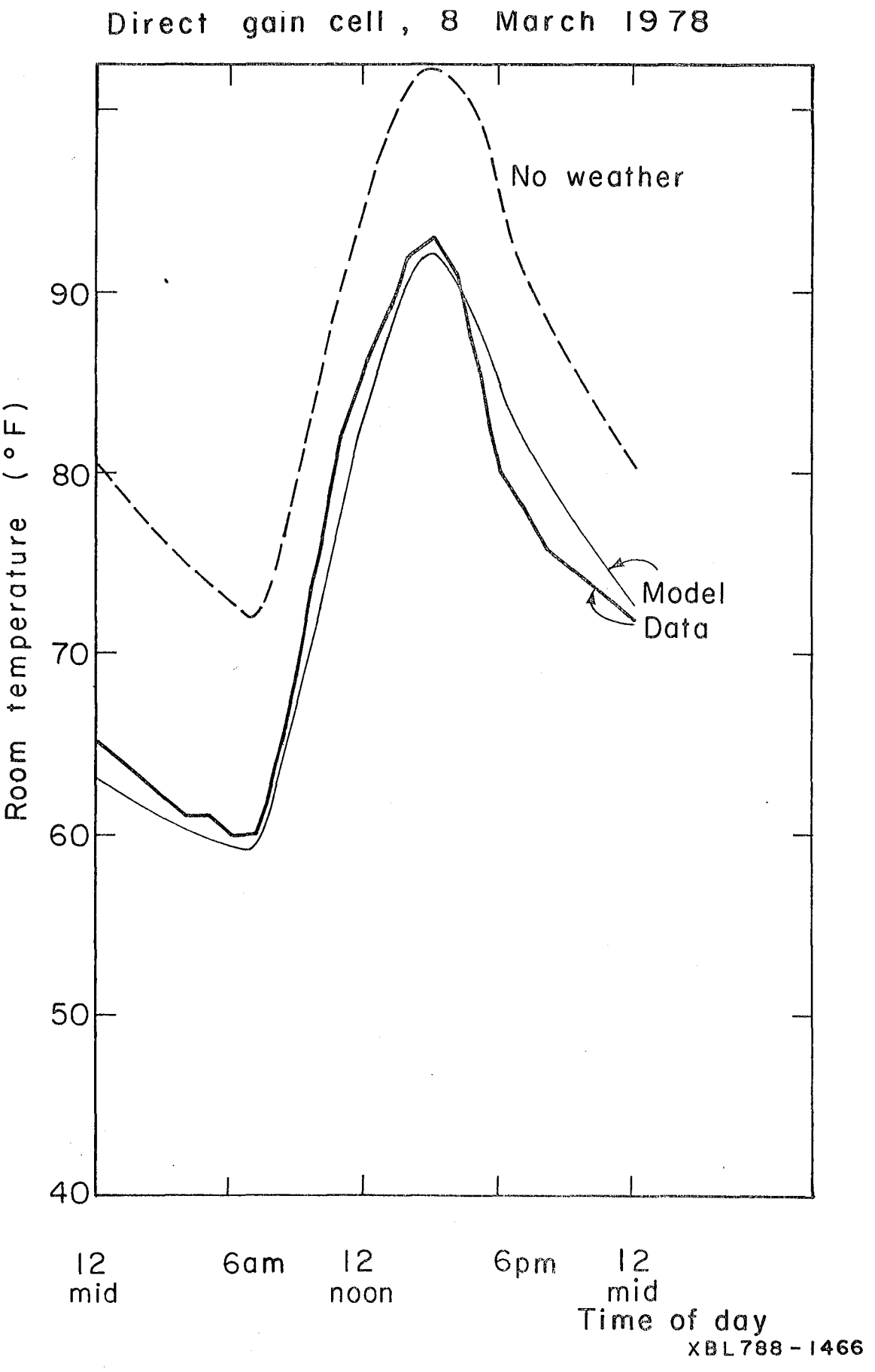
Direct gain cell, 8 March 1978
No weather
Model
Data
Room temperature (°F)
90
80
70
60
50
40
12
mid
6am
12
noon
6pm
12
mid
Time of day
XBL788-1466

Fig. 6.

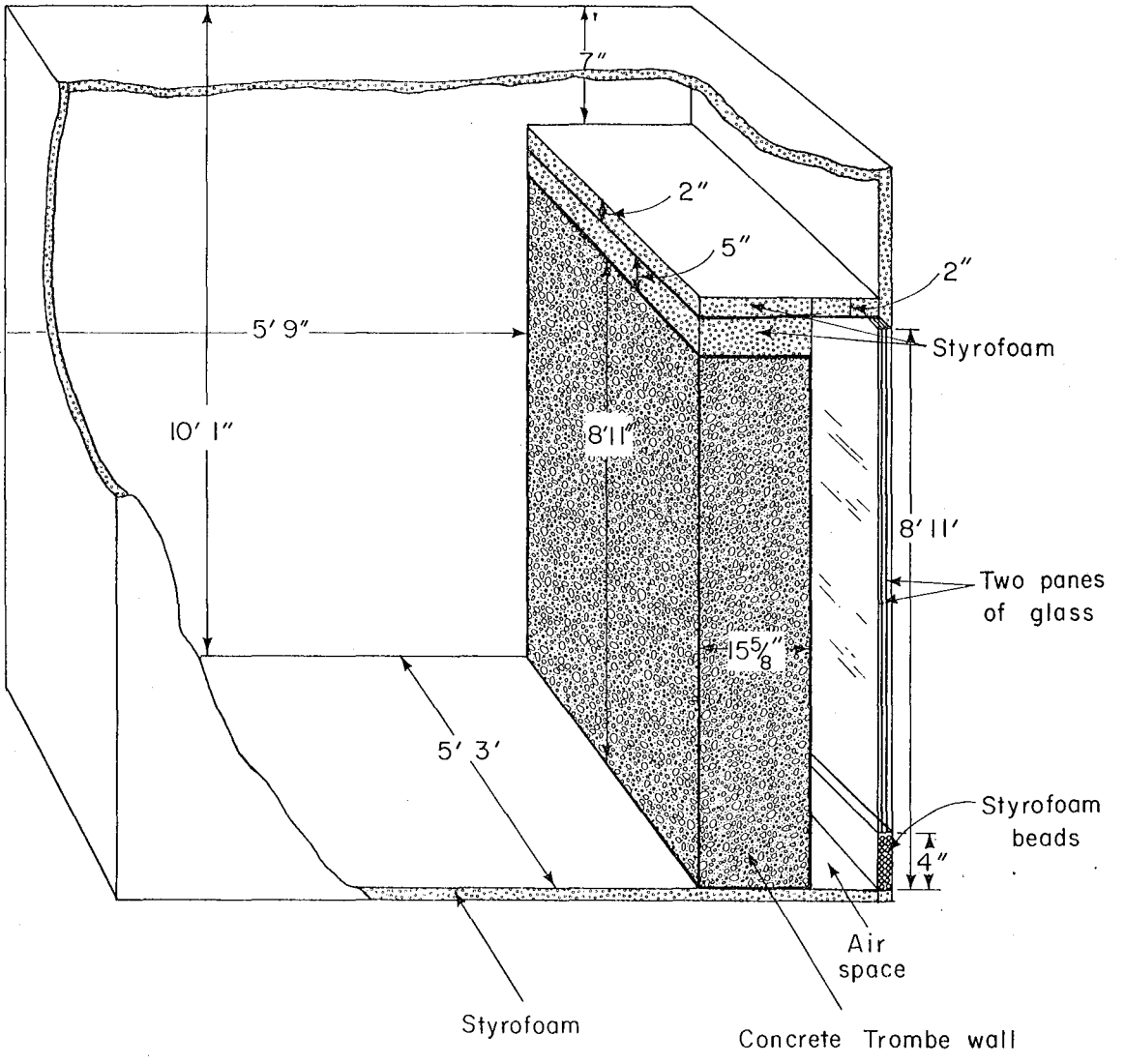


XBL 789-11086

Fig. 8. The Los Alamos Trombe wall cell. Dimensions are based on measurements by the author.

Section 3

Fig. 12. Comparison of temperature data and model calculations for the Sonoma house described in Section 3.5. The lower curves ($T_R$) graph temperature elevation ((room temperature)-(average ambient temperature)) as a function of time. The solid curve is the data for the day of 13 December 1975; the two dotted curves describe model simulations. The flatter dotted curve is calculated assuming that the solar gains through the small west-facing windows are unimportant, while the more peaked dotted curve includes a term approximating the effects of solar transmission through the west window.

The upper curve plots collector ("floor") temperature elevation ($T_f$) and compares to one data point measured on a similar day in February. The vertical error bars refer to the range in temperatures from the bottom to the top of the collector. The average temperature, "$T_f$", is probably closer to the top of the range (~80 - 85°F of elevation with respect to ambient average of 48°F).

# 4. OVERALL SUMMARY

Passive solar design is one of several promising conservation strategies which can, taken as a whole, reduce space heating needs to insignificance. Current efforts at solar building construction are impeded by a lack of theoretical understanding of the performance of passive solar buildings, and the concommitant inability to predict the results of various designs.

Existing public-domain building models do not yet handle solar gains correctly — they fail to consider where sunlight is absorbed within the building — and so are inaccurate for passive solar modeling. Even when they are revised to treat solar buildings precisely, they will still provide no insight into the thermally important features of the building. To address these problems, we derive an analytic model of passive solar building performance.

Of central importance in describing the heat transfers in passive solar buildings is the distribution of solar energy gains within the building. Our building models are therefore based on surface heat balance equations for the surfaces on which the sunshine is absorbed. In the distributed parameter model, we use the diffusion equation and the surface heat balance to derive response functions for surface temperatures as a response to sunlight and ambient temperature. These surface response functions are combined to form building response functions, which give the room temperature response to these weather variables or to heater output.

Using the building response functions, and simple sinusoidal representations of the input functions for a typical design day:

Analytic models are more limited in scope of application than computer models. They can easily be used to predict floating (that is, non-thermostated) behavior of internal temperatures, and to predict response to design conditions of weather, but they cannot easily model thermostat behavior in response to historic weather. These are tasks best left to computer models. However, as we have discussed, these models in the present form treat passive solar buildings incorrectly. We will use the results of the analytic models in a later paper to modify the program TWOZONE so that it simulates solar absorption in a manner parallel to that used in the analytic models.

9. Robert C. Sonderegger, "Dynamic Models of House Heating Based on Equivalent Thermal Parameters", Princeton University Center for Environmental Studies, 1977.

10. Philip W.B. Niles, "Modeling the Atascadero House" in Ref. 3b.

11. T. Kusuda, "NBSLD, Computer Program for Heating and Cooling Loads in Buildings", Center for Building Technology, National Bureau of Standards, NBS Building Science Series 69, 1976.

12. R. H. Henninger, "NECAP-NASA's Energy-Cost Analysis Program", U.S. Department of Commerce, National Technical Information Service N76-10751, 1975.

13. California Administrative Code Title 20 Chapter 1.

14. Robert H. Socolow and Robert C. Sonderegger, "The Twin Rivers Program on Energy Conservation in Housing: Four Year Summary Report. Princeton University, Center for Environmental Studies, Report #32 August 1976.

15. American Society of Heating, Refrigeration, and Air Conditioning Engineers, "Ashrae Handbook".

16. A. M. Neville, Properties of Concrete,(New York: John Wiley & Sons.)

17. C. W. Rose, Agricultural Physics,(Oxford, Pergamon Press, 1966), Ch. 2.1.

18. M. Lokmanhekim, F. C. Winkelmann, A. H. Rosenfeld, Z. Cumali, G. Leighton, "Cal-ERDA, A New State of the Art Computer Program for the Energy Utilization of Buildings", Presented at the Third International Symposium on the Use of Computers for Environmental Engineering Related to Buildings, Banff, Alberta, Canada, May 1978.

28. G. P. Mitalas and D. G. Stephenson, "Fortran IV Programs to Calculate Radiant Energy Interchange Factors." Computer Program No. 25 of the Division of Building Research, National Research Council of Canada, Ottawa, Canada, 1966.

29. D. G. Stephenson and G. P. Mitalas, "Calculation of Heat Conduction Transfer Functions for Multi-Layer Slabs." Ashrae Transactions 77 Part II, pp. 117-126, 1971.

30. J. H. Perry, Chemical Engineers Handbook, 5th Edition, 1973.

31. M. S. Ghausi and J. J. Kelly, Introduction to Distributed Parameter Networks (San Francisco: Holt, Rinehart, and Winston, 1968).

32. S. M. Berman, D. B. Goldstein, R. W. Richardson, "Lumped Parameters in Analytic Building Models", Lawrence Berkeley Laboratory, in process.

33. N. O. Milbank and J. Harrington-Lynn, "Thermal Response and the Admittance Procedure," British Building Research Establishment, Current Paper CP-61/74 (1974).

for the wall surface, where the symbols are those used in Sec. 2.3

We solve these equations for the surface temperatures $T_{fs}$, and $T_{ws}$:

$$T_{fs} = \frac{1}{\hat{U}_{fi} + \hat{h}_f} (\alpha_f S + \hat{h}_f T_R + \hat{U}_{fi} T_f) \qquad \text{(A2.3-2a)}$$

$$T_{ws} = \frac{1}{\hat{U}_{wi} + \hat{h}_w} (\alpha_w S + \hat{h}_w T_R + \hat{U}_{wi} T_w) \qquad \text{(A2.3-2b)}$$

and use the results in the room heat balance, Eq. (2.2)

$$\hat{U}_q(T_R - T_A) + \hat{h}_f(T_R - T_{fs}) + \hat{h}_w(T_R - T_{ws}) = H + \alpha_R S$$

to derive the result

$$T_R N_R = T_w N_w + T_f N_f + \frac{H}{\hat{U}_q} + S N_s + T_A \qquad \text{(A2.3-3)}$$

where

$$N_w = \frac{1}{\hat{U}_q} \frac{\hat{h}_w \hat{U}_{wi}}{\hat{h}_w + \hat{U}_{wi}}$$

$$N_f = \frac{1}{\hat{U}_q} \frac{\hat{h}_f \hat{U}_{fi}}{\hat{h}_f + \hat{U}_{fi}}$$

$$N_R = 1 + N_w + N_f$$

$$N_s = \frac{N_w \alpha_w}{\hat{U}_{wi}} + \frac{N_f \alpha_f}{\hat{U}_{fi}} + \frac{\alpha_R}{\hat{U}_q}$$

$$\dot{T}_w + \left[\lambda_w\left(1 - \frac{N_w}{N_R}\right) + \frac{\hat{U}_{wo}}{C_w}\right] T_w - \frac{\lambda_w N_f}{N_R} T_f \qquad \text{(A2.3-6a)}$$

$$= \frac{\lambda_w}{N_R \hat{U}_q} H + \left[\frac{\lambda_w}{N_R} + \frac{U_{wo}}{C_w}\right] T_A + \lambda_w \left[\frac{\alpha_w}{\hat{h}_w} + \frac{N_s}{N_R}\right] S$$

$$\dot{T}_f + \left[\lambda_f\left(1 - \frac{N_f}{N_R}\right) + \frac{\hat{U}_{fo}}{C_f}\right] T_f - \frac{\lambda_f N_w}{N_R} T_w \qquad \text{(A2.3-6b)}$$

$$= \frac{\lambda_f}{N_r \hat{U}_q} H + \left[\frac{\lambda_f}{N_R} + \frac{\hat{U}_{fo}}{C_f}\right] T_A + \lambda_f \left[\frac{\alpha_f}{\hat{h}_f} + \frac{N_s}{N_R}\right] S$$

where $$\lambda_w = \frac{\hat{U}_q}{C_w} N_w$$

$$\lambda_f = \frac{\hat{U}_q}{C_f} N_f$$

To simplify the algebra, we rewrite these as

$$\dot{T}_w + \Lambda_P T_w - \Lambda_F T_f = a_1 H + a_2 S + a_3 T_A \qquad \text{(A2.3-7a)}$$

$$\dot{T}_f + \Lambda_G T_f - \Lambda_Q T_w = a_4 H + a_5 S + a_6 T_A \qquad \text{(A2.3-7b)}$$

where the $\Lambda$'s and a's are defined by (A2.3-6 and 7) and have no special significance except to simplify the algebraic expressions. Their definitions are repeated in Table 2.1.

These are two linear first-order coupled differential equations. Their solution is simple, but some of the algebra becomes complicated. We first obtain the homogeneous solution, then a particular solution for

be the slower decay ($\Lambda_1 < \Lambda_2$). For a typical passive solar house $\Lambda_1 \sim \frac{1}{2 \text{ days}}$ while $\Lambda_2 \sim \frac{1}{5 \text{ hours}}$.

Inhomogeneous Solution

The inhomogeneous solution depends on the driving forces. We illustrate its solution with simplified driving forces which are sinusoidal in form. We approximate ambient temperature $T_A$ by a single term $T_A = \Delta T_A \, e^{i\omega_o t}$ where $\Delta T_A$ is complex. We have set average ambient air temperature equal to zero (that is, we measure all temperatures with respect to the average ambient temperature) and $\omega_o = 2\pi/\text{day}$. Solar gain is approximated by a sine wave of frequency $\omega_1$. This sine wave repeats every 24 hours, and is set equal to zero at night. Thus we take

$$S(t) = \begin{cases} S_1 \, e^{i\omega_1 t} & \text{day} \\ 0 & \text{night} \end{cases}$$

We take sunrise to be $t = 0$, and sunset at $t = t_d$. Heater output is taken as a constant, $H_o$. We further assume that the house parameters may change at night, producing two inhomogeneous solutions, one for day and one for night.

Ambient Temperature Response

The form of the solution for ambient temperature response is $T_w = \chi_{A_w} \Delta T_A \, e^{i\omega_o t}$ and $T_f = \chi_{A_f} \Delta T_A \, e^{i\omega_o t}$ where $\chi_{A_w}$ and $\chi_{A_f}$ have the values $\chi_{A_{wd}}$ and $\chi_{A_{fd}}$ for daytime parameters and $\chi_{a_{wn}}$ and $\chi_{A_{fn}}$ for the night. Substituting these expressions into (A2.3-7) we

$$(i\omega_o + \Lambda_p) \, \chi_{A_w} \Delta T_A - \Lambda_F \chi_{A_f} \Delta T_A = a_3 \, \Delta T_A$$

$$(i\omega_o + \Lambda_G) \, \chi_{A_f} \Delta T_A - \Lambda_Q \chi_{A_w} \Delta T_A = a_6 \, \Delta T_A$$

Complete Solution

The complete solution for a given problem is the sum of the homogeneous and inhomogeneous solutions. For a house whose temperature floats freely (e.g. no thermostatically controlled heater), and with the driving forces given above, we solve the equations (A2.3-7) separately for the day and night conditions. The solutions are joined smoothly using the assumption that the floor and wall temperatures do not change discontinuously. Note that this form of solution is for static weather: the same temperature and cloudiness conditions every day.

The boundary conditions are thus

$$T_w(t = 0^+) = T_w(t = 24\ \text{hrs}^-) \qquad \text{(A2.3-13)}$$

$$T_w(t = t_d^-) = T_w(t = t_d^+)$$

$$T_f(t = 0^+) = T_f(t = 24\ \text{hrs}^-)$$

$$T_f(t = t_d^-) = T_f(t = t_d^+)$$

These four equations determine the four unknowns $B_{1d}$ $B_{1n}$ $B_{2d}$ and $B_{2n}$. (Recall that the 'd' and 'n' subscripts refer to day and night solutions). These expressions are:

These four equations can be solved by first using (b) to find $B_{1n}$ and then using the result in (a). This produces an equation for $B_{2n}$ which can also be used in the $B_{1n}$ equation to express $B_{1n}$ and $B_{2n}$ in terms of $B_{1d}$ and $B_{2d}$. The results are

$$B_{1n} = Y_1 B_{1d} + Y_2 B_{2d} + Y_3$$

$$B_{2n} = Y_4 B_{1d} + Y_5 B_{2s} + Y_6$$

where the Y's are given explicitly in Table 2.1 .

Using these expressions above in (A2.3-14b) produces an equation of the form $B_{1d} Q_6 + B_{2d} Q_5 + Q_4 = 0$.

with the Q's given in Table 2.1.

Analogously using the $B_{1n}$ and $B_{2n}$ expressions on (A2.3-14d) we get

$$B_{1d} Q_2 + B_{2d} Q_3 - Q_1 = 0$$

Thus

$$B_{1d} = \frac{Q_3 Q_4 + Q_1 Q_5}{Q_2 Q_5 - Q_3 Q_6} \qquad \text{(A2.3-15)}$$

$$B_{2d} = \frac{Q_1 - Q_2 B_{1d}}{Q_3}$$

$$B_{1n} = Y_1 B_{1d} + Y_2 B_{2d} + Y_3$$

$$B_{2n} = Y_4 B_{1d} + Y_5 B_{2d} + Y_6$$

where the Q's and Y's are summarized in Table 2.1 . This determines the B's ; the complete solution for this problem can be written as

for night conditions and setting the initial values of $T_w$ and $T_f$ equal to their new calculated values at $t = t_d$. This process is illustrated in Sec. 3.3.5.

Further changes would include turning on the heater at some time before sunrise to simulate morning warm-up of the building (but this would involve matching boundary conditions at 3 times and finding 3 sets of B's), or adding the effects of a non-south facing window (discussed in Sec. 3.5).

One should note that the coefficients $\chi$ are actually linear response functions giving the response of wall or floor temperatures to solar or other excitations at a given frequency. They are similar to the response functions derived in Sec. 2.4 for the continuum model except that they describe the response of bulk material temperature rather than surface temperature.

The $\chi$ coefficients are shown here for walls and floor only; one can also derive response functions for room temperature as influenced by ambient temperature or sunlight using (A2.3-16). These response functions $\chi_{AR}$ and $\chi_{SR}$ can also be derived from the continuum model Eq. (A2.4-22), using lumped-parameter response functions in place of the distributed-parameter functions implied in that section. Lumped response functions are discussed in Appendix 2.5A.

$T_w$ is the lumped wall temperature.

This equation replaces (A2.3-1b); it says that the losses from the surface to the channel air plus the losses from sunlight (the minus sign indicates that these are really heat gains) plus the losses from the surface to the wall interior add to zero. Note that $\alpha_w \cong 1.0$ since almost all the sunlight passing through the window is absorbed on the wall.

We assume a constant channel temperature and constant wall temperature as a function of height; actually there will be a distribution of temperature. The channel air can then exchange heat with the outdoor air by conduction through the window or with room air through natural convection. Natural convection is a very complicated process; for this model we use a linear approximation and say that heat transfer from the channel air to the room is given by $\hat{U}_{cR}(T_c - T_R)$.

The heat balance for the channel air can then be expressed as

$$\hat{h}_{wc}(T_c - T_{ws}) + \hat{U}_{cA}(T_c - T_A) + \hat{U}_{cR}(T_c - T_R) = 0 \qquad \text{(A2.3-18)}$$

where $\hat{U}_{cA}$ is the heat transfer coefficient through the collector glazing (Btu/deg F-hr).

This simply says that the sum of the heat losses from the channel air is zero.

The room heat balance is altered in the Trombe model in two ways: the heat loss from the room to the wall surface occurs indirectly through the term $\hat{U}_{cR}(T_R - T_c)$ rather than directly through

We can use this to get an expression for wall surface temperature:

$$T_{ws} = \frac{1}{(\hat{U}_{wi} + \hat{U}_a)}\left(\alpha_w S + \hat{U}_{wi} T_w + \frac{\hat{h}_{wc} \hat{U}_{cA}}{\hat{\Sigma}} T_A + \frac{\hat{h}_{wc} \hat{U}_{cR}}{\hat{\Sigma}} T_R\right)$$

where $$\hat{U}_a = \frac{\hat{h}_{wc}(\hat{U}_{cA} + \hat{U}_{cR})}{\hat{\Sigma}} \qquad \text{(A2.3-21)}$$

We use these expressions along with (A2.3-2a) for floor surface temperature to derive a new room heat balance analogous to (A2.3-3); the expression has almost the same form as (A2.3-3) but the N's are different:

$$T_R N_R = T_w N_w + T_f N_f + \frac{H}{\hat{U}_q} + S N_S + T_A N_A$$

where $$N_w = \frac{\hat{h}_{wc} \hat{U}_{cR} \hat{U}_{wi}}{\hat{U}_q \hat{\Sigma}(\hat{U}_{wi} + \hat{U}_a)} + \frac{\hat{U}_{wo}}{\hat{U}_q} \qquad \text{(A2.3-22)}$$

$$N_f = \frac{1}{\hat{U}_q} \frac{\hat{h}_f \hat{U}_{fi}}{\hat{h}_f + \hat{U}_{fi}}$$

$$N_R = \left(1 + N_f + \frac{\hat{U}_{wo}}{\hat{U}_q} + \frac{\hat{U}_{cR}}{\hat{\Sigma}\hat{U}_q}\left(\hat{h}_{wc} + \hat{U}_{cA} - \frac{\hat{h}_{wc}^2 \hat{U}_{cR}}{\hat{\Sigma}(\hat{U}_{wi} + \hat{U}_a)}\right)\right)$$

$$N_S = \left(\frac{\alpha_w \hat{h}_{wc} \hat{U}_{cR}}{\hat{U}_q(\hat{U}_{wi} + \hat{U}_a)\hat{\Sigma}} + \frac{\alpha_f N_f}{\hat{U}_{fi}} + \frac{\alpha_R}{\hat{U}_q}\right)$$

$$N_A = \left(1 + \frac{\hat{U}_{cA} \hat{U}_{cR}}{\hat{U}_q \hat{\Sigma}} + \frac{\hat{h}_{wc}^2 \hat{U}_{cA} \hat{U}_{cR}}{\hat{\Sigma}^2 (\hat{U}_{wi} + \hat{U}_a)}\right)$$

To check this, consider a limiting case. Assume a perfectly insulated collector ($\hat{U}_{cA} \to 0$) and look at (A2.3- 23a). In this limit,

$\hat{U}_a \to \frac{\hat{h}_{wc}\hat{U}_{cR}}{\hat{h}_{wc}+\hat{U}_{cR}}$ , $\lambda_R \to \frac{\hat{U}_{wo}}{C_w} + \lambda_w$ , and the equation simplifies to:

$$\dot{T}_w + \left[\left(\lambda_w + \frac{\hat{U}_{wo}}{C_w}\right)\left(1 - \frac{N_w}{N_R}\right)\right]T_w - \frac{N_f}{N_R}\left(\lambda_w + \frac{\hat{U}_{wo}}{C_w}\right)T_f$$

$$= \left(\lambda_w + \frac{\hat{U}_{wo}}{C_w}\right)\frac{1}{N_R\hat{U}_q}H + \left(\frac{\alpha_w\lambda_w}{\hat{h}_w} + \left(\lambda_w + \frac{\hat{U}_{wo}}{C_w}\right)\frac{N_s}{N_R}\right)S + \left(\lambda_w + \frac{\hat{U}_{wo}}{C_w}\right)\frac{1}{N_R}T_A$$

Next consider solving the same problem with the earlier set of equations. We use (A2.3-5a) with (A2.3-2b) for $T_{ws}$ and use $\hat{U}_{wo}(T_w - T_R)$ in place of $\hat{U}_{wo}(T_w - T_A)$. This produces the identical differential equation; in addition, the expressions for $N_R$, $N_w$, etc. agree.

This shows that much of the algebraic complication in the Trombe wall solution comes from the use of channel temperature $T_c$ instead of pure series or parallel heat transfer paths in the direct gain model.

Thus the Trombe wall solution proceeds similarly to the direct gain building solution with the insertion of the definitions in Table 2.1a for those in Table 2.1 .

The lumped parameters for the Trombe wall are evaluated as in the case of an envelope wall with insulation outside, with $\hat{U}_a$ substituted for $\hat{h}_w$ ; and $\hat{U}_{wr}$, the coupling between rear Trombe-wall surface and the room, substituted for $\hat{U}_r$, the conductance of the insulation. As shown in Appendix 2.5A, the error in using lumped parameters to describe

Continuously heated house

In this part we discuss the solution to the lumped parameter model for a house kept at a fixed thermostat setting in which the heater output varies with time. This solution applies only in a very cold climate, when the heater is needed 24 hours a day. As we will show, "very cold" will turn out to be unreasonable for a typical passive solar design, rendering this solution of little practical interest.

We use the notation for the direct gain system described at the beginning of this appendix. The equations of motion are the room heat balance (A2.3-3)

$$N_R T_R = N_w T_w + N_f T_f + \frac{1}{\hat{U}_q} H = N_s S + T_R \qquad \text{(A2.3-25)}$$

and the differential equations (A2.3-5a and b)

$$C_w \dot{T}_w + \hat{U}_{wi}(T_w - T_{ws}) + \hat{U}_{wo}(T_w - T_A) = 0 \qquad \text{(A2.3-26a)}$$

$$C_f \dot{T}_f + \hat{U}_{fi}(T_f - T_{fs}) + \hat{U}_{fo}(T_f - T_A) = 0 \qquad \text{(A2.3-26b)}$$

In this case $T_R$ is fixed at the thermostat level $T_t$, so we solve these differential equations differently than before. Rather

$$\ddot{H} + \Lambda_w \dot{H} = -\hat{U}_q \left( N_s \ddot{S} + \left( \frac{N_w \lambda_w \alpha_w}{\hat{h}_w} + \frac{N_f \alpha_f \lambda_f}{\hat{h}_f} + N_s \Lambda_w \right) \dot{S} \right) - \hat{U}_q \left( \ddot{T}_A + \left( \Lambda_w + \frac{N_w \hat{U}_{wo}}{C_w} + \frac{N_f \hat{U}_{fo}}{C_f} \right) \dot{T}_A \right) - \hat{U}_q N_f \left( \Lambda_w' - \Lambda_f \right) \dot{T}_f \qquad \text{(A2.3-30)}$$

where $\Lambda_w = \lambda_w + \frac{\hat{U}_{wo}}{C_w}$

$$\Lambda_f = \lambda_f + \frac{\hat{U}_{fo}}{C_f}$$

We then add $\Lambda_f$ times (A2.3-30) to itself to get the equation of motion for H:

$$\ddot{H} + (\Lambda_w + \Lambda_f) \dot{H} + \Lambda_w \Lambda_f H = -\hat{U}_q \left( N_s \ddot{S} + \left[ (\Lambda_w + \Lambda_f) N_s + \frac{N_w \lambda_w \alpha_w}{\hat{h}_w} + \frac{N_f \lambda_f \alpha_f}{\hat{h}_f} \right] \dot{S} + \left[ N_s \Lambda_f \Lambda_w + \frac{N_w \lambda_w \Lambda_f \alpha_w}{\hat{h}_w} + \frac{N_f \Lambda_w \lambda_f \alpha_f}{\hat{h}_f} \right] S \right) - \hat{U}_q \left( \ddot{T}_A + \left( (\Lambda_w + \Lambda_f) + \frac{N_w \hat{U}_{wo}}{C_w} + \frac{N_f \hat{U}_{fo}}{C_f} \right) \dot{T}_A + \left( \Lambda_f \Lambda_w + \frac{N_w \hat{U}_{wo} \Lambda_f}{C_w} + \frac{N_f \hat{U}_{fo} \Lambda_w}{C_f} \right) T_A \right) + \hat{U}_q \left( \Lambda_w \Lambda_f N_R - \lambda_w \Lambda_f N_w - \lambda_f \Lambda_w N_f \right) T_t \qquad \text{(A2.3-31)}$$

The homogeneous solution of this equation is

$$A_1 e^{-\Lambda_w t} + A_2 e^{-\Lambda_f t}$$

Note that the decay constants are substantially different from the free-floating temperature time constants. In general, they are faster decays for example, for house #1 described later in this appendix, the free-floating temperature decay times are 1/(41 hrs) and 1/(2.35 hrs) whereas the heater decay constants are 1/(10 hrs) and 1/(8 hrs). However, the heater decay constants are still inversely proportional to the heat capacities.

The inhomogeneous solution can be expressed as $H_o + H_A e^{i\omega_o t} + H_s e^{i\omega_1 t}$ for ambient temperature given by $T_A = \Delta T_A e^{i\omega_o t}$ and solar

For house #1, we see the following departure from steady-state results:

$$H_o = 0.998\ (\hat{U}_q + \hat{U}_f + U_w)\ (T_t - T_A)$$

$$H_A = 0.946\ (\hat{U}_q + \hat{U}_f + \hat{U}_w)\ \Delta T_A\ e^{-i(\omega_o(0.16\ \text{hrs}))}$$

$$H_s = 0.581\ S_1\ e^{-i\omega_1(0.72\ \text{hrs})}$$

Thus the steady-state heater output agrees to within 1/4% with simple methods, while the response to ambient temperature is damped by 5% and phase-lagged by a trivial amount (10 minutes). The response to sunlight is greatly damped, but only phase-delayed by 45 minutes. The greater damping is to be expected; the sunlight falls on surfaces and some fraction of it is used to heat the materials under the surfaces; this portion is unavailable (at that time) for reducing furnace output.

However, the magnitude of these expressions shows that this constant-thermostat solution is unrealistic for a passive solar house. For house #1, with 250 $ft^2$ of solar collector window (1/6 of floor area) $H_s$ gets as large as 28,800 Btu/hr. Since $H_o \simeq 539$ Btu/°F-hr ($\Delta T$) and $H_1/\Delta T \cong H_o/\Delta T$ we would require an ambient temperature of 52° below thermostat for the solution to work. For a typical indoor temperature of 70°F, ambient temperatures would have to remain below 18°F. This is unlikely enough in any North American climate, but even if it occurred, the optimum passive house would likely have triple glazing rather than double and extra caulking and insulation, reducing $\hat{U}_q$ from 450 Btu/°F-hr

| | | |
|---|---|---|
| walls | $80\% \times 865\ ft^2 \times 0.05$ Btu/°F-$ft^2$-hr | = 35 Btu/°F-hr |
| ceiling | $90\% \times 1500\ ft^2 \times 0.05$ Btu/°F-$ft^2$-hr | = 67 |
| windows | $375\ ft^2 \times 0.60$ Btu/°F-$ft^2$-hr | = 225 |
| infiltration | $\frac{1}{2}\ hr^{-1} \times 8\ ft \times 1500\ ft^2 \times 0.018$ Btu/$ft^3$-°F | = 108 |
| doors | $2 \times 6\frac{2}{3}\ ft \times 3\ ft \times 0.37$ Btu/$ft^2$-°F | = 15 |
| | TOTAL $\hat{U}_q$ = | 450 Btu/°F-hr |

For the lumped parameter model, we divide the heavy materials into two surfaces, floor and walls. The floor parameters' evaluation is straightforward; we set $U_{fi}$ = 2.52 Btu/°F-$ft^2$-hr and $\bar{C}_f$ = 9.64 Btu/°F-$ft^2$ for concrete. Thus $\hat{U}_{fi}$ = 3780 Btu/°F-hr, $C_f$ = 14,460 Btu/°F.

The walls are a little more complicated, since we are combining the effects of two materials. We evaluate lumped parameters for wood (studs) and then for (non-wood-stud-backed) gypsum board, and then combine them.

Consider first the wood studs. The area in studs is $0.20 \times 865\ ft^2$ + $0.15 \times 1920\ ft^2$ + $0.10 \times 1500\ ft^2$ = 611 $ft^2$. We evaluate the lumped parameters $U_i$ and $\bar{C}$ for 6" wood, except that we hold off in evaluating $U_o$ until we have added the effects of the gypsum board. Note that some of the walls are partition walls.) When only part of the wall area communicates with outside, we want $(\hat{U}_i^{-1} + \hat{U}_o^{-1})^{-1}$ to equal the steady state heat loss, and we determine $\hat{U}_o$ accordingly. For the 6" wood, $U_i$ = 0.564 Btu/°F-$ft^2$-hr and $\bar{C}$ = 2.16 Btu/°F-$ft^2$. Next, the gypsum board has $\rho c_p$ = 13 Btu/°F-$ft^3$ and K = 0.0936 Btu/hr-deg F-ft. If the thickness is 5/8", the lumped parameters (for partition walls) are $U_i$ = 4.23 Btu/°F-$ft^2$-hr and $\bar{C}$ = 0.646 Btu/°F-$ft^2$. The areas (excluding

## APPENDIX 2.4: The Distributed Parameter Model

The distributed parameter model is an exact solution of the diffusion equations (2.3) for each of the heavy materials and the heat balance equations (2.1) and (2.2). The solution is computed in Fourier transform space; that is, we calculate response functions for room temperature (at a given frequency) as a function of the driving forces (sunlight, ambient temperature) at that frequency.

In this section, we solve the model for a case with three different material surfaces, floor ("f"), envelope walls ("e") and partition walls ("p"). We derive response functions relating material surface temperatures to sunlight, heater output, and ambient temperature. We then use these response functions to set up a simple approximate solution for room temperature as a function of time.

Note that our choice of three surfaces is arbitrary; extension to more surfaces is trivial.

We first write the equations of heat transfer for the model. For the floor, we have the diffusion equation (2.3) and the surface heat balance: (2.1):

$$\frac{K_f}{(\rho c_p)_f} \frac{\partial^2 T_f(z,t)}{\partial z^2} = \frac{\partial T_f(z,t)}{\partial t} \qquad \text{(A2.4-1)}$$

$$\hat{h}_f(T_f(0,t) - T_R) - \alpha_f S - A_f K_f \left.\frac{\partial T_f(z,t)}{\partial z}\right|_{z=0} = 0 \qquad \text{(A2.4-2)}$$

where $T_f(0,t)$ is the floor surface temperature and $-A_f K_f \left.\frac{\partial T_t}{\partial z}\right|_{z=0}$ is the surface heat flux into the floor.

$$T_f(z,t) = \left( T_f^{(+)} \; e^{k_f z} + T_f^{(-)} \; e^{-k_f z} \right) e^{i\omega t}$$

or $$T_f(z,t) = \left[ A_f \cosh k_f d_f \, (1-\xi) + B_f \sinh k_f d_f \, (1-\xi) \right] \; e^{i\omega t}$$

where $$k_f = \sqrt{\frac{i\omega(pC_\rho)_f}{K_f}} = \sqrt{\frac{\omega(pC_\rho)_f}{2K_f}} \; (1+i)$$

$$\xi = \frac{z}{d_f} , \qquad d_f = \text{the floor thickness}$$

These forms suggest that we look at a Fourier transform solution

$$\tilde{T}_f(z,\omega) = T_f^{(+)} \; e^{k_f z} + T_f^{(-)} \; e^{-k_f z}$$

or $$\tilde{T}_f(z,\omega) = A_f \cosh k_f d_f \, (1-\xi) + B_f \sinh k_f d_f \, (1-\xi)$$

So we will solve the Eqs. (A2.4-(1-7)) in Fourier transform space and drop the "~" notation.

Equations (A2.4(1-7)) provide 3 differential equations and 3 inside-surface boundary conditions. We also require boundary conditions on the outside surfaces. These will vary from case to case; we pick some representative cases below and present the appropriate boundary conditions.

Knowing the boundary conditions lets us represent a temperature distribution (e.g. $T_f(z,\omega)$) with one coefficient. That is, we can represent $B_f$ or $T_f^{(-)}$ in terms of $A_f$ or $T_f^{(+)}$.

For the floor, we assume a slab of masonry on top of the ground. (If instead we wish to treat a suspended floor, the boundary conditions are the same as for an envelope wall. Envelope walls are discussed below.)

where $d_e$ is the thickness of the envelope wall. We also require conservation of energy at the wall/resistance interface, so

$$Q = -A_e K_e \left.\frac{\partial T_e(\omega,y)}{\partial y}\right|_{y=d_e} \qquad \text{(A2.4-11)}$$

We look for a solution of the form $T_e = A \cosh k_e d_e(1-\xi) + B \sinh k_e d_e(1-\xi)$. Equation (A2.4-10) requires that $T_{int} = A$. Equating the right-hand sides of (A2.4-9 and 11), we see that $A = (R_e K_e k_e)B + T_A$ so that

$$T_e(\omega,y) = (R_e K_e k_e T_{e\omega} + T_A) \cosh k_e d_e(1-\xi) + T_{e\omega} \sinh k_e d_e(1-\xi) \qquad \text{(A2.4-12)}$$

where we have set $T_{e\omega} \equiv B$.

For the partition walls, the boundary condition embodies the fact that partition walls are two-sided. If they are driven by equal solar absorption on both sides, then the heat flux through the middle must be identically zero. Thus for a half-thickness $d_p$, we have

$$\left.\frac{\partial T_p}{\partial x}\right|_{x=d_p} = 0$$

We can then write $T_p$ as

$$T_p = T_{p\omega} \cosh k_p d_p(1-\xi) \qquad \text{(A2.4-13)}$$

where $d_p$ = the half-thickness of the wall.

This completes the discussion of boundary conditions; we use the results (A2.4-(8,12, and 13)) to derive the solution to the model. We first obtain expressions for the surface temperatures from the surface heat balance equations, then use these results in (A2.4-7).

For the partition walls, (A2.4-4 and 13) say that

$$T_{p\omega} = \frac{h_p T_R + \bar{\alpha}_p S}{h_p \cosh k_p d_p + K_p k_p \sinh k_p d_p} \qquad \text{(A2.4-18)}$$

Since by (A2.4-13), $T_p(\omega, x=0) = T_{p\omega} \cosh k_p d_p$ ,

$$T_p(\omega, x=0) = (h_p T_R + \bar{\alpha}_p S) \frac{\cosh k_p d_p}{h_p \cosh k_p d_p + K_p k_p \sinh k_p d_p} \qquad \text{(A2.4-19)}$$

Before substituting the surface temperature equations (A2.4-15,17, and 19) into the room heat balance (A2.4-7), we note the similarity in form of the three equations. Each computes the response of the surface temperature of the $i^{th}$ material to $T_R$, S, and $T_A$; in each there is a term $R_{1_i}$ $(h_i T_R + \bar{\alpha}_i S)$ where $R_{1_i}$ is a frequency-dependent linear response function. For the envelope walls, there is also a term $R_{2_i}$ $T_A$ where $R_{2_i}$ is another linear response function. Examination of the equations leading to this term ($R_{2_e}$ $T_A$) shows that any material surface whose outside is coupled to the ambient air will produce a similar term.

These response functions turn up again in Appendix 2.5A on optimal evaluation of the lumped parameters. They characterize the response of the continuum materials for this model; in other words, as we shall see below, the entire effect of distributed materials on room temperature can be expressed in terms of these response functions.

We can express this as $T_R \cdot A(\omega) = S \cdot B(\omega) + T_A \cdot C(\omega) + H$ (A2.4-22a)

where A, B, and C are frequency-dependent functions given by (A2.4-22).

We note several things about (A2.4-22). First, all the frequency-dependence is contained in the response functions; the coefficients in the equation ($\hat{U}_q$ ,$\hat{h}_e$, etc.) are all time-independent. Second, the response of the room to sunlight ($\frac{B}{A}$) differs substantially in form from its response to ambient temperature ($\frac{C}{A}$) or heater output ($\frac{1}{A}$). However, the responses to temperature and heater output are usually the same, since $\hat{h}_e R_{2e} << \hat{U}_q$ for most buildings.

Third, the form of (A2.4-22) shows all materials entering into the A,B and C coefficients in identical fashion. Thus adding another material 'x' to the system simply adds a term $\hat{h}_x(1-h_x R_{1x})$ to A, adds $h_x \alpha_x R_{1x}$ to B, and adds $\hat{h}_x R_{2x}$ to C. Extension of (A2.4-22) to any number of materials is thus trivial to do; we can write the equation for N materials as:

$$T_R\left[\hat{U}_q + \sum_{j=1}^{N} \hat{h}_j\left(1-h_j R_{1j}\right)\right] = S\left[\alpha_R + \sum_{j=1}^{N} h_j \alpha_j R_{1j}\right] + T_A\left[\hat{U}_q + \sum_{j=1}^{N} h_j R_{2j}\right] + H \qquad \text{(A2.4-22b)}$$

The form of (A2.4-22) also demonstrates an important linearity in the building response: linearity with respect to illuminated area. Suppose we have a surface, call it surface K, which receives an amount

the same material. That is, for a building with 8" concrete floor and walls, we can lump the floor and walls into a single heavy material, and not worry about the distribution of sunlight between walls and floor, or between the south part of the floor and the north part. (This may, however, introduce an error if the film coefficients h are different for walls and floor, or if the h's differ between the illuminated part of the floor and the shaded part.)

We note further that in the derivation of (A2.4-22), all the information about the heavy materials and their surface boundary conditions is contained in the response functions. Thus this equation is valid for the lumped parameter model as well as the distributed parameter model, provided we interpret the $R_1$ and $R_2$ functions as lumped-parameter response functions: Lumped parameter response functions are discussed extensively in Appendix 2.5A: they are of the form:

$$R_1 = \frac{U_i + U_o + i\omega\bar{C}}{(U_i + U_o + i\omega\bar{C})(h+U_i) - U_i^2}$$

$$R_2 = \frac{U_o U_i}{(U_i + U_o + i\omega\bar{C})(h + U_i) - U_i^2} \qquad \text{(A2.4-21a)}$$

(Alternately, a physically lumped-parameter material, such as a water wall, would be modelled using these response functions.)

To show some of the information contained in (A2.4-22), we look at its low frequency limit, noting that the semi-infinite floor approximation may produce an error in the floor term. The $\omega \to 0$ limit of this equation depends on the limits of the response functions. As $\omega$ becomes small, k becomes small, so cosh kd $\to$ 1 and sinh kd $\to$ kd.

the inside surface. Details of elements near the outside surface will be relatively unimportant, since they have little influence on the inside surface, except at very low frequencies. But at zero frequency, $R_1$ is simply related to the U-value of the wall, as shown in (A2.4-23), so if we get the correct U-value with a 1-layer-wall model, the $R_1$ function should be very closely approximated at all frequencies.

We expect that A, B, and C should have the property that $A(\omega) = A^*(-\omega)$; this is confirmed by looking at the form of (A2.4-22 and 21).

These equations show that $\omega$ appears only in the k's with $k = \sqrt{i\omega\rho C_p/K}$ If we change the sign of $\omega$, we change k to k*, which changes $R_1$ to $R_1^*$ and this changes A, B, and C to $A^*$, $B^*$, and $C^*$.

The thermal performance of the building is governed by Eq. (A2.4-22). When transformed back into the time domain, this says that

$$T_R = \int d\omega, \quad \text{or} \quad \sum_n \left( \frac{B(\omega)}{A(\omega)} S(n\omega_f) + \frac{C(\omega)}{A(\omega)} T_A(n\omega_f) + \frac{1}{A(\omega)} H(n\omega_f) \right) \quad \text{(A2.4-24)}$$

where the sum is taken over integral multiples of the fundamental frequency $\omega_f$ or else the integral over all $\omega$ is used. Note that the sum or integral is over all frequencies, both positive and negative.

We can convert to a sum or integral over positive frequencies by noting that since S, $T_A$, and H are real-valued $S(\omega) = S^*(-\omega)$, $T_A(\omega) = T_A^*(-\omega)$, etc. Thus for $\omega_p > 0$, the sum includes the terms $\frac{B}{A}(\omega_p)\, S(\omega_p) + \left(\frac{B}{A}\right)^*(\omega_p)\, S^*(\omega_p)$. These terms add to $2\mathrm{Re}\left(\left(\frac{B}{A}\right)(\omega_\rho) S(\omega_p)\right)$. Thus the sum or integral over only positive frequencies (not including zero frequency) will be exactly half the sum or integral over positive and negative frequencies (also not including $\omega = 0$). So we will take the Fourier transforms of S, $T_A$, and H to be twice their normal values for $\omega \neq 0$ and sum over positive frequencies only.

To show that the $d_n$'s converge quickly, we calculate the first five for $t_d$ = 7 hrs and $t_d$ = 8 hrs.

| $\frac{n}{t_d}$ | 0 | 1 | 2 | 3 | 4 | 5 |
|---|---|---|---|---|---|---|
| 7 | .186 | $.343e^{-.916i}$ | $.266e^{1.833i}$ | $.167e^{-2.748i}$ | $.0601e^{2.618i}$ | $.0065e^{1.702i}$ |
| 8 | .212 | $.382e^{-1.047i}$ | $.272e^{-2.094i}$ | $.141e^{-i\pi}$ | $.0465e^{2.094i}$ | $.0210e^{-2.094i}$ |

As shown in (A2.4-25) for large n, $d_n \propto \frac{1}{n^2}$. Thus we see that truncating the Fourier series at n = 3 will not lead to serious (~10%) error.

The response of the building to the simple diurnal cycle described above is given by

$$T_R(t) = |S_1| \sum_{n=1}^{3} \frac{B(n\omega_o)}{A(n\omega_o)} d_n e^{in\omega_o t} + |S_1| \frac{B(0)}{A(0)} d_o + \frac{C(\omega_o)}{A(\omega_o)} \Delta T_A e^{i\omega_o t} + \bar{T}_A + \frac{H}{A(0)} \qquad \text{(A2.4-26)}$$

where the real part of complex quantities is taken after multiplication. Note again that A(0) is just the steady-state heat loss coefficient for the building.

We have derived the response of the distributed-parameter house to diurnal weather cycles; we next discuss the response to longer-duration weather.

Weather patterns can be Fourier-analyzed into a number of frequencies slower than $\omega_o = 2\pi$/day. We choose one such frequency and call it $\omega_w$ and discuss the response of the building to a design weather

This is derived as follows: $S(t)$ is the product of two functions: an envelope function $F(t) = \bar{S} + \Delta S_w \cos \omega_w t$ and a daily solar gain function $G(t) = \begin{cases} \sin \omega_1 t & \text{day} \\ 0 & \text{night} \end{cases}$. Each of these functions can be written as a Fourier integral: $S(t) = \int_{-\infty}^{\infty} d\omega\ s(\omega)\ e^{i\omega t}$,

$F(t) = \int_{-\infty}^{\infty} d\omega\ f(\omega)\ e^{i\omega t}$, $G(t) = \int_{-\infty}^{\infty} d\omega g(\omega)\ e^{i\omega t}$, with s, t, and g given by $s(\omega) = \frac{1}{2\pi}\int_{-\infty}^{\infty} dt\ S(t)\ e^{-i\omega t}$ and t and g given by analogous expressions. We also know that $g(\omega) = |S| c_n\ \delta(\omega_o n)$ from the daily cycle analysis and that $f(\omega) = \bar{S}\ \delta(0) + \frac{\Delta S_w}{2}\ (\delta(\omega_w) + \delta(-\omega_w))$ from inspection, where $\delta$ is the Dirac delta function.

We are interested in finding $s(\omega)$; we write an expression for it as follows:

$$s(\omega) = \frac{1}{2\pi}\int_{-\infty}^{\infty} S(t)\ e^{-i\omega t}\ dt = \frac{1}{2\pi}\int_{-\infty}^{\infty} F(t)\ G(t)\ e^{-i\omega t}\ dt \qquad \text{(A2.4-28)}$$

We replace $F(t)$ and $G(t)$ by their Fourier expansions:

$$s(\omega) = \frac{1}{2\pi}\int_{-\infty}^{\infty} dt^{-i\omega t} \int_{-\infty}^{\infty} d\omega'\ e^{i\omega' t}\ f(\omega') \int_{-\infty}^{\infty} d\omega''\ e^{i\omega'' t}\ g(\omega'')$$

$$= \frac{1}{2\pi}\int_{-\infty}^{\infty} d\omega'\ f(\omega') \int_{-\infty}^{\infty} d\omega''\ g(\omega'') \int_{-\infty}^{\infty} dt\ e^{i(\omega'+\omega''-\omega)t} .$$

$$= \frac{1}{2\pi}\int_{-\infty}^{\infty} d\omega'\ f(\omega') \int_{-\infty}^{\infty} d\omega''\ g(\omega'') \times 2\pi\ \delta(\omega'+\omega''-\omega)$$

We use the $\delta$-function in the $f(\omega')$ integral to get

$$s(\omega) = \int_{-\infty}^{\infty} d(\omega'')\ f(\omega-\omega'')\ g(\omega'')$$

We have now derived a Fourier-expansion for the weather-varying solar gain function; we next look at how this expansion can be used to calculate $T_R$. We have shown that adding a weather-varying component to $T_A$ simply adds the terms $\Delta T_{A_w} \frac{B(\omega_w)}{A(\omega_w)} e^{i\omega_w t}$ to (A2.4-27). Adding a weather-varying effect onto S(t) will replace the steady-state term $|S_1|\frac{B(0)}{A(0)} d_o$ with the analogous term $\bar{S} \frac{B(0)}{A(0)} d_o$. It will also add a term at frequency $\omega_w$ :

$$\Delta S_w \frac{B(\omega_w)}{A(\omega_w)} d_o e^{i\omega_w t}$$

In addition, it will replace each of the terms

$$|S_1| \frac{B(n\omega_o)}{A(n\omega_o)} d_n e^{in\omega_o t} \text{ with a triplet } \bar{S} \frac{B(n\omega_o)}{A(n\omega_o)} d_n e^{in\omega_o t}$$

$$+ \Delta S_w \frac{d_n}{2} \left( \frac{B(n\omega_o + \omega_w)}{A(n\omega_o + \omega_w)} e^{i(n\omega_o+\omega_w)t} + \frac{B(n\omega_o - \omega_w)}{A(n\omega_o - \omega_w)} e^{i(n\omega_o-\omega_w)t} \right)$$

Since $\frac{B}{A}$ will generally not vary too much with small changes in $\omega$ (note that $\omega_w$ will be about 10% of $n\omega_o$ or less), we can approximate the triplet by $(\bar{S} + \Delta S_w \cos \omega_w t) \frac{B(n\omega_o)}{A(n\omega_o)} d_n e^{in\omega_o t}$, as shown below.

Suppose $\frac{B}{A}$ varies only slowly with $\omega$; so let

$$\frac{B}{A}(\omega_n \pm \omega_w) = \frac{B}{A}(\omega_n)(1 \pm \varepsilon_n) \left( \text{ignoring terms of order } \frac{\partial^2 (B/A)}{\partial \omega^2} \omega_w^2 \right)$$

This equation is useful in evaluating the response of the building to design weather conditions. The design conditions for checking whether the house overheats might be that for $\Delta S_w \cos \omega_w t$ in phase with $\Delta T_{Aw}$, we calculate the response of $T_R$ on the hottest day of the cycle. We then determine the response on the coldest day, for the same weather conditions. These two daily-temperature calculations then bracket the range of performance of the building under all expected weather conditions.

Design weather conditions could be determined in principle from Fourier analysis of real weather data; but such analysis has not been done to present.

The preceding analysis has been done for a "direct gain" building. Extension to include Trombe wall structures is relatively straightforward and is shown below.

Trombe Wall Solution

In this section we show how to include the effects of a Trombe wall. Because of the constraints of the Fourier solution, the Trombe wall must be completely unmanaged in this solution; that is, the degree of thermocirculation from wall surface to room cannot change from day to night, nor can the glazing on the Trombe wall be insulated at night.

We use the same parameters to describe the wall's coupling to the room and to the outside as are used in the lumped parameter model, Appendix 2.3. The Trombe wall surface is coupled to the channel air through the film heat transfer coefficient $\hat{h}_{Tc}$. The channel air is then coupled to the ambient air by $\hat{U}_{cA}$. which describes heat loss through the collector glazing; it is also coupled convectively to the

Note that we have made the approximation of one-dimensional heat flow — that there is no temperature variation from bottom to top in the Trombe wall or air channel. In fact, temperature gradients will exist; however, they will not be important unless they affect the heat transfer coefficients $\hat{h}_{Tc}$, $\hat{U}_{TR}$, etc. If these heat transfers are really linear, then by the arguments of the previous section we can take $T_{\hat{c}}$, $T_T$, and $T_{int}$ to be averages over all heights and the solution will not be affected.

The diffusion equation is solved by

$$T_T(x,t) = A_T \cosh k_T d_T (1-\xi) + B_T \sinh k_T d_T (1-\xi) \qquad \text{(A2.4-34)}$$

where $\xi = x/d_T$.

Since $T_{int}$ is the rear surface temperature of the Trombe wall, $T_T(x = d_T,t) = T_{int}$. Then by (A2.4-33), $B_T = \dfrac{\hat{U}_{TR}}{A_T K_T k_T} (A_T - T_R)$ so that

$$T_T(x,t) = T_{T_\omega} \left( \cosh k_T d_T(1-\xi) + \frac{(T_{T_\omega} - T_R)\, \hat{U}_{TR}}{A_T K_T k_T} \sinh k_T d_T(1-\xi) \right) \qquad \text{(A2.4-35)}$$

where $T_{T_\omega} \equiv A_T$.

Before we substitute this into (A2.4-32), we eliminate $T_c$ using the channel heat balance (A2.3-20); then using (A2.4-35) for $T_T$ and its derivatives; we find that

Note that $R_{1T}$ and $R_{2T}$ have exactly the same form as (A2.4-21) for $R_{1e}$ and $R_{2e}$ except that $U_{TR}$ replaces $\frac{1}{R_e}$. This replacement is a matter of definition only; both $U_{TR}$ and $\frac{1}{R_e}$ are the conductances away from the back wall surface.

This completes the derivation of Trombe wall surface temperature as a function of materials properties; we use the result in the room heat balance to obtain the solution for room temperature. The room heat balance is slightly altered to take into account the Trombe wall; instead of A2.4-7, we have:

$$\hat{h}_e\left(T_R - T_e(0,t)\right) + \hat{h}_p\left(T_R - T_p(0,t)\right) + \hat{h}_f\left(T_R - T_f(0,t)\right) + \hat{U}_q(T_R - T_A) + \hat{U}_{cR}(T_R - T_c) + \hat{U}_{TR}(T_R - T_{int}) = \alpha_R S + H \tag{2.4-38}$$

This equation is the same as (A2.4-7) except for the addition of the last two terms on the left-hand side. We can write these terms as

$$(\hat{U}_{cR} + \hat{U}_{TR})T_R - \hat{U}_{cR}\left(\frac{\hat{U}_{cA}}{\hat{\Sigma}} T_A + \frac{\hat{U}_{cR}}{\hat{\Sigma}} T_R + \frac{\hat{h}_{Tc}}{\hat{\Sigma}} T_T(x=0)\right)$$

$$-\hat{U}_{TR}\left(\frac{\hat{U}_{cA}\hat{h}_{Tc}}{\hat{\Sigma}} \frac{1}{D_T} T_A + \frac{\alpha_T}{D_T} S + T_R \frac{1}{D_T}\left(\hat{U}_{TR}\cosh k_T d_T + \frac{\hat{U}_{TR}\hat{U}_a}{A_T K_T k_T} \sinh k_T d_T + \frac{\hat{U}_{cR}\hat{h}_{Tc}}{\hat{\Sigma}}\right)\right)$$

using (A2.3-20) for $T_c$ and (A2.4-36) for $T_{int} = T_{T\omega}$. Then with (A2.4-37) for $T_T(x=0)$, we can derive the relationship between $T_R$, $T_A$, S, and H as:

So for a Trombe wall building, we use (A2.4-39) above in place of (A2.4-22) to derive $A(\omega)$, $B(\omega)$, and $C(\omega)$; the $T_R(t)$ equations (A2.4-26 and 30) still are valid with these new A, B, and C functions.

For a non-convecting Trombe wall ($\hat{U}_{cR} = 0$), these expressions simplify considerably, and the A, B, and C functions of (A2.4-39) compare to the earlier form (A2.4-22) as follows:

$$A(\omega) = (\ldots. \text{ old terms } \ldots. + \hat{U}_{TR}\ (1-U_{TR}\ R'_{1T}))$$

$$B(\omega) = (\ldots. \text{ old terms } \ldots. + \alpha_T\ R_{2T}) \qquad \text{(A2.4-40)}$$

$$C(\omega) = \left(\ldots. \text{ old terms } \ldots. + \frac{\hat{h}_{Tc}\ \hat{U}_{cA}}{\hat{h}_{Tc} + \hat{U}_{cA}}\ R_{2T}\right)$$

These are not quite analogous to the forms for interior walls, due to the appearance of $R'_{1T}$ in $A(\omega)$ instead of $R_{1T}$, and due to the use of $R_{2T}$ in $B(\omega)$ rather than $R_{1T}$. However, the new term in $C(\omega)$ is analogous to that for an envelope wall.

All the material derived above for Trombe walls works equally well for water walls, with the lumped response functions (A2.4-21a) replacing the continuum functions (A2.4-37).

We also have continuity of temperature at the interface (e.g. perfect thermal contact) or

$$T_1(d_1) = T_2(0) \tag{A2.4-44}$$

Finally, we have perfect thermal contact between the outside surface of layer 2 and the outside air.

$$T_2(d_2) = T_A \tag{A2.4-45}$$

Using (A2.4-41) in (A2.4-45) we see that $C = T_A$. Then (A2.4-42) requires that

$$S' = A(h \cosh k_1d_1 + K_1k_1 \sinh k_1d_1) + B(h \sinh k_1d_1 + K_1k_1\cosh k_1d_1) \tag{A2.4-46}$$

while (A2.4-42) says that

$$K_1k_1B = K_2k_2T_A \sinh k_2d_2 + K_2k_2D \cosh k_2d_2 \tag{A2.4-47}$$

Finally, from (A2.4-44), we get

$$A = T_A \cosh k_2d_2 + D \sinh k_2d_2 \tag{A2.4-48}$$

We solve the last of these equations for D and use the result in (A2.4-47) to express B in terms of A and $T_A$. This result is then used in (A2.4-46) to obtain the following expressions for A and B:

$$A = \frac{S}{D_{en}} + \frac{T_A}{D_{en}}\left(K_2k_2 \frac{\cosh k_2d_2}{\sinh k_2d_2} + \frac{K_2k_2}{K_1k_1} h \frac{\sinh k_1d_1}{\sinh k_2d_2}\right) \tag{A2.4-49}$$

Radiative Coupling Solution

In this section we derive the modifications necessary to precisely calculate convection and radiation exchanges within a building. Previously, we assumed that each material surface was in thermal contact with the room air through a coupling coefficient $\hat{h}$ which combined the effects of convection and radiation.

In this section, we model the more realistic case where the surface j is coupled to the air through the convective coefficient $\hat{h}'_j$, and is also coupled to each other surface i through the coefficient $\hat{h}_{ij}$. This radiation coefficient includes a geometric form factor.

The surface heat balance for the $j^{th}$ surface is then modified to read:

$$\hat{h}'_j \; T_R + \alpha_j \; S + \sum_{\substack{i=1 \\ i\neq j}}^{N} \hat{h}_{ij} \; T_{si} - \hat{h}'_j \; T_{sj} - \sum_{\substack{i=1 \\ i\neq j}}^{N} \hat{h}_{ij} \; T_{sj} - A_j K_j \left.\frac{\partial T_j}{\partial x}\right|_{x=0} = 0 \qquad \text{(A2.4-51)}$$

where $T_{sj}$ is the temperature of the $j^{th}$ surface and N is the number of material surfaces in the building.

We can simplify the notation somewhat if we define $\hat{h}'_j \equiv \hat{h}_{jj}$ and

$$\sum_{i=1}^{N} \hat{h}_{ij} \equiv \hat{h}_{j,tot}.$$

Then we have

$$\hat{h}_{jj} \; T_R + \alpha_j \; S + \sum_{\substack{i=1 \\ i\neq j}}^{N} \hat{h}_{ij} \; T_{si} - \hat{h}_{j\,tot} \; T_{sj} - A_j K_j \left.\frac{\partial T_j}{\partial x}\right|_{x=0} = 0 \qquad \text{(A2.4-52)}$$

$$\underset{\sim}{T}_s = \underset{\sim}{T}_{eq} + \underset{\approx}{M}\,\underset{\sim}{T}_s \tag{A2.4-55}$$

where $\underset{\sim}{T}_{eq}$ is a column vector whose $j^{th}$ component is

$$R_{1j}(h_{jj}\,T_R + \bar{\alpha}_j\,S) + R_{2j}\,T_A$$

and $\underset{\approx}{M}$ is an $N \times N$ matrix whose $ij^{th}$ component is

$R_{1j}\,h_{ij}$ and whose diagonal elements are all zero.

Solving (A2.4-55) formally, we have

$$\underset{\sim}{T}_s = (\underset{\approx}{1} - \underset{\approx}{M})^{-1}\,\underset{\sim}{T}_{eq} \tag{A2.4-56a}$$

where $\underset{\approx}{1}$ is the $N \times N$ identity matrix; or

$$T_{sj} = \sum_{i=1}^{N} \left\{(\underset{\approx}{1} - \underset{\approx}{M})^{-1}\right\}_{ji} \left\{R_{1i}(h_{ii}\,T_R + \bar{\alpha}_i\,S) + R_{2i}\,T_A\right\} \tag{A2.4-56b}$$

Let $\underset{\approx}{L} \equiv (\underset{\approx}{1} - \underset{\approx}{M})^{-1}$ ; then we can write (A2.4-54) as

$$T_R\left\{\hat{U}_q + \sum_{j=1}^{N} \hat{h}_{jj}\,(1 - \sum_{i=1}^{N} L_{ji}\,h_{ii}\,R_{1i})\right\}$$

$$S\left\{\sum_{j=1}^{N}\sum_{i=1}^{N} h_{jj}\,L_{ji}\,\alpha_i\,R_{1i}\right\}$$

$$+\,T_A\left\{\hat{U}_q + \sum_{j=1}^{N} \hat{h}_{jj} \sum_{i=1}^{N} L_{ji}\,R_{2i}\right\}$$

$$+\,H \tag{A2.4-57}$$

## APPENDIX 2.5A: Simulating Distributed Walls with Lumped Parameters

Fourier transform techniques allow the exact solution of the passive solar house model for distributed walls. However, these techniques are practical only in those cases where the parameters of the house are not time-dependent. For time-dependent parameters, such as night insulation of the windows, it is much simpler to solve the model using lumped parameters. This section discusses the derivation of lumped parameters which approximate the behavior of a distributed wall.

The most important elements of the house to model are those which receive and store solar energy (e.g. a slab floor). At the surface of the massive solar receiver, the temperature $T_S$ will be determined by a heat balance between solar gain, convection/radiation to the room, and diffusion into the receiver. Call the receiver a "floor" although the analysis would be the same if it were a wall. The heat balance of the surface is given by

$$A_f K_f \left.\frac{\partial T_f(z,t)}{\partial z}\right|_{z=0} + \alpha_f S + \hat{h}_f (T_R - T_S) = 0 \qquad \text{(A2.5A-1)}$$

where
- $A_f$ is the area of the floor
- $K_f$ is the conductivity of the floor
- $\hat{h}_f$ is the floor surface film coefficient times the floor area
- $T_R$ is the room temperature
- $T_S$ is the floor surface temperature
- $\alpha_f S$ is the solar gain on the floor (in Btu $h^{-1}$ or W)
- $z$ is the distance into the floor material

In a lumped model, this heat balance is given by

lumped parameters which allow $R_1$ and $R_2$ to be approximately the same over the relevant range of frequencies.

"The relevant range of frequencies" is from $\omega = 0$ to $\omega \approx 2\pi/1$ day $\times$ 3. The lower limit is important because there is a fairly large DC component (or at least yearly component) to the response of the house. The fundamental frequency for solar gain and ambient temperature is usually one day, while the first few harmonics are necessary to describe day and night solar gain conditions.

We will discuss several cases of walls to be modeled. The simplest case is the single-layer wall of finite thickness. We then model a semi-infinite wall. The results for the semi-infinite wall are extended to cover moderately thick walls. The moderately thick wall solution will be compared to the thin-wall solution.

We next discuss insulated walls: that is, walls of a homogeneous material with nonzero heat capacity covered by a pure insulator. There are two cases of interest: insulation outside (e.g. concrete block with exterior foam insulation) and insulation inside (e.g. carpeted slab floors). In addition, we look at simulations for interior walls. To avoid complication we model each element (floor, walls, etc.) separately; that is, we do not consider the properties of the walls in choosing the lumped parameters for the floor. The validity of this approach is demonstrated by the form in which the response functions $R_1$ and $R_2$ appear in (A2.4-22); each element enters independently.

Using expression (A2.5A-5b) for B, we obtain the result that

$$T_S = R_1 \bar{\alpha}_f S + R_2 T_A + R_1 (h_f T_R) \qquad \text{(A2.5A-6a)}$$

The last term in this expression comes about because when we look at only one heavy material, the room temperature is indeterminate and must be considered as a separate independent excitation. This is not a problem since the response of $T_S$ to $T_R$ is given by the function $h_f R_1$ which is proportional to $R_1$; thus if we match $R_1$ correctly in the lumped and distributed models, we have automatically modeled the response to $T_R$ correctly.

It should be noted that $R_1$ is <u>not</u> the response of the surface temperature $T_S$ to solar gain, since solar gain affects $T_S$ indirectly through $T_R$ as well as directly. $R_1$ is the response of $T_S$ to a unit heat flux input on the inside. For this particular case, the heat flux is given by $h_f T_R + \bar{\alpha}_f S$, but $R_1$ characterizes the surface temperature's response to <u>any</u> heat flux on the surface, just as $R_2$ characterizes the response to temperature input on the <u>opposite</u> surface.

In obtaining (A2.5A-6a) we find that

average of $T_f(z,t)$; thus it cannot be measured or compared to anything in the continuum model or in the real world. It should, however, lead to the correct values of $T_S$ and other measurable quantities.

Solving (A2.5A-7) and (A2.5A-2) in Fourier transform space, we get

$$\tilde{T}_f(i\omega C_f + \hat{U}_i + \hat{U}_o) = \hat{U}_i \tilde{T}_S + \hat{U}_o \tilde{T}_A \qquad \text{(A2.5A-8a)}$$

$$-\hat{U}_i \tilde{T}_f + (\hat{h}_f + \hat{U}_i)\tilde{T}_S = \overline{\alpha}_f \tilde{S} + \hat{h}_f \tilde{T}_R \qquad \text{(A2.5A-8b)}$$

Solving this gives

$$\tilde{T}_S = \frac{\hat{U}_o + \hat{U}_i + i\omega C_f}{(\hat{U}_o + \hat{U}_i + i\omega C_f)(\hat{h}_f + \hat{U}_i) - \hat{U}_i^2} (\hat{h}_f \tilde{T}_R + \alpha_f \tilde{S}) + \frac{\hat{U}_i \hat{U}_o}{(\hat{U}_o + \hat{U}_i + i\omega C_f)(\hat{h}_f + \hat{U}_i) - \hat{U}_i^2} \tilde{T}_A \qquad \text{(A2.5A-9a)}$$

We can identify the first coefficient as the lumped version of $R_1$ and the second as the lumped version of $R_2$. That is, writing (A2.5A-9a) for a unit area of floor,

$$R_{1_\ell} = \frac{U_i + U_o + i\omega \overline{C}_f}{(U_i + U_o + i\omega \overline{C}_f)(h_f + U_i) - U_i^2} \qquad \text{(A2.5A-9b)}$$

$$R_{2_\ell} = \frac{U_i U_o}{(U_i + U_o + i\omega \overline{C}_f)(h_f + U_i) - U_i^2} \qquad \text{(A2.5A-9c)}$$

where $\overline{C}_f = C_f/A_f$.

To sum up, we have derived an expression for the Fourier transform of the inside receiver surface temperature $\tilde{T}_S$ in terms of the driving functions $\tilde{T}_A$ and $\tilde{S}$. We have done this for both the continuum and the lumped models. We next attempt to find values of $\hat{U}_o$, $\hat{U}_i$, and $C_f$ which

where $p_n$ is the $n^{th}$ solution of $\tan p_n = -p_n K_f/dh_f$.

The numerator of $R_{2_c}$ is a constant, while the denominator of $R_{2_c}$ is the same as the denominator of $R_{1_c}$: thus we get no new poles or zeros from looking at $R_{2_c}$.

To make use of (A2.5A-10) in choosing $U_i U_o$ and $C_f$, we approximate the exact function $R_1$ by following three rules:

1) The steady-state conductance $\left((U_i)^{-1} + (U_o)^{-1}\right)^{-1}$ is equal to the steady-state conductance in the continuum model ($K_f/d$). This ensures that the limit of $R_1$ and $R_2$ as $\omega \to 0$ is the same in both models.
2) The <u>first pole</u> of the continuum $R_1$ occurs at the same frequency as the only pole of the lumped $R_1$.
3) The <u>first zero</u> of the continuum $R_1$ occurs at the same frequency as the only zero of the lumped $R_1$.

These conditions say that the truncated product for $R_1$ will approximate the exact function for $R_1$, if they agree for $\omega = 0$ and if the interesting range of $\omega$ ($0 \leq \omega \lesssim 3 \times 2\pi/\text{day}$) is smaller than the second pole or zero of the expansion. If $\omega << p_2$ and $z_2$ we say the wall is "thin." If $\omega \gtrsim p_2$ and $z_2$ then the approximation breaks down and we treat the wall as "thick" (see the section on thick walls for numerical definitions of thick and thin).

This can be understood intuitively in the following way: If a function F of a complex $\omega$ has an isolated pole at $\omega = \omega_p$ on the positive imaginary $\omega$ axis, then a graph log F vs. log $\omega$ will be approximately constant for $\omega << \omega_p$ and will have a derivative of -1 for $\omega >> \omega_p$. If it has an isolated zero at $\omega = \omega_z$, it will be constant for $\omega << \omega_z$ and have a

$$\hat{U}_i = \frac{\pi^2}{p_1^2}\frac{A_f K_f}{d} + \left(\frac{\pi^2}{p_1^2} - 1\right)\hat{h}_f \qquad \text{(A2.5-12a)}$$

$$\hat{U}_o = \frac{\frac{A_f^2 K_f^2}{d} + \left(1 - \frac{p_1^2}{\pi^2}\right)(K_f A_f)\hat{h}_f}{\left(1 - \frac{p_1^2}{\pi^2}\right)\left(K_f A_f + d\hat{h}_f\right)} \qquad \text{(A2.5-12b)}$$

$$C_f = \frac{d^2 \rho c_p (\hat{U}_i + \hat{U}_o)}{\pi^2 K_f} = \frac{(U_i + U_o)}{U_f}\frac{1}{\pi^2} C_{fo} \qquad \text{(A2.5-12c)}$$

where $C_{fo}$ is the bulk heat capacity $\rho C_p dA_f$. Note that these are expressed in terms of the extensive parameters $\hat{h}_f$ and $A_f K_f$, and are proportional to area.

We look at the limiting behavior of these quantities as $d \to 0$ (thin wall/floor)

$$U_i \to 4\frac{K_f}{d} = 4U_f$$

where $U_f$ is the steady-state "U"-value of the floor

$$U_o \to 4/3\ U_f$$

Thus the wall has the correct static U-value, but 3/4 the resistance is on the outside and only 1/4 on the inside.

$$C_f \to \frac{16\ A_f d \rho c_p}{3\pi^2} = \frac{16}{3\pi^2} C_{fo} \cong 0.540\ C_{fo}$$

where $C_{fo}$ is the static heat capacity of the floor $(=(dA_f)(\rho c_p))$.

For thick walls, $d \to \infty$ and $p_n \to \pi$,

$$\hat{U}_i \to \frac{A_f K_f}{d} = U_f A_f \to 0$$

The agreement between the exact $R_1$ and $R_2$ and the simulated functions for 4-inch wood is shown in Fig. 2.8 and Table 2.5. As seen, the agreement is good, despite the fact that 4 inches of wood is not especially thin. For 2-inch concrete the agreement is even better, as shown in Table 2.4

For thicker walls, the method starts to break down. Tables 2.6 and 2.8 show $R_1$ and $R_2$ for two simulation techniques. In the pole-and-zero method $|R_1|$ is 20% off for $\omega = 2\pi/\text{day}$ and 50% off for $\omega = 2\pi/8$ hrs. $|R_2|$ is even less accurate. Finally, for a 20-foot concrete wall (or 20 feet of concrete slab floor plus dry soil) the agreement is very poor (Table A2.5-1).

Semi-Infinite and Thick Walls

As we approach the limit of the semi-infinite wall, a large number of poles and zeroes occur at low frequencies, so the pole-and-zero approach is useless. Instead we choose $\hat{U}_i$ and $C_f$ ($\hat{U}_o$ is now zero) in such a way that $R_1$ is exactly the same in lumped and continuum models at a particular frequency. The frequency at which the match occurs is arbitrary; we choose $\omega = 2\pi/\text{day}$ for the match frequency because most of the spectrum of the driving functions (sunlight and ambient temperatures) occur at or near this frequency.

We now calculate $R_1$ for the continuum and lumped models. For the continuum model, the diffusion equation is solved by $\tilde{T}(\omega,z) = \tilde{T}_s e^{-k_f x}$ for a semi-infinite wall. Then the heat balance equation (A2.5-1) says

$$-A_f K_f k_f \tilde{T}_s + \hat{h}_f \tilde{T}_R + \alpha_f \tilde{S} - \hat{h}_f \tilde{T}_s = 0$$

or

$$\tilde{T}_s = \frac{1}{\hat{h}_f + K_f k_f A_f} (\hat{h}_f T_R + \alpha_f \tilde{S})$$

so

This models the semi-infinite slab as being equivalent to a finite-thickness penetration depth. The heat capacity is equal to that of one penetration depth of material (penetration depth = $\sqrt{2}/k_f$), while $\hat{U}_i$ is equal to the heat transfer coefficient for one-half a penetration depth. (The penetration depth is for a frequency $\omega = 2\pi/\text{day}$.)

The semi-infinite model is not useful by itself, since real walls have finite thickness. However, it can be extended to finite walls by letting $\hat{U}_o$ have nonzero value.

We know in the limit of $\omega \to 0$ that the heat transfer coefficient of a thick slab of homogeneous material is $K_f/d$. We also know that $R_1$ and $R_2$ should have the same steady-state behavior in the simulation as in the exact solution since a significant part of the driving forces occur at zero frequency. Therefore we set the value of $U_o$ such that $\left((\hat{U}_o)^{-1} + (\hat{U}_i)^{-1}\right)^{-1} = A_f K_k/d$ where $\hat{U}_i$ is obtained from the semi-infinite model.

To reiterate, for thick walls, we set

$$\hat{U}_i = \sqrt{2}\, A_f K_f\, |k_f| \qquad \text{(A2.5A-20a)}$$

$$C_f = \frac{\sqrt{2}\,\rho c_p A_f}{|k_f|} \qquad \text{(A2.5A-20b)}$$

$$\hat{U}_o = \left(\left(\frac{A_f K_f}{d}\right)^{-1} - (\hat{U}_i)^{-1}\right)^{-1} \qquad \text{(A2.5A-20c)}$$

This assures that $R_{1\,\text{lumped}}$ and $R_{2\,\text{lumped}}$ have the same limit as $\omega \to 0$ as the continuum response functions.

Table 2.9 and Fig. 2.9 for 20-ft (or semi-infinite) concrete walls, and Table 2.8 and Fig. 2.9 for 1½-ft concrete walls illustrate how well the

the others. Thus we can divide the range of material thickness into two regions:

1) Walls thinner than the thickness at which the two techniques produce equal parameter values,

2) Walls thicker than this.

From the tables we see that the dividing point between thick and thin wall is 5 to 6 inches for wood and 10 inches for concrete. This dividing point is logical for another reason. The semi-infinite model shows that only a finite amount of heat capacity is effective no matter how thick the material is. It is unreasonable to simulate a finite-thickness wall using a larger value of $C_f$ than for a semi-infinite wall.

Thus, a reasonable decision-rule seems to be to use the pole-and-zero approach when it produces a heat capacity less than $\sqrt{2}\ \rho c_p A_f / |k_f|$ and to use the thick-wall method otherwise. At the dividing point it should make little difference which method is used since they apparently produce approximately the same results for $\hat{U}_i$ and $\hat{U}_o$.

To show that the two methods should describe all walls, we note that the semi-infinite approximation should work well when the wall is thicker than the penetration depth: when

$$d \gtrsim \sqrt{\frac{2K_f}{\omega_o \rho c_p}}$$

where $\omega_o = 2\pi/\text{day}$. Sonderegger[1] says that the pole-and-zero approach is within 10% for $\omega RC < 10$, where $C = \rho c_p d$ and $R = d/K_f$. This condition says

$$d < \sqrt{\frac{10K_f}{\rho c_p \omega}} \quad .$$

$$-A_f K_f \left.\frac{\partial T_f}{\partial z}\right|_{z=d} = \hat{U}_r (T_{int} - T_A) \qquad \text{(A2.5A-21a)}$$

$$T_f(z=d) = T_{int} \qquad \text{(A2.5A-21b)}$$

and

$$A_f K_f \left.\frac{\partial T_f}{\partial z}\right|_{z=0} + \alpha_f S + \hat{h}_f (T_R - T_S) = 0 \qquad \text{(A2.5A-1)}$$

where $T_{int}$ is the temperature of the resistance/continuum interface

$\hat{U}_r$ is the heat transfer coefficient of the resistance.

Using the equation for $T_f$ in these three boundary conditions, and recalling that $T_s = T_f(z=0)$, we get

$$A_1 = T_A \frac{U_r \cosh k_f d + \frac{U_r h_f}{K_f k_f} \sinh k_f d}{D} + (h_f T_R + \bar{\alpha}_f S) \frac{1}{D} \qquad \text{(A2.5A-22a)}$$

$$B_1 = T_A \times \left( \frac{\frac{U_r h_f}{K_f k_f} \cosh k_f d + U_r \sinh k_f d}{D} \right) + (h_f T_R + \bar{\alpha}_f S) \frac{U_r}{K_f k_f} \frac{1}{D} \qquad \text{(A2.5A-22b)}$$

where $D = (U_r + h_f)\cosh k_f d + \left( K_f k_f + \frac{U_r h_f}{K_f k_f} \right) \sinh k_f d$ .

We set $T_s = T_f(z=0)$ and solve for $R_1$ and $R_2$. The result is

$$R_1 = \frac{\cosh k_f d + \frac{U_r}{K_f k_f} \sinh k_f d}{(U_r + h_f)\cosh k_f d + \left( K_f k_f + \frac{U_r h_f}{K_f k_f} \right) \sinh k_f d} \qquad \text{(A2.5A-23a)}$$

be the same. This requires

$$\frac{1}{\hat{U}_o} + \frac{1}{\hat{U}_i} = \frac{d}{A_f K_f} + \frac{1}{\hat{U}_r} \qquad \text{(A2.5A-26a)}$$

$$-\frac{p_1^2 K_f}{\rho c_p d^2} = \frac{1}{C_f}\left(\frac{\hat{U}_i}{\hat{h}_f + \hat{U}_i} - [\hat{U}_o + \hat{U}_i]\right) \qquad \text{(A2.5A-26b)}$$

$$-\frac{z_1^2 K_f}{\rho c_p d^2} = -\frac{1}{C_f}(\hat{U}_o + \hat{U}_i) \qquad \text{(A2.5A-26c)}$$

These are similar in form to (A2.5A-11a,b,c,), and have similar solutions:

$$\hat{U}_i = \frac{z_1^2}{p_1^2}\frac{A_f K_f}{d\hat{U}_r + A_f K_f}\hat{U}_r + \left(\frac{z_1^2}{p_1^2} - 1\right)\hat{h}_f \qquad \text{(A2.5A-27a)}$$

$$\hat{U}_o = \left(\frac{d}{A_f K_f} + \hat{U}_r^{-1} + \hat{U}_i^{-1}\right)^{-1} \qquad \text{(A2.5A-27b)}$$

$$C_f = \frac{d^2 \rho c_p (\hat{U}_i + \hat{U}_o)}{z_n^2 K_f} \qquad \text{(A2.5A-27c)}$$

For the thick wall case, we use the same values (A2.5A-20a,b) for $\hat{U}_i$ and $C_f$ and use (A2.5A-26a) to solve for $\hat{U}_o$:

$$\hat{U}_o = \left\{\left(\frac{A_f K_f}{d}\right)^{-1} + \hat{U}_r^{-1} - \hat{U}_i^{-1}\right\}^{-1}$$

Then conservation of energy at the interface gives us

$$\hat{U}_c(T_S - T_{int}) = - A_f K_f \left.\frac{\partial T_f}{\partial z}\right|_{z=0} \qquad \text{(A2.5A-29)}$$

also

$$T_{int} = T_f(z=0) \qquad \text{(A2.5A-30a)}$$

$$T_A = T_f(z=d) \qquad \text{(A2.5A-30b)}$$

$T_f$ solves the diffusion equation, and is given by

$$T_f(z) = A_2 \cosh k_f d\left(1 - \frac{z}{d}\right) + B_2 \sinh k_f d\left(1 - \frac{z}{d}\right)$$

Equation (A2.5A-30b) requires that $A_2 = T_A$. Using this expression for $T_f$ in (A2.5A-29) and (30a) gives two equations in two unknowns ($B_2$ and $T_s$). These are solved by

$$B_2 = T_A\left(\frac{\left(\frac{U_c}{h_f + U_c} - 1\right)\cosh k_f d - \frac{K_f k_f}{U_c}\sinh k_f d}{D}\right) + (h_f T_R + \bar{\alpha}_f S)\frac{1}{(h_f + U_c)D} \qquad \text{(A2.5A-31)}$$

where

$$D = \frac{K_f k_f}{U_c}\cosh k_f d + \frac{h_f}{h_f + U_c}\sinh k_f d$$

$$T_S = \frac{K_f k_f}{(h_f + U_c)D}\,T_A + \frac{\frac{K_f k_f}{U_c}\cosh k_f d + \sinh k_f d}{(h_f + U_c)D}(h_f T_R + \bar{\alpha}_f S) \qquad \text{(A2.5A-32)}$$

So we conclude that the continuum version of $R_1$ is given by

the same form irrespective of whether the real wall is insulated; only the values of $\hat{U}_i$ and $\hat{U}_o$ and $C_f$ change. The results are

$$\hat{U}_i = \frac{z_1^2}{p_1^2} \frac{A_f K_f}{A_f K_f + d\,\hat{U}_c} \hat{U}_c + \left(\frac{z_1^2}{p_1^2} - 1\right) \hat{h}_f \qquad \text{(A2.5A-34a)}$$

$$\hat{U}_o = \frac{\hat{U}_i^2}{\left(1 - \frac{p_1^2}{z_1^2}\right)(\hat{h}_f + \hat{U}_i)} - \hat{U}_i \qquad \text{(A2.5A-34b)}$$

$$C_f = \frac{d^2 \rho c_p (\hat{U}_i + \hat{U}_o)}{z_1^2 \; K_f} \qquad \text{(A2.5A-34c)}$$

These are the same as (A2.5A-26abc) with different values of $z_1$ and $p_1$ and with $\hat{U}_c$ replacing $\hat{U}_r$.

A thick-wall model would set $\hat{U}_i = \left\{\left(\sqrt{2}\, A_f K_f |k_f|\right)^{-1} + (\hat{U}_c^{-1})\right\}^{-1}$

and $\hat{U}_o = \left(\frac{d}{A_f K_f} + \hat{U}_i^{-1}\right)^{-1}$. (A2.5A-35)

Again, the switch between pole-zero and semi-infinite models is done whenever d is so large that $C_{p.z.} > C_{s.i.}$ Table A2.5-3 shows the response functions for a carpeted concrete floor, compared to a bare floor. Note the drastic difference in shape between the response function for bare concrete, which drops with frequency as $\omega \gtrsim 2\pi/2$ days, while the carpeted response function is nearly frequency independent. Results are tabulated in Table A2.5-4.

For the lumped case, $R_1 = \dfrac{U_i + i\omega\bar{C}_f}{(h_f+U_i)(U_i+i\omega\bar{C}_f) - U_i^2}$ as before.

In this case there are only two match conditions, first pole and first zero, since the steady-state conduction is zero. The conditions are:

$$\frac{-p_1^2 K_p}{\rho c_p d^2} = -\frac{1}{C_f}\,\frac{\hat{h}_f\hat{U}_i}{\hat{h}_f+\hat{U}_i} \qquad \text{(A2.5A-38a)}$$

$$-\frac{\pi^2 K_f}{4\rho c_p d^2} = -\frac{\hat{U}_i}{C_f} \qquad \text{(A2.5A-38b)}$$

The solution is:

$$\hat{U}_i = \hat{h}_f\left(\frac{\pi^2}{4p_1^2} - 1\right) \qquad \text{(A2.5A-39a)}$$

$$C_f = \frac{4\hat{U}_i \rho c_p d^2}{\pi^2 K_f} \qquad \text{(A2.5A-39b)}$$

Note that this solution is the same as that for an outside-insulated envelope wall in the limit that $\hat{U}_r \to 0$ (perfect insulation).

Trombe wall lumped parameters

Modelling a Trombe wall differs from the previous models for envelope walls in three ways. First, the surface heat balance involves the channel air temperature instead of the room temperature. That is, Eq. (A2.3-17) is used as the surface heat balance in place of (A2.3-16) or (2.1). Second, the back-side-of-material boundary condition involves room temperature rather than ambient temperature. Third, the back-side boundary condition is not perfect thermal contact but rather coupling through a film coefficient.

We discuss next how these changes affect the process of evaluating lumped parameters, and how the accuracy of the lumped model is impaired. We focus the discussion on the thick wall model, since most distributed Trombe walls are "thick".

Since the basic equations differ, we must rederive the lumped and distributed response functions from scratch. We first consider the continuum case.

The solution to the diffusion equation is

$$T_w(x,\omega) = A_4 \cosh k_w d(1 - \frac{x}{d}) + B_4 \sinh k_w d(1 - \frac{x}{d}) \qquad \text{(A2.5A-39)}$$

The outside boundary condition is similar to that given in the "insulation outside" case (A2.5A-21):

$$-A_w K_w \frac{\partial T_w}{\partial x}\bigg|_{x=d} = \hat{U}_{wR}(T_{int}-T_R)$$

where $\hat{U}_{wR}$ is the film coefficient coupling the back of the Trombe wall to the room air (Btu/deg-h)

and $T_{int}$ is the back surface temperature of the wall

Using (A2.5A-40) on this equation, and rearranging terms we find that

$$A_4 = T_R \frac{U_{wR} \cosh k_w d + \frac{U_a U_{wR}}{K_w k_w} \sinh k_w d + \frac{h_{wc} U_{cR}}{\Sigma}}{D}$$

$$+ \bar{\alpha}_w S \frac{1}{D} + T_A \frac{h_{wc} U_{cA}}{\Sigma} \frac{1}{D} \qquad \text{(A2.5A-43a)}$$

$$B_4 = -T_R \left( \frac{\frac{U_a U_{wR}}{K_w k_w} \cosh k_w d + U_{wR} \sinh k_w d - \frac{h_{wc} U_{cR}}{\Sigma} \frac{U_{wR}}{K_w k_w}}{D} \right) \qquad \text{(A2.5A-43b)}$$

$$+ \bar{\alpha}_w S + \frac{h_{wc} U_{cA}}{\Sigma} T_A \frac{U_{wR}}{K_w k_w} \frac{1}{D}$$

where $D = (U_a + U_{wR}) \cosh k_w d + \left( K_w k_w + \frac{U_a U_{wR}}{K_w k_w} \right) \sinh k_w d$ .

We note that $T_{ws} = A_4 \cosh k_w d + B_4 \sinh k_w d$; thus the previous equation shows that

$$T_{ws} = T_R \left( \frac{U_{wR} + \frac{h_{wc} U_{cR}}{\Sigma} \left( \cosh k_w d + \frac{U_{wR}}{K_w k_w} \sinh k_w d \right)}{D} \right) \qquad \text{(A2.5A-44)}$$

$$+ \left( \bar{\alpha}_w S + \frac{h_{wc} U_{cA}}{\Sigma} T_A \right) \left( \frac{\cosh k_w d + \frac{U_{wR}}{K_w k_w} \sinh k_w d}{D} \right)$$

This can be expressed as linear sums of the response functions $R_1$ and $R_2$ for insulated walls given in (A2.5A-23) with $U_{wR}$ replacing $U_r$, $U_a$ replacing $h_f$ and wall subscripts replacing floor subscripts. Written in this fashion, we have

Using (A2.5A-9) for the lumped response functions, we find that we can express the surface temperature as

$$T_{ws} = R_1\left(\bar{\alpha}_w S + \frac{h_{wc}U_{cA}}{\Sigma} T_A\right) + \left(\frac{h_{wc}U_{cR}}{\Sigma} R_1 + R_2\right) T_R \qquad \text{(A2.5A-48)}$$

in the lumped model; note that this is precisely the same form as that given in (A2.5A-45) for the distributed parameter model. Thus the Trombe wall response functions are just linear combinations of the envelope wall response functions, and the same matching procedures should work, (again using $U_{wR}$ instead of $U_r$ and $U_a$ instead of $h_f$).

However, one new problem crops up. While the response function coupling $T_{ws}$ with $T_A$ was relatively unimportant for an envelope wall (being relatively small in magnitude and in parallel with much larger couplings) the Trombe response function coupling $T_{ws}$ and $T_R$ is important. This is because the coupling works in both directions; we are concerned with how $T_{ws}$ affects $T_R$ as well as how $T_R$ affects $T_{ws}$. (The analogous statement was not true for the envelope wall. We are <u>not</u> concerned with how $T_R$ affects $T_A$; we know that the influence is infinitesimal).

Thus while for the envelope wall, we were only concerned with the accuracy of $R_1$, we are now concerned with the accuracy of $h_{wc}U_{cR}/\Sigma \times R_1 + R_2$. Consider the following typical values of the U's for a Trombe wall: $h_{wc}$, the coupling from receiver surface to channel air is about 4 Btu/ft$^2$-deg F-hr; $U_{cA}$ linking the channel air to the outside is about 0.75 for double glazing, and $U_{cR}$, the convective heat flow to the room, is about 0.35. Then $h_{wc}U_{cR}/\Sigma \cong 0.275$, so we look at the comparison between lumped and continuum versions of $R_2 + 0.275\ R_1$.

listed in Table A2.5-6. As seen, the form of these response functions differs greatly from the thick-wall model. The thin $R_2$ is more accurate, although still twice as large as the continuum $R_2$ at $\omega = 2\pi/\text{day}$. The thin $R_1$ is slightly more accurate for $\omega$ small, but reaches its high frequency limit near $\omega = 2\pi/\text{day}$, and starts disagreeing with the continuum $R_1$ by a large factor for $\omega \sim 2\pi/8$ hrs. Error in the thin-wall function ($R_2$ + 275 $R_1$) is only 1% for $\omega = 2\pi/\text{week}$, 6% for $\omega = 2\pi/2$ days, 11% for $\omega = 2\pi/\text{day}$, but rises to 17% for $\omega = 2\pi/8$ hrs and 30% for $\omega = 2\pi/3$ hrs.

All three functions, $R_1$, $R_2$ and $R_2$ + 275 $R_1$ are plotted in Fig. 2.5-4 for both the thin and the thick models. This graph is done on semi-log paper to provide with reader with a better estimate of error magnitudes.

What is happening is that the thick-wall model is calculating the collector surface temperature better, and estimating surface-to-room and surface-to-outdoors heat transfers more accurately, but the thin wall model is doing a better job of calculating heat diffusion through the wall.

It is not surprising that the $R_2$ function is simulated most poorly, since that function describes heat transfers through the wall. For a very thick wall, the continuum nature of the wall is very important in describing heat flow from one side to the other; no choice of lumped parameters would provide an adequate simulation. To see this, note in Table A2.5-5 that the daily heat transmission is phase delayed by more than $\pi$, while the <u>maximum</u> phase delay for any

Appendix 2.5A Footnotes

1) See Ref. 9, Chapter IV.

2) See, for example, Ref. 31, Chapter 3.

3) See Ref. 19.

TABLE A2.5-2

Response Functions for Insulated* 8-inch Concrete† Block.

| $\omega$ | Continuum Model $R_1$ | Continuum Model $R_2$ | Lumped Model (Thick Wall) $R_1$ | Lumped Model (Thick Wall) $R_2$ |
|---|---|---|---|---|
| 0 | 0.622 | 0.067 | 0.622 | 0.067 |
| $2\pi$/month | $0.618\ e^{-0.070i}$ | $0.067\ e^{-0.144i}$ | $0.620\ e^{-0.048i}$ | $0.067\ e^{-0.080i}$ |
| $2\pi$/week | $0.567\ e^{-0.268i}$ | $0.060\ e^{-0.578i}$ | $0.594\ e^{-0.194i}$ | $0.064\ e^{-0.330i}$ |
| $2\pi$/2 days | $0.391\ e^{-0.456i}$ | $0.032\ e^{-1.403i}$ | $0.442\ e^{-0.428i}$ | $0.043\ e^{-0.875i}$ |
| $2\pi$/day | $0.316\ e^{-0.451i}$ | $0.016\ e^{-1.955i}$ | $0.332\ e^{-0.411i}$ | $0.026\ e^{-1.175i}$ |
| $2\pi$/8 hrs | $0.234\ e^{-0.529i}$ | $0.004\ e^{+3.082i}$ | $0.261\ e^{-0.196i}$ | $0.009\ e^{-1.433i}$ |
| $2\pi$/3 hrs | $0.161\ e^{-0.614i}$ | $5 \times 10^{-4}\ e^{+1.284i}$ | $0.251\ e^{-0.078i}$ | $0.004\ e^{-1.519i}$ |

*Insulation is R - 8: $\frac{1}{U_r} = 8\ \frac{ft^2\text{-hr-}^\circ F}{Btu}$

†Assumes $\rho = 144\ lb/ft^3$, $c_p = 0.156\ Btu/lb$, $K = 0.54\ \frac{Btu}{^\circ F\text{-hr-ft}}$, $h = 1.5\ \frac{Btu}{^\circ F\text{-hr-ft}^2}$

TABLE A2.5-4

Response Functions for Carpeted* Concrete† Floor, 8-inch-thick.

| | Continuum Model | | Lumped Model (Thin Wall) | |
|---|---|---|---|---|
| $\omega$ | $R_1$ | $R_2$ | $R_1$ | $R_2$ |
| 0 | 0.525 | 0.213 | 0.525 | 0.213 |
| $2\pi$/month | $0.525\ e^{-0.006i}$ | $0.212\ e^{-0.060i}$ | $0.525\ e^{-0.005i}$ | $0.212\ e^{-0.045i}$ |
| $2\pi$/week | $0.523\ e^{-0.024i}$ | $0.209\ e^{-0.253i}$ | $0.523\ e^{-0.023i}$ | $0.209\ e^{-0.189i}$ |
| $2\pi$/2 days | $0.506\ e^{-0.062i}$ | $0.175\ e^{-0.813i}$ | $0.506\ e^{-0.059i}$ | $0.177\ e^{-0.591i}$ |
| $2\pi$/day | $0.484\ e^{-0.070i}$ | $0.124\ e^{-1.372i}$ | $0.484\ e^{-0.064i}$ | $0.127\ e^{-0.930i}$ |
| $2\pi$/8 hrs | $0.461\ e^{-0.048i}$ | $0.042\ e^{-2.592i}$ | $0.464\ e^{-0.033i}$ | $0.051\ e^{-1.327i}$ |
| $2\pi$/3 hrs | $0.450\ e^{-0.037i}$ | $0.008\ e^{+1.949i}$ | $0.461\ e^{-0.013i}$ | $0.020\ e^{-1.478i}$ |
| $\infty$ | 0.433 | 0 | 0.460 | 0 |

*Assumes carpet is a pure resistance with $U_c = 0.81$ Btu/ft$^2$-°F-hr. (ASHRAE value for carpet with foam pad)

†Assumes $\rho = 144$ lb/ft$^3$, $c_p = 0.156$ Btu/lb-°F, $K = 0.54$ Btu/°F-hr-ft, $h = 1.5$ Btu/°F-hr-ft$^2$

Table A2.5-6 A Comparison of Two Alternate Lumped Parameter Approaches to the Trombe Wall Response Functions of Table A2.5-5

| $\omega$ | Thin-Wall Model | | | | Naive* Lumped Parameters | | | |
|---|---|---|---|---|---|---|---|---|
| | $R_1$ | $R_2$ | $R_2$ | $\frac{h_{wc}U_{cR}}{\Sigma}$ $R_1$ | $R_1$ | $R_2$ | $R_2$ | $\frac{h_{wc}U_{cR}}{\Sigma}$ |
| 0 | .877 | .255 | .496 | | .877 | .255 | .496 | |
| $2\pi$/month | $.865e^{-.081i}$ | $.249e^{-.203i}$ | $.486e^{-.143i}$ | | $.856e^{-.085i}$ | $.241e^{-.324i}$ | $.473e^{-.206i}$ | |
| $2\pi$/week | $.743e^{-.240i}$ | $.191e^{-.722i}$ | $.384e^{-.473i}$ | | $.724e^{-.156i}$ | $.145e^{-.963i}$ | $.317e^{-.492i}$ | |
| $2\pi$/4 days | $.647e^{-.253i}$ | $.139e^{-.945i}$ | $.298e^{-.555i}$ | | $.675e^{-.122i}$ | $.094e^{-1.193i}$ | $.245e^{-.465i}$ | |
| $2\pi$/2 days | $.565e^{-.186i}$ | $.079e^{-1.257i}$ | $.205e^{-.531i}$ | | $.648e^{-.071i}$ | $.050e^{-1.375i}$ | $.197e^{-.318i}$ | |
| $2\pi$/day | $.533e^{-.106i}$ | $.041e^{-1.410i}$ | $.162e^{-.352i}$ | | $.640e^{-.037i}$ | $.025e^{-1.472i}$ | $.181e^{-.174i}$ | |
| $2\pi$/8 hrs | $.523e^{-.037i}$ | $.014e^{-1.517i}$ | $.146e^{-.133i}$ | | $.637e^{-.012i}$ | $.008e^{-1.538i}$ | $.176e^{-.057i}$ | |
| $2\pi$/3 hrs | $.522e^{-.014i}$ | $.005e^{-1.531i}$ | $.144e^{-.049i}$ | | $.637e^{-.005i}$ | $.003e^{-1.558i}$ | $.175e^{-.022i}$ | |

*Sets $U_i = U_o = 2K/d$ and $\overline{C} = \rho c_p d$

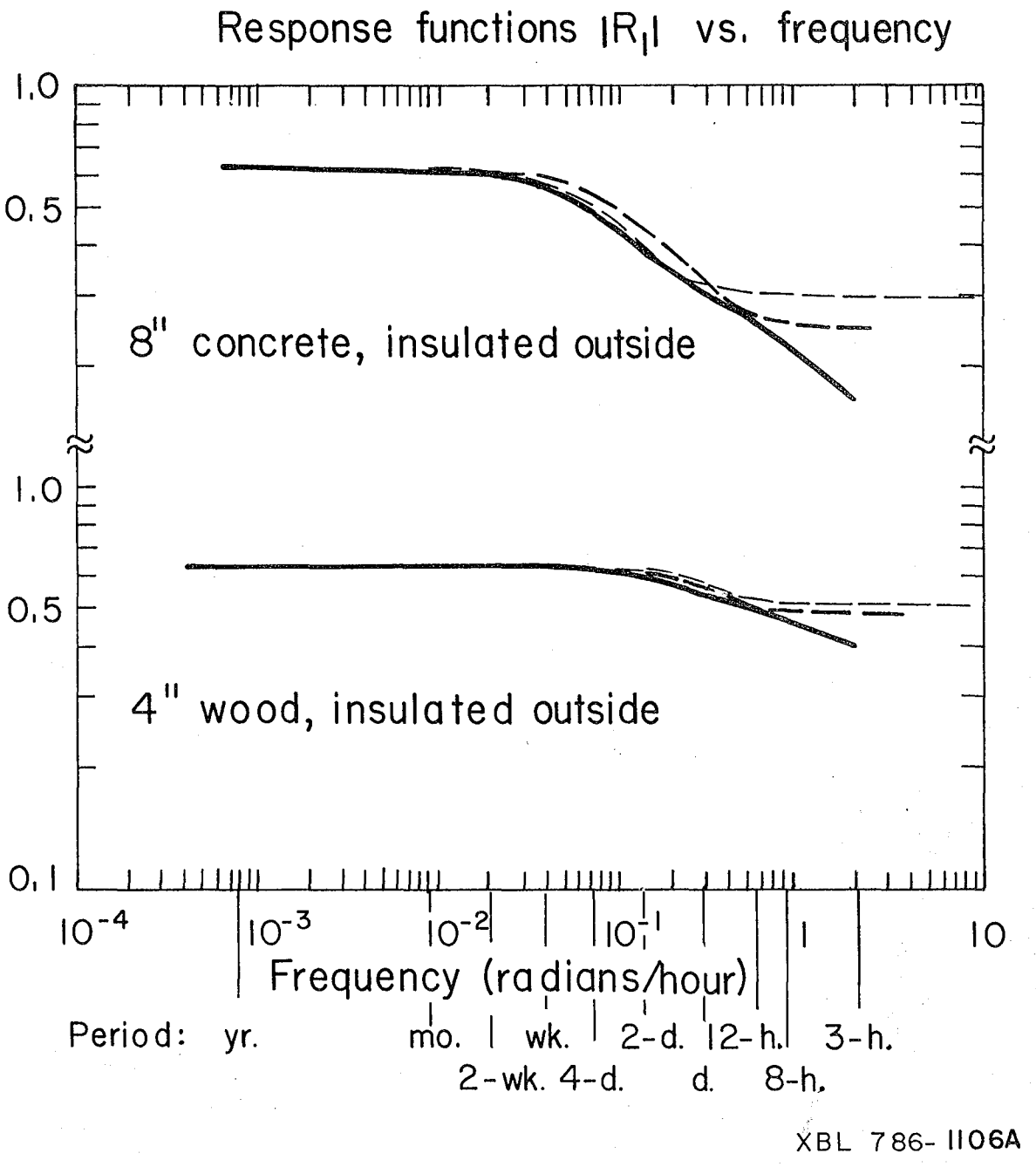


Fig. A2.5-2. Response functions for insulated materials as a function of frequency. Log$|R_1|$ is plotted vs log $\omega$ for two materials with insulation of R-8 (8 ft$^2$-hr-°F/Btu) on the outside. The solid lines represent the continuum response functions. The heavy dashed lines describe the thick-wall lumped model response functions, while the light dashed lines represent the thin-wall functions.

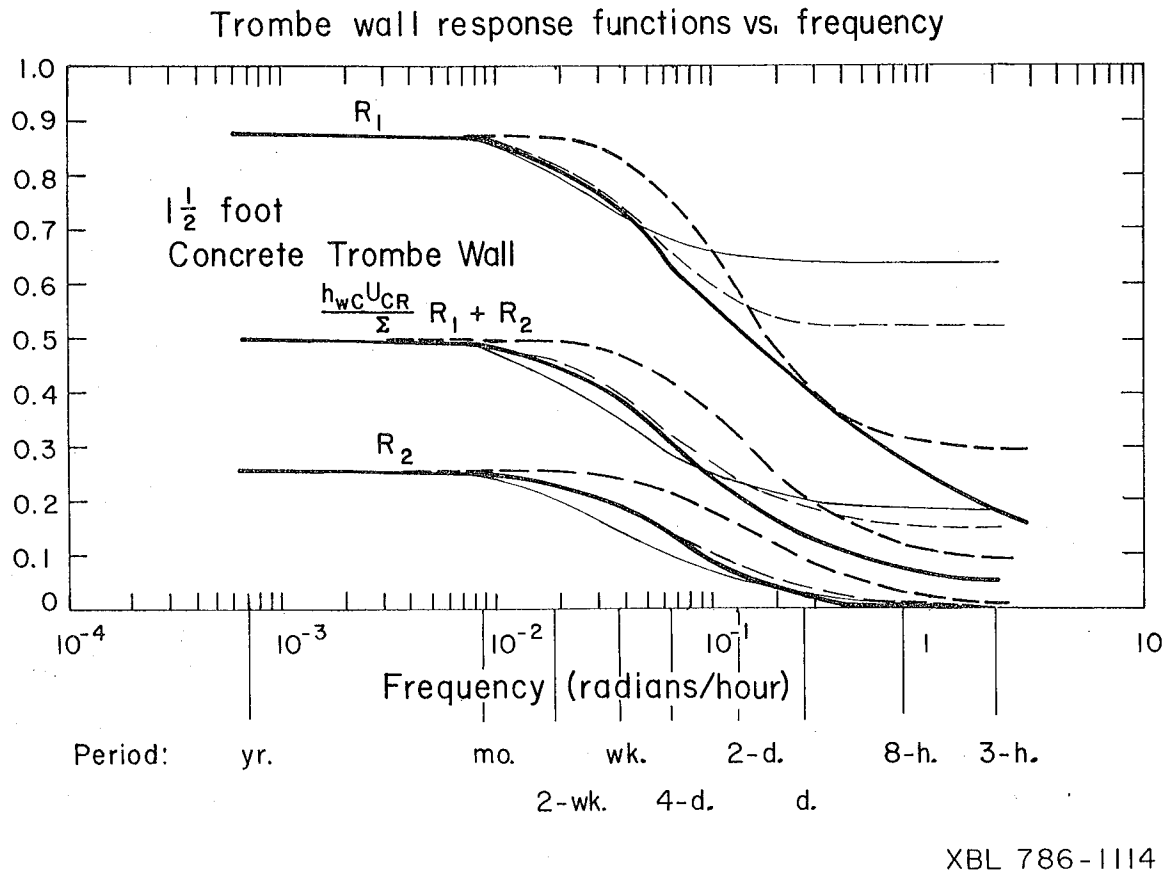


Fig. A2.5-4. Response functions for a 1.5-ft-thick Trombe wall. The most important function is $(h_{wc}U_{cR}/\Sigma)\ R_1 + R_2$. In this figure the y-axis is $|R|$ rather than $\log|R|$ to better display the magnitude of errors. The heavy solid lines represent the continuum response functions. The heavy dashed lines describe the thick-wall lumped model response functions, while the light dashed lines represent the thin-wall functions. The light solid line describes the naive lumped parameter case where $U_i = U_o = 2U_w$ and $C_w = (\rho c_p)_w A_w d$.

solution plotted as a dotted line. Figure A2.5B-1 is a similar representation of wall surface temperature.

Both figures show the same pattern of agreement. Except for the first hour or two after the windows are shuttered, both solutions are identical to within 5% or less. During the transition periods, the lumped parameter model shows discontinuous changes in temperature, which occur because the room and wall surface have no heat capacity. The distributed model requires continuous temperatures as a function of time, because the surface layer has finite heat capacity (per unit thickness). However, the sudden difference between the two models decreases quickly as the faster exponential decays in the continuum model go to zero.

The equations for the house to be modelled are presented next. The "floor" subscripts are used to describe the solar collector. The heat balance for the floor surface is (from (2.1) and (2.6))

$$\hat{h}_f(T_{f_s} - T_R) - \alpha_f S(t) + \hat{U}_{fi}\,(T_{f_s} - T_f) = 0$$

where $\hat{h}_f$ is heat transfer coefficient from floor surface to room air (Btu/°F-hr, or W/°C)

$T_{f_s}$ is the floor surface temperature (°F or °C)

$\hat{U}_{fi}$ is the heat transfer coefficient from floor surface to floor interior (Btu/°F-hr, or W/°C),

and the other symbols are defined in Sec. 2.2.

Heat flows within the wall are described by the diffusion equation (2.3)

$$\frac{\partial T_w}{\partial t} = \frac{K_w}{(\rho c_p)_w} \frac{\partial^2 T_w}{\partial x^2} \qquad \text{(A2.5B-3)}$$

The boundary conditions are

$$T_w(0,t) = T_{ws} \qquad \text{(A2.5B-4)}$$

which is true by definition and

$$T_w(d,t) = T_A \qquad \text{(A2.5B-5)}$$

where $d$ is the wall thickness. This equation assumes perfect thermal contact between the outside wall surface and the outside air.

Finally, the room heat balance from (2.2) is (in the limit of $\hat{U}_{fi} \to \infty$ )

$$\hat{h}_f(T_R - T_f) + \hat{h}_w(T_R - T_{ws}) + \hat{U}_q(T_R - T_A) = 0 \qquad \text{(A2.5B-6)}$$

where $\hat{U}_q$ is the quick heat transfer coefficient for all heat losses except those through the floor and walls (e.g. infiltration, windows) (Btu/°F-hr, or W/°C).

These six equations will be solved under the assumption that $\hat{U}_{fo}$ changes values between day and night (corresponding to the fact that the window covering the collector is shut at night). Thus the equations will be solved for the day period using the daytime value of $\hat{U}_{fo}$ and then solved again for the night period, and the two solutions will be joined continuously at sunrise and sunset, as was done in the lumped parameter case (see Section 2.3).

To begin the solution, we note that the two independent variables or driving forces are $T_A$ and S, while the two dependent variables are

where we have defined

$$\Lambda_1 = \frac{1}{C_f}\left(\frac{\hat{h}_f \hat{U}_q}{\hat{h}_f + \hat{U}_q} + \hat{U}_{fo}\right)$$

$$\Lambda_2 = \frac{1}{C_f}\left(\hat{U}_{fo} + \frac{\hat{h}_f \hat{U}_q}{\hat{h}_f + \hat{U}_q}\right) = \Lambda_1$$

$$\Lambda_3 = \frac{1}{C_f} \frac{\hat{h}_f A_w K_w}{(\hat{h}_f d + A_w K_w)}$$

$$\Lambda_3 = \alpha_f + \frac{\alpha_w \hat{h}_f}{\hat{h}_f + \hat{U}_q}$$

$$\xi = \frac{x}{d}$$

The above solutions for $T_R$ and $T_{ws}$ also transform (A2.5B-2) into

$$T_w\big|_0 - D_1 \frac{\partial T_w}{\partial \xi} - D_2 T_f = D_3 T_A + D_4 S \qquad \text{(A2.5B-8)}$$

where $\xi = x/d$ (so $\xi$ goes from 0 to 1).

and where

$$D_1 = \frac{(\hat{h}_f + \hat{h}_w + \hat{U}_q) A_w K_w}{d\hat{h}_w (\hat{h}_f + \hat{U}_q)}$$

$$D_2 = \frac{\hat{h}_f}{\hat{h}_f + \hat{U}_q}$$

We let $T_A = \Delta T_A \, e^{i\omega_0 t}$ where $\omega_0 = 2\pi/\text{day}$.

We measure all temperatures with respect to daily average $T_A$ so that the steady-state part of $T_A$ is zero.

Thus the inhomogeneous solution is

$$T_R(t) = \begin{cases} \chi_s(\omega_1)\, S(t) + \chi_A(\omega_0) T_A(t) & 0 \leqslant t < t_d \\ \chi'_A(\omega_0) T_A(t) & t_d \leqslant t < 24 \text{ hrs} \end{cases}$$

where $\chi_A'$ is calculated using nighttime values of the parameters.

We also will need to calculate the inhomogeneous solution for $T_f$ and $T_w$; these can be obtained from the $T_R$ solution by calculating the response of each to stimulation by either S or $T_A$. We expect solutions of the form

$$T_f = \chi_{s_f} S(t) + \chi_{A_f} T_A(t)$$

and

$$T'_w(x,t) = \chi_{s_w}(x)\, S(t) + \chi_{A_w}\, T_A(t)$$

Equations (A2.4-20) and (A2.5-9bc) imply that

$$T_{f\omega} = \left( \frac{\hat{h}_f}{\hat{U}_{fo} + \hat{h}_f + i\omega C_f} \right) T_{R\omega} + \frac{\alpha_f}{\hat{U}_{fo} + \hat{h}_f + i\omega C_f}\, S + \frac{\hat{U}_{fo}}{\hat{U}_{fo} + \hat{h}_f + i\omega C_f}\, T_A \qquad \text{(A2.5B-9)}$$

while (A2.4-12 and 16) (with $R_e = 0$) require that

Thus

$$\chi_{S_f} = \frac{\hat{h}_f \chi_S + \alpha_f}{\hat{U}_{fo} + \hat{h}_f + i\omega_1 C_f} \qquad \text{(A2.5B-12b)}$$

$$\chi_{S_w} = \frac{h_w \chi_s + \alpha_w}{D} \left( \sinh k_w d(1-\xi) \right)$$

$$\chi_{A_f} = \frac{\hat{h}_f \chi_A + \hat{U}_{fo}}{\hat{U}_{fo} + \hat{h}_f + i\omega_0 C_f} \qquad \text{(A2.5B-13b)}$$

$$\chi_{A_w} = \cosh k_w d(1-\xi) + \frac{\hat{h}_w \chi_A - \left( \hat{h}_w \cosh k_w d + A_w K_w k_w \sinh k_w d \right)}{D} \sinh k_w d\,(1-\xi)$$

(A2.5B-13b)

Homogeneous Solution

We look for solutions of the form

$$T_f = T_{f_o} e^{-\lambda t}$$

$$T_w(x,t) = T_{wo}(x)\, e^{-\lambda t}$$

since we are solving a diffusion equation and a lumped parameter heat balance, both of which are solved by a series of (one or infinitely many) decaying exponentials.

The diffusion equation (A2.5B-3) tells us that for this form of solution

$$-\lambda T_{wo} = \frac{K_w}{\rho c_p} \frac{\partial^2 T_w}{\partial x^2} = \Lambda_w \frac{\partial^2 T_w}{\partial \xi^2}$$

where $\xi = \frac{x}{d}$ and $\Lambda_w = \frac{\hat{U}_w}{C_w} = \frac{K_w/d}{\rho c_p d}$

Orthogonality

We next show that we can arrange the homogeneous solutions to this set of equations in a vector format, with one vector for each decay constant $\lambda_n$. We will show that the vectors can be chosen in such a way that the solutions at each $\lambda_n$ are orthogonal to each other.

First, consider the relationship between $T_f$ and $T_{ws}$. We showed that

$$T_{wo}^{(n)}(\xi) = B \sin \ell_n (1 - \xi)$$

then (A2.5B-8) requires that

$$B = \frac{D_2}{\sin\ell_n + D_1 \ell_n \cos \ell_n} T_{fo} \qquad \text{(A2.5B-15a)}$$

Thus it is reasonable to look at basis vectors of the form:

$$T_n \left( \left( \frac{1}{\frac{D_2 \sin \ell_n (1 - \xi)}{\sin\ell_n + D_1 \ell_n \cos \ell_n}} \right) \right) \qquad \text{(A2.5B-15b)}$$

We show next that such basis vectors are orthogonal to each other, and in the process calculate the form of scalar product between two vectors.

Consider two vectors

$$\begin{pmatrix} T_f^{(n)} \\ T_w^{(n)} \end{pmatrix} \quad \text{and} \quad \begin{pmatrix} T_f^{(m)} \\ T_w^{(m)} \end{pmatrix}$$

Then by (A2.5B-3),

$$\frac{\partial^2 T_w^{(n)}}{\partial \xi^2} + \ell_n^2 T_w^{(n)} = 0 \qquad \text{(A2.5B-16)}$$

and

$$\frac{\partial^2 T_w^{(m)}}{\partial \xi^2} + \ell_m^2 T_w^{(m)} = 0$$

Then we use (A2.5B-8) in homogeneous form to eliminate $T_f$ from the righthand side of (A2.5B-19); the result is

$$\Lambda_w(\ell_n^2 - \ell_m^2) T_f^{(n)} T_f^{(m)} = \frac{\Lambda_3}{D_2}\left(T_w^{(n)}(0)\ T_w^{(m)\prime}(0) - T_w^{(m)}(0)\ T_w^{(n)\prime}(0)\right)$$

This result is used to replace the bracketed term in (A2.5B-18), to yield the final result

$$\left(\ell_n^2 - \ell_m^2\right)\left\{\frac{D_2\Lambda_w}{\Lambda_3}\ T_f^{(n)} T_f^{(m)} + \int_0^1 d\xi\ T_w^{(m)}(\xi)\ T_w^{(n)}(\xi)\right\} = 0$$

or

$$\left(\ell_n^2 - \ell_m^2\right)\left(C_f\ T_f^{(n)} T_f^{(m)} + C_w \int_0^1 d\xi\ T_w^{(m)}(\xi)\ T_w^{(n)}(\xi)\right) = 0 \qquad \text{(A2.5B-20)}$$

where $C_w = (\rho c_p)_w\ d\ A_w$

This equation gives the form of the scalar product between two basis vectors and proves their orthogonality. The scalar product is in an intuitively appealing form, it is the sum of the product of the $T_f$ components of each sector, weighted by the floor heat capacity, and the integral of the $T_w$ components, weighted by the wall heat capacity. This form is analogous to the scalar product derived in Ref. 32.

Orthogonality comes about because (A2.5 B2-20) requires the product of $\ell_m^2 - \ell_n^2$ and the scalar product of basic vectors m and n to be zero; if $m \neq n$, then $\ell_m^2 - \ell_n^2 \neq 0$ and the scalar product must be zero. This equation also allows us to normalize the vectors, such that the scalar

This completes the solution to the homogeneous equations. The solution can be written as

$$\sum_{n=1}^{\infty} A_n \, e^{-\Lambda_w \ell_n^2} \, \mathcal{J}_n \qquad \text{(A2.5B-24)}$$

where $A_n$ are arbitrary constants determined by the boundary conditions, and $\mathcal{J}_n$ are basis vectors, given by

$$\mathcal{J}_n = N_n \begin{pmatrix} 1 \\ \left( \dfrac{D_2 \sin \ell_n (1 - \xi)}{\sin \ell_n + D_1 \ell_n \cos \ell_n} \right) \end{pmatrix}$$

Complete Solution

For a house which changes the parameter $\hat{U}_{fo}$ from day to night, we can write the complete solution for each period as the sum of the homogeneous and inhomogeneous solutions. This solution is

$$\mathcal{J}(t) = \begin{cases} \displaystyle\sum_{n=1}^{\infty} A_n \mathcal{J}_n \, e^{-\Lambda_w \ell_n^2} + \underset{\sim}{\chi}_s \, S(t) + \underset{\sim}{\chi}_A \, T_A(t) & 0 \leq t < t_d \\ \displaystyle\sum B_n \mathcal{J}_n' \, e^{-\Lambda_w \ell_n'^2} + \underset{\sim}{\chi}'_A \, T_A(t) & t \leq t_d < 24 \text{ hr} \end{cases}$$

(A2.5B-25)

where a primed variable is evaluated using nighttime parameter values and where the $\chi$'s are vectors $\begin{pmatrix} \chi_f \\ \chi_n \end{pmatrix}$ whose form is given by (A2.5B-12 and 13).

To derive a numerical solution, we must solve for the $A_n$'s and $B_n$'s. The boundary conditions are the same as in the lumped parameter solution: continuity and periodicity. We require that

$$A_m = \sum_{\substack{n=1\\ \ell=1}}^{\infty} O_{mn} O_{\ell n} \; e^{-\Lambda_w(\ell_\ell^2 t_d + \ell_n'^2 t_n)} \; A_\ell + \sum_{n=1}^{\infty} O_{mn} \; e^{-\Lambda_w \ell_n'^2 t_n} \; D_n + C_m \qquad \text{(A2.5B-29a)}$$

$$B_m = \sum_{\substack{n=1\\ \ell=1}}^{\infty} O_{nm} O_{n\ell} \; e^{-\Lambda_w(\ell_n^2 t_d + \ell_\ell'^2 t_n)} \; B_\ell + \sum_{n=1}^{\infty} O_{mn} \; e^{-\Lambda_w \ell_n^2 t_d} \; C_n + D_m \qquad \text{(A2.5B-29b)}$$

Evaluation of the Solution

To evaluate (A2.5B-25 and 29) requires the determination of three expressions: $O_{mn}$, $\underset{\sim}{\chi}_S \cdot \mathcal{J}_m$, $\underset{\sim}{\chi}_A \cdot \mathcal{J}_m$. We find equations for these three next; following that we evaluate a numerical solution based on the Sonoma house.

First, $O_{mn} = \mathcal{J}_m \cdot \mathcal{J}'_n$

$$O_{mn} = N_m N_n' \left( C_f + C_w \int_0^1 d\xi \; \frac{D_2 D_2' \sin \ell_m(1-\xi) \sin \ell_n'(1-\xi)}{(\sin \ell_m + D_1 \ell_m \cos \ell_m)(\sin \ell_m' + D_1' \ell_m' \cos \ell_m')} \right)$$

Since $D_2 = D_2'$ and $D_1 = D_1'$, we can write this as

$$O_{mn} = N_m N_n' \left( C_f + C_w \; \frac{D_2^2 \left( \dfrac{\sin(\ell_m - \ell_n')}{\ell_m - \ell_n'} - \dfrac{\sin(\ell_m + \ell_n')}{\ell_m + \ell_n'} \right)}{2(\sin \ell_m + D_1 \ell_m \cos \ell_m)(\sin \ell_n' + D_1 \ell_n \cos \ell_n')} \right)$$

As in the case of the $N_n$'s, this expression is very sensitive to small errors in the $\ell$'s. It could be expressed elegantly as $O_{mn} = N_m N_n' \; C_f (\Lambda_1 - \Lambda_1') / \Lambda_w (\ell_m^2 - \ell_n'^2)$, but this is even more sensitive to errors in evaluating the $\ell$'s. A more useful form for

$$I = -2e^{-\theta(1+i)}\frac{1}{2i}\left\{\frac{e^{\theta(1+i)} - e^{i\ell_m}}{\theta + i(\theta - \ell_m)} - \frac{e^{\theta(1+i)} - e^{-i\ell_m}}{\theta + i(\theta + \ell_m)} - e^{2\theta(1+i)}\right.$$

$$\left.\times\left[\frac{e^{-\theta(1+i)} - e^{i\ell_n}}{-\theta + i(-\theta_e - \ell_m)} - \frac{e^{-\theta(1+i)} - e^{-i\ell_m}}{-\theta + i(-\theta + \ell_m)}\right]\right\} \qquad \text{(A2.5B-31)}$$

Then

$$\underset{\sim}{\chi}_s \cdot \mathcal{J}_m = N_m\left(C_f\,\frac{\hat{h}_f\chi_s + \alpha_f}{\hat{U}_{fo} + \hat{h}_f + i\omega_1 C_f} - \frac{C_w(\chi_s\hat{h}_w + \alpha_w)\, I\,((\Lambda_1 - \Lambda_w\ell_m^2)D_1 + \Lambda_3 D_2)}{D\Lambda_3 \sin\ell_m}\right)$$

(A2.5B-32)

For $\underset{\sim}{\chi}_s$ we use the primed values of $\ell_m$ and $\Lambda_1$ (as well as I).

The final expression we need is $\mathcal{J}_m \cdot \underset{\sim}{\chi}_A$

This calculation is analogous to the preceding:

$$\mathcal{J}_m \cdot \underset{\sim}{\chi}_A = N_m\left(C_f\,\frac{\hat{h}_f\chi_A + \hat{U}_{fo}}{\hat{h}_f + \hat{U}_{fo} + i\omega_0 C_f} + C_w\,\frac{J((\Lambda_1 - \Lambda_w\ell_n^2)D_1 + \Lambda_3 D_2)}{D\Lambda_3 \sin\ell_m}\right)$$

where

$$J = \int_0^1 d\xi\,\frac{(A_w K_w k_w + \hat{h}_w)e^{k_w d} - \chi_A\hat{h}_w}{2\,e^{\theta(1+i)}\,D}\,\frac{e^{i\ell_m(1-\xi)} - e^{-i\ell_m(1-\xi)}}{2i}$$

$$\times\left(e^{\theta(1+i)\xi} - e^{2\theta(1+i)}\;e^{-\theta(1+i)}\right) + \int_0^1 d\xi\,\frac{e^{i\ell_m(1-\xi)} - e^{-i\ell_m(1-\xi)}}{2i}$$

$$\times\left(e^{\theta(1+i)(1-\xi)}\right)$$

Note that $K_e$ and $\theta_e$ are evaluated for $\omega = \omega_0$ here.

Floor thermal mass: $C_f = 3535$ Btu/°F

$$\hat{U}_{fo} = \begin{cases} 400 \text{ Btu/°F (day)} \\ 30 \text{ Btu/°F (night)} \end{cases}$$

Floor-to-room film coefficient: $\hat{h}_f = 75$ Btu/°F

Area of walls: $A_w = 198$ ft$^2$

Thickness of walls: $d = \frac{1}{2}$ ft

Heat capacity of walls: $\rho C_p = 9$ Btu/°F ft$^3$

Total heat capacity of walls: $\rho C_p A_w d = 891$ Btu/°F

Walls-to-room film coefficient: $\hat{h}_w = 198$ Btu/°F-hr

Quick house heat transfer coefficient: $\hat{U}_q =$ Btu/°F-hr

Fraction of sun absorbed on floor: $\alpha_f = 952$

Fraction of sun absorbed on walls: $\alpha_w = 048$

Solar gain during the day: $S_1 e^{i\omega_1 t}$

(where $S_1 = 65{,}000\ e^{-9903i}$ Btu/hr)

Length of day period: $t_d = 6.5$ hrs

Solar frequency: $\omega_1 = 0.3415$

For simplicity, we take $\Delta T = 0$, steady outdoor temperature. The lumped parameters are:

$$\hat{U}_{wi} = 112 \text{ Btu/°F-hr}$$

$$\hat{U}_{w_0} = 35.4 \text{ Btu/°F-hr}$$

$$C_w = 428 \text{ Btu/°F}$$

along with the parameters $\hat{h}_w, \hat{h}_f$, $C_f$, $\hat{U}_{fo}$ $\hat{U}_q$ above.

We now proceed to calculate the exact solution. From (A2.5B-7 and 8) we evaluate the D's and $\Lambda$'s:

$$\Lambda_1 = 0.127 \quad \text{(day)}$$
$$\text{or } 0.02257 \quad \text{(night)} \qquad D_1 = 0.025675$$
$$\Lambda_3 = 0.002562 \qquad D_2 = 0.336$$
$$\Lambda_w = 0.03022$$

We next use (A2.5B-14) for the decay parameters $\ell_m$

$$\ell_1 = 2.0402 \qquad \ell_1' = 0.8743$$
$$\ell_2 = 2.578 \qquad \ell_2' = 2.56754$$
$$\ell_3 = 5.34435 \qquad \ell_3' = 5.3441$$
$$\ell_4 = 8.2937 \qquad \ell_4' \cong \ell_4$$
$$\ell_5 = 11.327 \qquad \ell_5' \cong \ell_5$$
$$\ell_6 = 14.4015 \qquad \ell_6' \cong \ell_6$$

Then we can use (A2.5B-23) to evaluate the normalization factors

$$N_1 = 1.6495 \times 10^{-2} \qquad N_1' = 1.6756 \times 10^{-2}$$
$$N_2 = 3.243 \times 10^{-3} \qquad N_2' = 1.3607 \times 10^{-3}$$
$$N_3 = 4.986 \times 10^{-4} \qquad N_3' = 4.366 \times 10^{-4}$$
$$N_4 = 2.146 \times 10^{-4} \qquad N_4' = 2.037 \times 10^{-4}$$
$$N_5 = 1.177 \times 10^{-4} \qquad N_5' \cong N_5$$
$$N_6 = 7.47 \times 10^{-5} \qquad N_6' \cong N_6$$

We note that the test $\sum_{n\ or\ m} O_{mn}^2 = 1$ checks to three significant figures. We note also that except for $O_{21}$ and $O_{12}$, all off-diagonal terms are very small. *All* diagonal terms are very close to one. We use these results to calculate $\underset{\sim}{\chi}_s \cdot \mathcal{J}_m$ from (A2.5B-31) and (32) using the result [from Appendix 2.4, Eq.(A2.4-22 )] that $\chi_s = 2.872 \times 10^{-4}\ e^{-0.9747i}$. After a very long and tedious calculation (evaluating I in (A2.5B-31) in a 98-step calculation on an HP programmable calculator), we find that

$$\underset{\sim}{\chi}_s \cdot \mathcal{J}_1' = 4.546 \times 10^{-2}\ e^{-1.2173i}\ ; \qquad \underset{\sim}{\chi}_s \cdot \mathcal{J}_1' = 4.573 \times 10^{-2}\ e^{-1.2151i}$$

$$\underset{\sim}{\chi}_s \cdot \mathcal{J}_2' = 5.12 \times 10^{-3}\ e^{-1.0323i} \qquad \underset{\sim}{\chi}_s \cdot \mathcal{J}_2' = 9.453 \times 10^{-4}\ e^{0.4917i}$$

$$\underset{\sim}{\chi}_s \cdot \mathcal{J}_3' = 1.453 \times 10^{-3}\ e^{2.7509i} \qquad \underset{\sim}{\chi}_s \cdot \mathcal{J}_3' = 1.572 \times 10^{-3}\ e^{2.6727i}$$

$$\underset{\sim}{\chi}_s \cdot \mathcal{J}_4' = 8.984 \times 10^{-4}\ e^{2.9675i} \qquad \underset{\sim}{\chi}_s \cdot \mathcal{J}_4' = 9.138 \times 10^{-4}\ e^{2.9396i}$$

$$\underset{\sim}{\chi}_s \cdot \mathcal{J}_5' = 5.402 \times 10^{-4}\ e^{3.0432i} \qquad \underset{\sim}{\chi}_s \cdot \mathcal{J}_5' = 5.592 \times 10^{-4}\ e^{3.0289i}$$

$$\underset{\sim}{\chi}_s \cdot \mathcal{J}_6' = 3.56 \times 10^{-4}\ e^{3.0765i} \qquad \underset{\sim}{\chi}_s \cdot \mathcal{J}_6' = 3.58 \times 10^{-4}\ e^{3.0679i}$$

In the second sum, the exponential kills off all terms with $n \geq 3$. This reduces the sum to two terms for $m=1$ or 2, and eliminates it for $m > 3$ (since $O_{3i} \cong 0$ for $i \neq 3$). Thus we can solve for $A_m$ as follows:

$$A_1 = O_{11}^2(0.2947)A_1 + O_{11}O_{21}(0.181)A_2 + O_{11}(0.6675)D_1 + C_1$$

where we have dropped:

$O_{12}^2 \; e^{-\Lambda_w(\ell_1^2 t_d + \ell_2'^2 t_n)} \; A_1$ because $O_{12}^2 \sim 0.01$ and $e^{-(\;)} \sim 0.01$

$O_{12}O_{22} \; e^{-\Lambda_w(\ell_2^2 t_d + \ell_2'^2 t_n)} \; A_2$ because $|O_{12}O_{22}| \sim 0.1$ and $e^{-(\;)} \sim 0.01$

$O_{12} \; e^{-\Lambda_w \ell_2'^2 t_n} \; D_2$ because $|O_{12}| \sim 0.1$ and $e^{-(\;)} \sim 0.03$ and $D_2 << D_1$

Thus

$$A_1 = 0.0286\, A_2 + 5007$$

$$A_2 = O_{21}O_{11}(0.2947)A_1 + \left(O_{21}^2(0.181) + O_{22}^2(0.0083)\right)A_2 + O_{21}(0.6675)D_1 + O_{22}(0.0306)D_2 + C_2$$

where we have dropped

$O_{22}O_{12} \; e^{-\Lambda_w(\ell_1^2 t_d + \ell_2'^2 t_d)} \; A_1$ because $|O_{12}| \sim 0.1$ and $e^{-(\;)} \sim 0.01$

So, $A_2 = 0.0312\, A_1 + 355$, $A_3 = -0.00238\, D_1 + C_3 = 23.96$,

$A_4 = C_4 = 21.98$, $A_5 = C_5 = 15.50$,

Since the solution (A2.5B-25), we encounter the quantities $A_nN_n$ rather than just $A_n$ (the $N_n$ is part of the expression for $\mathcal{J}_n$) we solve the preceding equation for $A_nN_n$ and list the results below:

$$A_1N_1 = 82.83°F \qquad B_1N_1' = 85.06°F$$
$$A_2N_2 = 1.659°F \qquad B_2N_2' = 0.16311°F$$
$$A_3N_3 = 0.01195°F \qquad B_3N_3' = 0.03193°F$$
$$A_4N_4 = 0.004717°F \qquad B_4N_4' = 0.005958°F$$
$$A_5N_5 = 0.001824°F \qquad B_5N_5' = 0.001788°F$$
$$A_6N_6 = 0.0008°F \qquad B_6N_6' = -0.0006587°F$$

We next display the numerical values of the exponential decay constants $(\Lambda_w \ell_n^2)$

$$\lambda_1 = 0.1258\ hr^{-1} \qquad \lambda_1' = 0.02310\ hr^{-1}$$
$$\lambda_2 = 0.2008 \qquad \lambda_2' = 0.1992$$
$$\lambda_3 = 0.8631 \qquad \lambda_3' = 0.8631$$
$$\lambda_4 = 2.079 \qquad \lambda_4' = \lambda_4$$
$$\lambda_5 = 3.877 \qquad \lambda_5' = \lambda_5$$
$$\lambda_6 = 6.268 \qquad \lambda_6' = \lambda_6$$

The value of $\underset{\sim}{\chi}_S$ is computed to be

$$\left(7.290 \times 10^{-4}\ e^{-1.2144i},\quad 3.436 \times 10^{-4}\ e^{-1.6041} \left(\frac{\sinh kd(1-\xi)}{\sinh kd}\right)\right)$$

This completes the numerical work necessary to evaluate a solution which can be compared to the lumped parameter solution. To make the comparison, we shall calculate $T_f, T_R$ and the wall surface temperature $T_{ws}$.

We note that wall surface temperature is $T_w(0)$. The room

This concludes the calculation. We discuss its significance next.

Floor (Storage) Temperature

As is readily apparent from the coefficients, there is excellent agreement between the lumped solution and the exact solution. The inhomogeneous terms agree in phase and are 2% apart in magnitude; in general, the lumped and exact temperatures agree within about 2%. This agreement is to be expected since the floor is an inherently lumped material which is described identically in both models.

Note the fast convergence of the coefficients ($A_n N_n$). This convergence should go as $1/n^3$ in the limit of large n. This is because by (A2.5B-29), $A_n$ goes proportionally to $\mathcal{J}_m \cdot \chi_s$, which in turn goes as 1/n (since $\ell_n \sim n\pi$ for large n and $\mathcal{J}n \cdot \underset{\sim}{\chi}_s \propto \ell^2$ I/N while $I \propto 1/\ell_n$). Thus since $N_n \propto 1/n^2$, $A_n N_n \propto 1/n^3$. Thus only the first one or two terms are important.

Room Temperature

Since the room has no thermal mass, and is coupled to the solar-receiving wall surface, which also has no thermal mass in the lumped model, it can change temperature discontinuously. It does so when the collector panel is opened or closed.

In the real world temperatures do not change discontinuously. Thus we would expect to "round off the corners" on the graph of temperature versus time for the lumped model. When one does this, it looks quite similar to the exact solution (see Fig. 2.11).

This is apparent looking at the equations for room temperature. The coefficients of the slowest decaying exponential at night are 26.7

terms are left out by truncating the series at n = 6. This can also be seen by calculating $T_R$ ($t = 0$ or $t = t_d$) with both the night and day equations. By (A2.5B-26), $T_R$ should not change discontinuously, but the truncated solution jumps by about 1°F at sunset and 1½°F at sunrise. These truncation errors die off quickly, of course, since the seventh term decays to 0.01% of its original magnitude after one hour.

Wall Surface Temperature

Wall surface temperature is the most sensitive comparison of the lumped parameter model with the exact solution, since it is a variable which refers to the continuum which is being approximated in the lumped model. In the continuum solution, the wall behavior is characterized by a function $T_w(x,t)$, while the lumped model approximates this with a wall-storage temperature $T_w(t)$, which is *not* the average of $T_w(x,t)$, but rather is chosen to simulate the response of the wall surface to excitations.

Wall surface temperature is analogous in both solutions so it is a good variable to compare. In this case the wall surface temperature comparison checks the validity of the thick-wall model for 6"-thick wood.

As in the case with room temperature, the wall surface temperature in the lumped parameter model can change discontinuously because the wall surface has no thermal mass as idealized in that model. Large (5 - 8°F, or 15 - 50%) jumps in wall surface temperature are in fact calculated in the lumped parameter model.

The exact solution requires continuous surface temperature; however the change from day to night generates a series of relatively important,

$$T_{ws} = \begin{cases} 18.42\, e^{-0.09891t} + 5.36\, e^{-0.1299t} + 25.828\, e^{i(\omega_1 t - 4.26\ \text{hrs})} & \text{day} \\ 24.19\, e^{-0.2312(t-t_d)} + -0.06\, e^{-0.10104(t-t_d)} & \text{night} \end{cases}$$

This solution yields decay constants which are substantially different than either of the previous cases. While the slow night decay constant is unchanged, the faster decay constant differs from the previous models by a factor of 2. The slow day decay constant is 20% smaller than before, while the fast constant is 35% smaller.

The coefficients are also different, with the exception of the dominant night coefficient. The faster night decay has a coefficient of essentially zero in this model, compared to 3° in the previous cases. While before the first two day coefficients had opposite signs, the present model gives coefficients of the same sign. The inhomogeneous term is also different from the previous models, with 15% (3.5°F) larger amplitude and about 1 hour less phase lag than the exact solution.

The results of this model compared to the other two are graphed in Fig.A2.5B-1. As seen in the figure, agreement is generally worse than for the "optimal" lumped parameters. All three models converge on the same temperature in the early morning hours, but the rest of the time the "dumb" lumped parameter model disagrees with the exact model by two or three times as much as the "optimal" lumped parameter model (and in the same direction). That is, during the day, the "dumb" lumped parameter model is off by 10 to 14% (not counting the first 2 hours), while during the night, the agreement is within 8%, improving to better than 3% by midnight. The "dumb" lumped parameter model also has larger day/night discontinuities of 10.7° (or 65%) at sunrise and 6.5°F (27%) at sunset.

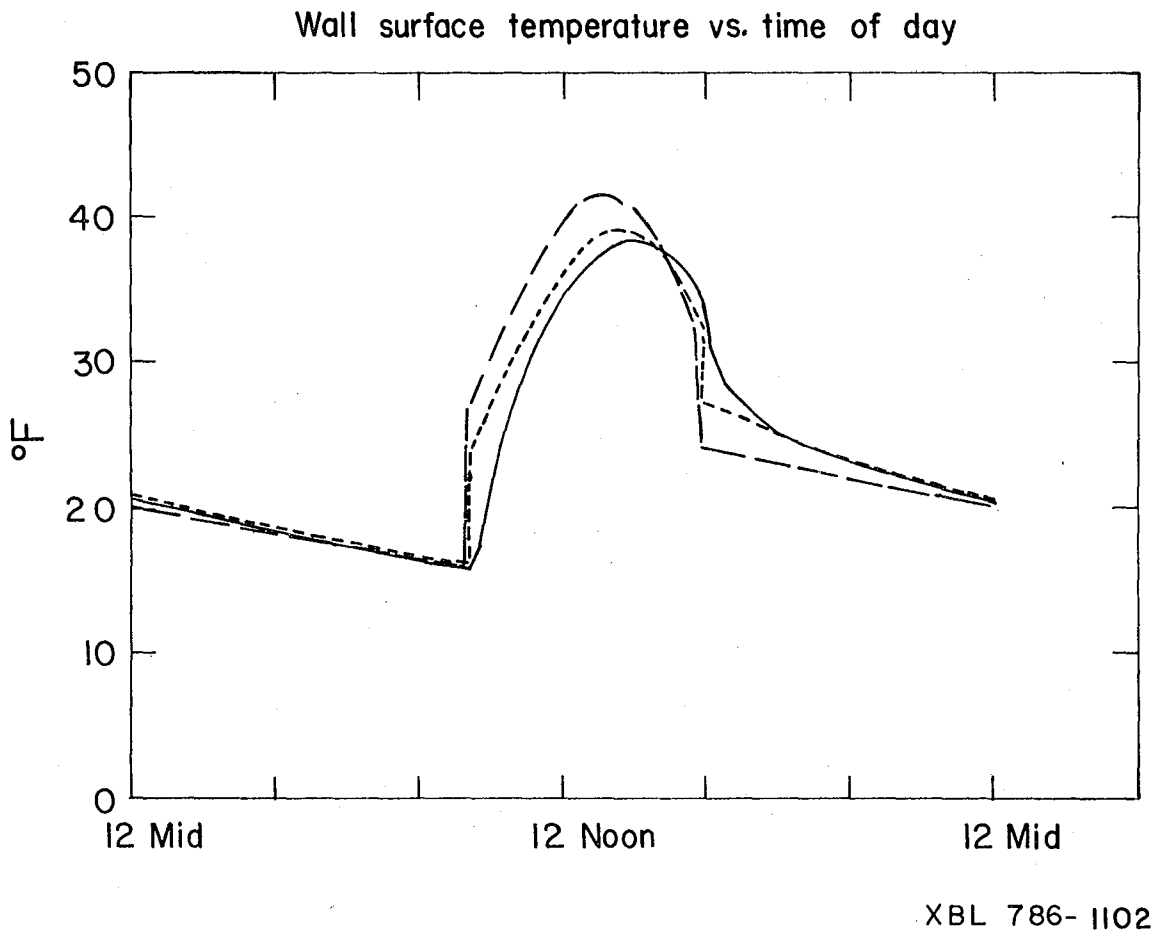


Fig. A2.5B-1. Comparison of wall-surface temperature elevations for the lumped parameter model and an exact solution of the problem. The solid line represents the exact solution, while the light dotted line describes the lumped parameter approximation. The heavy dashed line describes the performance of a naive lumped parameter approach.

This report was done with support from the Department of Energy. Any conclusions or opinions expressed in this report represent solely those of the author(s) and not necessarily those of The Regents of the University of California, the Lawrence Berkeley Laboratory or the Department of Energy.